Stabilisation of Self Mode-Locked Quantum Dash Semiconductor Lasers

Haroon Asghar
M.Sc (Physics), M.Phil (Physics)
114224233

Thesis submitted for the degree of Doctor of Philosophy

NATIONAL UNIVERSITY OF IRELAND, CORK

School of Science

Department of Physics

June 2018

Head of Department: Professor John. G. McInerney

Supervisor: Professor John. G. McInerney

Contents

List of Figures

List of Tables

Abstract

Semiconductor mode-locked lasers are compact pulsed sources which produce high quality optical pulses with high repetition rates and subpicosecond pulse duration. In order to use these sources in real applications, low timing jitter and robust feedback control stabilisation is highly desirable. In this thesis, a series of experimental studies have been performed to achieve stabilisation of two-section self mode-locked quantum-dash laser emitting at $\sim$ 1.55 μm and operating at 21 GHz repetition rate.

First, stabilisation of self mode-locked quantum-dash laser over a wide range of delay tuning was achieved using symmetric dual-loop feedback. Optimum levels were determined for narrowest RF linewidth and reduced timing jitter for single- and symmetric dual-loop feedback. Two symmetric dual-loop configurations, with balanced and unbalanced feedback ratios, were studied. We have demonstrated unbalanced symmetric dual-loop feedback, with the inner cavity resonant and fine delay tuning of the outer loop, produced narrowest RF linewidth and reduced timing jitter over a wide range of delay, unlike single and balanced symmetric dual-loop configurations. This configuration with feedback lengths 80 and 140 m reduced the RF linewidth by $\sim$ 4-67x ($\sim$ 2-9x timing jitter reduction) and $\sim$ 10-100x ($\sim$ 2.5-10x timing jitter reduction), respectively, across the widest delay range, compared to free-running. For symmetric dual-loop feedback, the influence of different power split ratios through the feedback loops was also determined.

We achieved the optimum stabilisation of self mode-locked quantum-dash laser over a wide range of delay tuning using asymmetric dual-loop feedback. Various feedback schemes were investigated and feedback levels far narrowest RF linewidth and low timing jitter were identified, for single- and asymmetric dual-loop feedback. We demonstrated that asymmetric dual-loop feedback, with the shorter feedback cavity tuned to be fully resonant, followed by fine-tuning of the phase of the longer feedback cavity, gave stable narrow RF spectra across the widest delay range, unlike single-loop feedback and free-running conditions. This asymmetric dual-loop scheme reduced the RF linewidth $\sim$ 2.5-4x compared to single-loop and $\sim$ 4-100x relative to free-running conditions. In addition, for asymmetric dual-loop feedback, significant suppression in fundamental side-mode was achieved relative to single-loop feedback.

In addition, we have demonstrated an asymmetric dual-loop feedback scheme

to suppress external cavity side-modes induced in self mode-locked quantum-dash lasers with conventional single- and dual-loop feedback. We reported optimal suppression of spurious tones by optimising the delay in the second loop. We observed that asymmetric dual-loop feedback, with large ($\sim$ 8x) disparity in loop lengths, produced significant suppression in external-cavity side-modes and yielded flat RF spectra close to the main peak with low timing jitter, compared to single-loop feedback. Significant reduction in RF linewidth and reduced timing jitter was also produced by optimising delay time in the second feedback loop. Experimental results based on this feedback configuration validate predictions of recently published numerical simulations.

Finally, we reported stabilisation of our self mode-locked quantum-dash laser on the widest range of delay tuning using simultaneous continuous-wave optical injection and optical feedback. With optical injection, various wavelength detuning ranges (1568 to 1578 nm) and optimum wavelengths (1571.725 to 1572.710) were determined which yielded narrowest RF linewidth and reduced timing jitter. We demonstrated that under double resonance, with both optical feedback and continuous-wave injection, a minimum RF linewidth of $<$ 1 kHz (instrument limited) was achieved which was 2x lower than external optical feedback and $>$ 100x lower than the free-running condition.

I, Haroon Asghar, certify that this thesis is my own work and has not been submitted for another degree at University College Cork or elsewhere.

_____

Haroon Asghar

In the Name of Allah, the Most Beneficent, the Most Merciful

Dedicated to the loving memory of my mother

Acknowledgements

I would like to extend my sincere and heartiest thanks to all of those who provide me immense help and guidance during my Ph.D. Degree.

First and foremost, it is a genuine pleasure to express my deep sense of thanks and gratitude to my supervisor Prof. John. G. McInerney for his scholarly guidance, generous encouragement, pleasant attitude, and kind behavior throughout my research work. Despite his busy schedule and engagements, he was always available to solve any problem I ever came across. His useful support and guidance at every stage helped me a lot to complete my Ph.D. Degree.

I would extend my gratitude to Dr. Ehsan Sooudi for his guidance throughout my research project. His prompt inspirations, timely suggestions with kindness have enabled me to complete my thesis.

This really gives me pleasure to thank my seniors; Dr. Pramod Kumar and Dr. Wei Wei for their keen interest and skillful help. A special mention goes to my Laboratory fellows; Alfonso, Thibault, and Pierpaolo for being friendly, helpful and cooperative behavior. My special thanks to David Rea, Robin Gillen, Sean Knott and John O'Riordan. The memories of the time, which I spent in the lab with them, will always refresh my mind. I also express great gratitude to my friends Rehan, Asfandyar, Usman, Saim, Danish, Mohsin, Razaq, Sohail, Junaid, Ghalib and Imran for your company and friendship.

Many thanks to Dr. Francois Lelarge from Almae Technologies SAS, France and Prof. Abderrahim Ramdane from LPN, CNRS, France for providing quantum dash mode-locked laser devices.

I acknowledge with thanks to the Science Foundation Ireland (SFI) and the European Office of Aerospace Research and Development (EOARD) for providing me financial support for this work.

Finally, I am thankful to my father (Muhammad Asghar) for his unlimited moral support and encouragement in every aspect. I also would like to acknowledge the patience which my wife (Sumaira) and children (Ayesha and Abdul Haseeb), showed during my Ph.D. I owe profound thanks to my other family members, sisters (Saba, Nida, and Rida) and brother (Mamoon) who always pray for my success. May God bless them with health and happiness.

Last but not the least, I absolutely find no words to express my deepest feelings for my loving mother who is now not with me, dreamed of my success and sacrificed too much. It is all due to her prayers where today I am. At these memorable moments, I can't forget her. May Allah give her place in heavens (Ameen)

List of Publications

Journal Papers:

- **Haroon Asghar**, E. Sooudi, and John. G. McInerney, “stabilisation of self-mode-locked QDash lasers subject to simultaneous continuous-wave (CW) optical-injection and optical feedback,” Appl. Opt. **57**(22) (2018).
- **Haroon Asghar**, W. Wei, P. Kumar, E. Sooudi, and John. G. McInerney, “stabilisation of self-mode-locked quantum dash lasers by symmetric dual-loop optical feedback,” Opt. Express. **26**(3), 4581–4592 (2018).
- **Haroon Asghar**, and John. G. McInerney, “Asymmetric dual-loop feedback to suppress spurious tones and reduce timing jitter in self-mode-locked quantum dash lasers emitting at 1.55 μm,” Opt. Letter. **42**(18), 3714–3717 (2017).
- **Haroon Asghar**, E. Sooudi, P. Kumar, W. Wei, and John. G. McInerney, “Optimum stabilisation of self-mode-locked quantum dash lasers using dual optical feedback with improved tolerance against phase delay mismatch,” Opt. Express. **25**(14), 15796–15805 (2017).
- **Haroon Asghar**, E. Sooudi, and John. G. McInerney, "Effects of power-split ratio and phase delay on performance of self-mode-locked QDash lasers subject to symmetric and asymmetric dual-loop optical feedback" Opt. Express. (2018) **In Review**

Conference Papers

- **Haroon Asghar**, E. Sooudi, and John. G. McInerney, “stabilisation and jitter reduction in mode-locked quantum dash lasers by asymmetric dual-loop optical feedback,” *Conference on Lasers and Electro-Optics **(CLEO)***, paper. JTu2A. 31, (2018)
- **Haroon Asghar**, E. Sooudi, P. Kumar, W. Wei, A. Gonzalez, and John. G. McInerney, “Optimum stabilisation of self-mode-locked quantum dash lasers using dual-loop optical feedback,” *International Conference on Transparent Optical Networks **(ICTON)***, paper We.P.30, (2017)

- **Haroon Asghar**, E. Sooudi, W. Wei, P. Kumar, A. Gonzalez, and John. G. McInerney, "A novel symmetric dual-loop feedback scheme insensitive to phase tuning using self-mode-locked two-section quantum dash laser," *International Conference on Transparent Optical Networks **(ICTON)***, paper We.P.29, (2017)
- **Haroon Asghar**, W. Wei, P. Kumar, D. Marah, and John. G. McInerney, "A novel dual-loop feedback scheme to reduce spurious tones in self-mode-locked two-section quantum Dash laser emitting at 1.55 μm," *Conference on Lasers and Electro-Optics **(CLEO)***, paper JTu5A.98, (2017)
- **Haroon Asghar**, W. Wei, A. Gonzalez, and John. G. McInerney, "Influence of controlled feedback intensity through symmetric dual-loop feedback on the noise characteristics of passively mode-locked two-section quantum dash laser," Photonics Ireland, paper B33, (2017)
- **Haroon Asghar**, W. Wei, P. Kumar, D. Marah, and John. G. McInerney, "Sub-picosecond pulse stability of passively mode-locked two-section quantum dash laser at 1550 nm subject to single and dual optical feedback," *Conference on Lasers and Electro-Optics **(CLEO)***, paper STh4L.4, (2016)
- W. Wei, **Haroon Asghar**, P. Kumar, D. Marah, and John. G. McInerney, "Sub-kHz RF linewidth of quantum-dash mode-locked laser by self-injection from symmetric dual-loop feedback and fibre delay," *Conference on Lasers and Electro-Optics **(CLEO)***, paper STh4L.3, (2016)
- P. Kumar, **Haroon Asghar**, W. Wei, D. Marah, E. Sooudi and John. G. McInerney, "Dynamical complexity induced by frequency dependent optical feedback in dual-section passive mode-locked quantum-dash laser at 1.55 μm," **(CHAOS)**, (2016)
- D. Marah, P. Kumar, **Haroon Asghar**, S. Keshri, R. Kumar, John. G. McInerney, "Pulse characteristics of passively mode-locked dual-section quantum-dash laser subjected to optical feedback," *International Symposium on Physics and Applications of Laser Dynamics **(IS-PALD)***, (2015)
- **Haroon Asghar**, E. Sooudi, and John. G. McInerney, "stabilisation of self-mode-locked QDash lasers using simultaneous continuous-wave (CW) optical-injection and optical feedback," Photonics Ireland, (2018) (Submitted)

- A. González, T. Bondaz, **Haroon Asghar**, P.A. Porta, and John. G. McInerney, "Observation of relaxation oscillations in vertical-external-cavity surface-emitting lasers," Photonics Ireland, (2018) (Submitted)

Chapter 1

Introduction

Semiconductor mode-locked lasers (MLLs) have attracted much attention in recent years due to their potential applications in various fields including optical sampling [1], frequency comb generation [2-5], optical clock recovery [6 ,7], optical clock distribution [5], telecommunications [8-11] and spectroscopy [12]. Pulsed semiconductor MLLs with wavelengths near 1550 nm are of particular interest in optical telecommunications because the transmission window of an ideal silica optical fibre lies within the wavelength range of 1280 nm to 1580 nm. These lasers can also be used as pulse sources for time-domain multiplexed systems [13] and as synchronised pulse sources or multi-wavelength lasers for wavelength-division multiplexed systems [14, 15]. Some ideal features of semiconductor MLLs include compactness, low fabrication costs, low threshold current, fast carrier dynamics, inhomogeneously broadened spectrum, and low amplified spontaneous emission [16, 4]. To improve the performance and to extend applications of semiconductor MLLs high timing stability is paramount. In the last two decades, significant progress has been made in the area of mode-locked laser diodes. However, many open problems still exist and need to be addressed in depth, including stabilisation of semiconductor MLLs. In order to improve the stabilisation of self-mode-locked (SML) quantum-dash (QDash) lasers, a series of experimental studies has been conducted and are described in this thesis.

In the following sections, a brief introduction to semiconductor lasers, mode-locking, and quantum nanostructure-based semiconductor MLLs is given, with essential discussions on the stabilisation techniques (external optical feedback and optical injection techniques) analysed in this thesis. Finally, the motivation

for this work and outline of the thesis is presented in sections 1.5 and 1.6, respectively.

1.1 Semiconductor Lasers

In 1917, Einstein published his classic paper [17] in which he introduced the concept of stimulated emission, which became the basis of Lasers [1]. Stimulated emission is a quantum mechanical phenomenon in which an electron in the excited state is stimulated by the interaction of an incoming photon to return to the lower state with simultaneous emission of a second photon. This emitted photon has identical properties (polarisation, frequency, phase and direction of travel) to the incident photon. The basic sketch of the phenomenon of stimulated emission is illustrated in Fig. 1.1 (a).

All types of lasers consist of three fundamental components: a pump generating population inversion, a gain medium providing amplification and a resonant cavity confining the optical field. A schematic of a laser cavity including these three main components is shown in Fig. 1.1 (b).

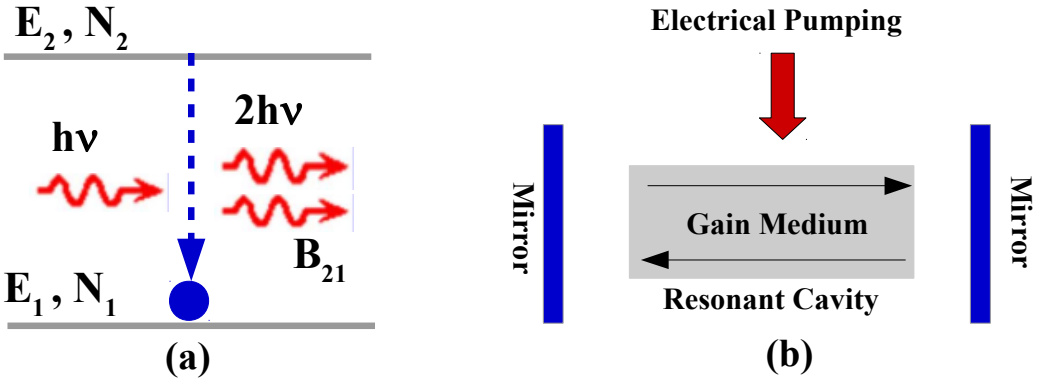

Figure 1.1: (a) Sketch of the phenomenon of stimulated emission (b) Schematic diagram of a laser cavity including the three main components.

The invention of the semiconductor laser can be considered as a revolutionary development in the field of science and technology. The first report on the process of stimulated emission in the GaAs based *p-n* junction was discovered at the Ioffe Institute, Russia in 1962 [18]. However, a practical semiconductor device based on the principle of stimulated emission was first demonstrated by Hall *et al.* [19], which is now used in many everyday applications, such as

[1] The word "laser" is an acronym for "light amplification by stimulated emission of radiation."

read/write data on compact discs, laser pointers, displays, printers and most optical fibre telecommunications systems. The first reports on semiconductor lasers were published by the following four institutions within a period of five weeks in 1962.

- General Electric (GE Schenectady) [19]
- International Business Machines Corporation (IBM Yorktown Heights, NY) [20]
- General Electric (GE Syracuse, NY) [21]
- Lincoln Lab Massachusetts Institute of Technology (MIT, Cambridge) [22]

Semiconductor lasers are based on semiconductor gain media and population inversion is achieved when an electric current is injected. The basic mechanism responsible for light emission from a semiconductor material is the recombination of electrons and holes at a *p-n* junction. A basic schematic of *p-n* junction based semiconductor laser is depicted in Fig. 1.2. A cavity, formed by placement of high and partially reflecting mirrors, provides the selective feedback mechanism to emitted photons travelling through the gain media. The stimulated emission occurs within the active region and produces optical gain. If the injected carrier density is large enough, the stimulated emission of the photons overcomes the losses and lasing takes place at particular wavelengths related to the length of the cavity and properties of the materials of the active region.

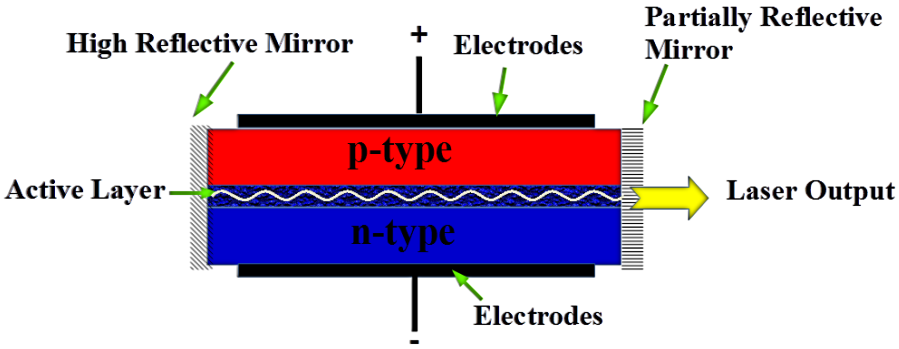

Figure 1.2: Schematic of semiconductor laser with main components.

The first report of semiconductor lasers [19] was based on homojunction semiconductor diodes which consist of two layers made from the same compound, generally gallium arsenide (GaAs). Semiconductor lasers based on homojunction materials involved very high threshold current densities because electrons and holes are free to diffuse and therefore dilute the gain which yields poor carrier confinement. Furthermore, the poor overlap of the optical mode with the

gain leads very high optical losses. To overcome such primary disadvantages of homojunction based semiconductor lasers, in 1970 Alferov [23] demonstrated the first double heterostructure (DH) laser. This DH structure consisted of GaAs active region surrounded by $Al_xGa_{1-x}As$ layers and continuous-wave (CW) operation followed by the lower threshold current density was achieved at room temperature [24]. The DH structure provides lateral confinement of the electric field to the active region due to the higher refractive index of the central region to that of the cladding material. In addition, the surrounding semiconductor layer with wider band-gap results in lower absorption of light, reducing the optical losses significantly. Due to this remarkable discovery and seminal role in the development of practical semiconductor lasers, Alferov shared the Nobel Prize in Physics with Kroemer in 2000. The discovery of DH structures made possible the production of inexpensive commercially available semiconductor lasers and subsequently revolutionised optical communication and data storage. Nowadays, most semiconductor lasers are based on DH structures due to their improved carrier and optical confinement relative to homojunction lasers. Materials used for development of DH semiconductor laser systems include GaAs/AlGaAs, InGaAsP/GaInAs/InP and InGaAs/AlGaInAs/InP [25].

In recent decades, optimisation and development of semiconductor materials have led to new low threshold and high-performance semiconductor lasers, including quantum-well and quantum-dot/dash lasers, vertical cavity surface emitting lasers (VCSELs), distributed feedback (DFB) lasers, and quantum cascade lasers which are suitable for a broad range of applications. In DH structures, a thin layer of GaAs (< 20 nm) confined between two layers of AlGaAs, traps electrons and holes in the central region. Due to the small thickness of the GaAs, the confinement energies become quantised and the resulting DH structure is known as a quantum-well laser [26]. Confinement in two and three spatial dimensions is also possible, leading to quantum-wires and quantum-dots respectively. Maximum quantum confinement occurs for quantum-dots in which the densities of states are discrete and electrons are confined in all three dimensions. This, in turn, can result in lower threshold current density and higher optical material gain [27]. The density of states for a different degrees of confinement is shown in Fig. 1.3. In recent years quantum-dot (QDot) and QDash semiconductor lasers have attracted much attention for reasons of stability, compactness, and low fabrication costs, and are ideal for generating stable picosecond pulses with high repetition rates.

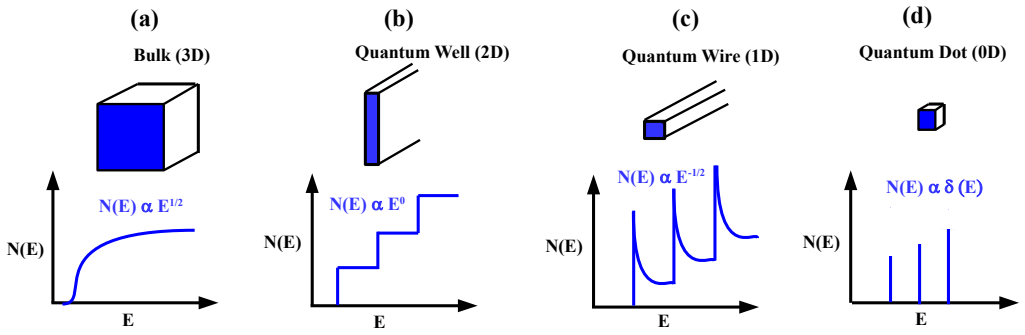

Figure 1.3: Quantum confinement and density of states. (a) Bulk structure (no quantum confinement) (b) Quantum confinement in one dimension (quantum well) (c) Quantum confinement in two dimensions (quantum-wire) (d) Quantum confinement in three dimensions (quantum-dot).

1.2 Pulse Generation in Semiconductor Lasers

Optical pulses are flashes of light, which are often generated with lasers by exploiting their unique properties [28]. Repetition rate, pulse duration, peak and average powers, chirp and timing jitter are the fundamental properties of the laser pulse. Semiconductor lasers are a suitable candidate to generate high-quality pulses in terms of high repetition rates (up to 500 GHz) [29], short pulses up to order of femtoseconds [30] with low timing jitter [31]. In order to achieve ultrashort optical pulses from semiconductor lasers, generally, there are three techniques: gain switching [32-34], Q-switching [32, 33, 35] and mode-locking [32, 36, 37]. In Q-switching, intense short pulses (of the order of nanoseconds) are generated from the laser rather than CW operation. The basic idea of Q-switching is that the energy stored in the laser medium can be released suddenly by increasing the Q-value of the cavity so that the laser reaches the threshold. This can be done actively [38], by moving one of the resonator mirrors in place or passively [39, 40] by inserting a saturable absorber inside the resonator. Gain switching is a method in which the light of extremely short pulses (of the order of picoseconds) is generated by quick modulation of the laser gain via the pump power. Unlike Q-switching, gain-switching does not require the insertion of active/passive elements in the laser cavity, but it requires external elements (RF signal sources) to modulate the laser gain [34, 41, 42]. In comparison to Q-switching, the major advantage of gain-switching is that it is wavelength tunable [43]. Among the above-discussed techniques, mode-locking [44, 45] is the simplest technique, resulting in shorter and higher quality optical pulses with lower timing jitter, and is sometimes simple to im-

plement.

1.2.1 Mode-Locking in Semiconductor Lasers

Semiconductor MLLs are attractive sources of ultrashort optical pulse trains with high repetition rates. Applications for MLLs include telecommunications, optical data storage, defense, security, metrology, medical systems, and many other emerging areas. Mode-locking is a technique that allows the generation of light pulses of extremely short duration (on the order of picoseconds or femtoseconds), and occurs when the longitudinal modes of the laser's resonant cavity are forced to oscillate with fixed amplitudes and locked phases. Mode-locking in semiconductor lasers can be achieved by three broad categories: active mode-locking [46], passive mode-locking [47-50], and hybrid mode-locking [51]. In all these techniques, optical modes of the laser cavity are forced to oscillate with stable amplitudes and fixed relative phases.

1.2.1.1 Active Mode-Locking

Active mode-locking in semiconductor lasers can be implemented by modulating the gain or an absorber in the laser cavity at frequencies synchronised to the cavity round-trip time [32, 52]. To modulate the absorption, an electro-absorption modulator monolithically embedded in the laser cavity can be used to lock the phases of the longitudinal modes together. An external RF source is used to synchronise the modulating signal frequency with the inverse round trip time of the resonator or an integer multiple of it, generating windows of positive gain. During a short period of net gain, optical pulses of the order of picoseconds are generated with low timing jitter.

1.2.1.2 Passive Mode-Locking

In passive mode-locking, ultra-short optical pulses are generated without any external source for modulating the gain or absorption. This technique requires a saturable absorber embedded within the laser cavity. A saturable absorber acts as an intensity dependent transmission which absorbs low-intensity light and leads to selective amplification of high-intensity light, so that highly intense pulses are produced. After many round trips, the pulses are generated in a

steady stream by temporal interaction of gain and absorber dynamics, where the absorber is saturated faster than the gain, and recovers before the gain, enabling a positive net gain window which sharpens the pulses with a repetition rate corresponding to the round-trip time of the cavity.

1.2.1.3 Hybrid Mode-Locking

Hybrid mode-locking is a combination of both active and passive mode-locking. With this approach, as external RF source synchronises the pulse timing, as in active mode-locking, while an absorber also generating optical pulses as in passive mode-locking. This technique has the advantage of stabilising the phase-noise of the laser which leads a significant reduction in RF linewidth and has many applications in telecommunication systems, where synchronisation of pulses is required.

1.3 Quantum Dash/Dot Mode-locked Lasers Emitting at 1.55 μm

The device investigated in this thesis was a two-section self mode-locked QDash laser emitting at $\sim$ 1550 nm and operating at $\sim$ 21 GHz pulse repetition rate. In this section, we describe a brief history of InP based QDash/Dot MLLs.

Renaudier *et al.* [53] first demonstrated single-section QDot Fabry-Pérot semiconductor lasers emitting at 1.5 μm and operating at 45 GHz repetition rates. Mode-locking in these lasers was obtained without saturable absorbers and record low RF linewidth (100 kHz) was achieved relative to bulk and quantum-well lasers. Later, Gosset *et al.* [54, 55] reported pulse generation in one-section passive mode-locked QDash semiconductor lasers emitting at 1.5 μm with a repetition rate of 134 GHz. Optical pulses of width 800 fs were achieved with a time-bandwidth product of 0.46. In addition, a record low RF linewidth (50 kHz) was demonstrated for passive mode-locked QDash laser operated at 42 GHz with few ps range pulse-width. Such low RF linewidth highlights the potential of quantum nano-structure based semiconductor lasers to design high-performance pulse sources and low timing-jitter devices for potential application in optical communications. Similar investigations have been performed by another group [56] who demonstrated femtosecond pulses from

InAs/InP based single-section passive mode-locked QDot lasers. Optical pulses with duration 312 fs were generated at a repetition rate of 92 GHz with RF linewidths as low as 20 kHz. The most interesting part was the fact that these deliberate pulsations were observed for single-section Fabry-Pérot lasers without any desirable passive (absorber section) or active mode-locking schemes. Mode-locked lasers which automatically start mode-locking in the absence of any active/passive scheme in the device are called self-mode-locked lasers. In self-mode-locking, non-linear effects such as self-phase modulation (SPM) [57, 58], cross-phase modulation (XPM) [59] and four-wave-mixing (FWM) [60, 61] inside the laser medium contribute to maintain fixed phase relationship between the longitudinal modes inside the laser cavity [56]. Further self-mode-locking has been demonstrated in InGaAsP based bulk lasers [62], GaAs bulk lasers [63], quantum-well lasers emitting at 980 nm [64] and 1.55 μm [65, 66]. Self-mode-locked quantum dot lasers allow reduction of device complexity and simplify packaging and cost, with improved performance including low RF linewidth and corresponding timing jitter relative to quantum-well and bulk semiconductor lasers [31, 53].

1.4 Stabilisation of Semiconductor QDash Mode-Locked Lasers

The focus of this thesis will be to achieve stabilisation of our SML QDash lasers using controlled external optical feedback and optical injection techniques. In this section, a brief introduction and overview of external optical feedback and optical injection will be presented.

1.4.1 External Optical Feedback

In 1980, Lang and Kobayashi [67] reported some aspects of the dynamics of a semiconductor laser exposed to optical feedback. In optical feedback approach, photons emitted from the active medium are partially reflected by an external mirror back into the gain medium of the laser cavity, as shown in Fig. 1.4.

Semiconductor lasers under external optical feedback are of high interest to study the dynamical behavior of the systems because external optical feedback introduces a delay in the system. This delay results in rich dynamical states like

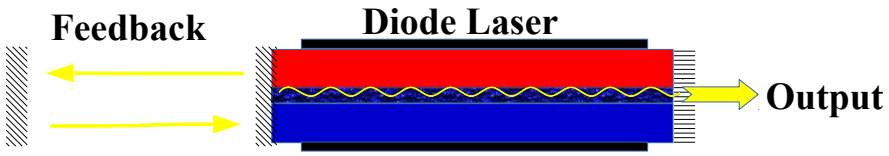

Figure 1.4: Schematic of semiconductor laser subject to external optical feedback.

multistability [68, 69], chaos [70, 71], and low-frequency fluctuation regimes [72]. Furthermore, the amount of feedback into the laser cavity significantly affects the characteristics of semiconductor lasers and yields complex dynamical states due to high sensitivity of semiconductor lasers to external optical feedback. The effects of small amounts of external optical feedback with proper phase matching can be highly beneficial for the characteristics of semiconductor lasers, and a considerable reduction in RF linewidth and timing jitter can be obtained. Goldberg *et al.* [73] experimentally observed changes in spectra of GaAlAs semiconductor lasers subject to external optical feedback, and minimum RF linewidth as low as 100 kHz was achieved. In 1983, Tamburrini *et al.* [74] reported phase-noise measurements on semiconductor lasers with considerable reduction in RF linewidth in the presence of external optical feedback. Later, Patzak *et al.* [75] and Agrawal [76] showed that proper phase-matching and weak optical feedback conditions produced linewidth reduction of the semiconductor lasers by a factor of ~ 10. In the early 90's, Solgard and Lau [77] experimentally demonstrated that external optical feedback can be used to reduce the RF linewidth close to two orders of magnitude compared to free-running conditions. It was also determined that the effects of optical feedback change periodically as the length of the feedback loop is varied, and the feedback level required to stabilise the laser was further identified. During the last two decades, a number of experimental [77-81] and numerical [81-85] investigations have been performed to evaluate the properties of semiconductor lasers under external optical feedback. Recently, Lin *et al.* [79] experimentally investigated the influence of external optical feedback on two-section passively mode-locked QDot lasers operating at 5.1 GHz repetition rate. It was found that under fully resonant feedback level up to -36 dB, the RF linewidth was reduced to 8 kHz from 100 kHz for the free-running. In addition, for a passively mode-locked QDash laser emitting at 1580 nm and operating at 17 GHz repetition rate, RF linewidth reduction to as low as 500 Hz occurs at significantly stronger feedback -22 dB [80]. These differences in feedback level are explicable by the likelihood that the anti-guiding (phase-amplitude coupling) factor

is lower in quantum-dashes. Most recently, 99% reduction in RF linewidth and 23 fs pulse-to-pulse jitter was reported using single cavity feedback for a 40 GHz QDot mode-locked laser [78]. Five different feedback regimes were identified along with the regime of resonant optical feedback most favorable and desirable for practical applications.

The introduction of a high fraction of the back-reflected light into the gain medium of the laser cavity can be disadvantageous and restrict practical applications of semiconductor lasers. For example, to use semiconductor lasers as transmitters in optical networks, expensive optical isolators are needed to avoid back reflections that influence the temporal stability of the lasers. In 1984, Cho and Umeda [86] claimed that high feedback ratio (5-10%) into the laser cavity leads the laser into a state of chaos. Lenstra *et al.* [87] first observed the dramatic increase in linewidth broadening ($\sim$ 25 GHz) at moderate higher feedback level as a form of chaos, referred to as coherence collapse. Since then much attention has been devoted to understand and explore such complex dynamical states. Research on the phenomenon of low-frequency fluctuation and coherence collapse regime is still going on [88, 89].

1.4.2 Optical-Injection of Semiconductor Lasers

The phenomenon of optical injection can be described as two coupled oscillators, where one oscillator represents the injection field and the other diode laser: shown in Fig. 1.5. For optical injection, the relevant parameters include pump power, feedback level injected into the slave laser, and frequency detuning between the injected field and the free-running laser.

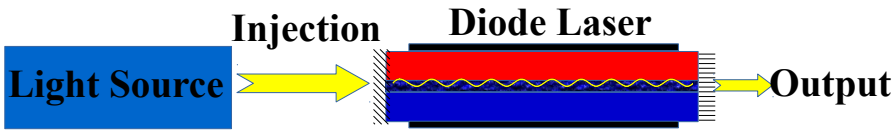

Figure 1.5: Schematic of semiconductor laser subject to optical-injection.

At theoretical prediction of the locking of electrical oscillators was presented by Van der Pol in 1927. In the middle of the 20^{th} century, Adler reported [90] that the oscillation frequency of an electrical oscillator can be locked to the frequency of the injected oscillator. The first injection-locking was demonstrated by Stover and Steier and successful phase-locking was achieved by direct injection of the first laser into the cavity of the other laser [91]. Both lasers used

in this experimental study were He-Ne lasers operating in a single longitudinal mode at 632.8 nm [91]. In 1980, Kobayashi *et al.* reported the first observations of injection-locking in DH structure AlGaAs semiconductor lasers [92] and measured experimental results agreed well with theoretical values based on Adler's theory [90]. Later, Lang [93] analysed the injection-locking properties of a semiconductor laser and found that injection carrier density results in peculiar asymmetric tuning curves and a dynamic instability. A detailed theoretical and experimental investigation of the locking conditions of semiconductor lasers was presented by Mogensen *et al.* [94] in 1985. From a purely physical point of view, many studies have been done on the analysis of stability and behaviour of laser systems under optical injection as a system of nonlinear coupled oscillators. For further details on optical injection, see the review article [95] and references therein.

1.5 Motivation for This work

Quantum nanostructure-based semiconductor MLLs are of increasing interest for various applications in optical communication systems, such as multi-carrier transmission systems in orthogonal frequency division multiplexing (OFDM) [96, 15], coherent wavelength division multiplexing (CoWDM) [13], arbitrary waveform generation [97], all-optical signal processing [98] and millimeter-wave generation [99]. While picosecond pulses from these lasers have been demonstrated routinely, these pulses have significant chirp and poor timing jitter. The latter is usually determined by measuring the linewidth of the repetition rate peak in the RF intensity fluctuation spectrum. To improve the phase-noise of passively MLLs, several experimental methods such as external optical feedback [77-81, 100], coupled optoelectronic oscillators (OEOs) [101-104], hybrid mode-locking [105] and injection-locking [100, 106-108] techniques have been proposed and demonstrated. Optoelectronic feedback has been utilized to stabilise timing jitter by conversion of the optical signal (using a fast photodetector) to an electrical oscillation for use in a long feedback loop. This technique does not utilize an RF source but requires optical-to-electrical conversion. Hybrid mode-locking requires electrical modulation of the gain or absorber bias, while optical injection needs an external laser, making these techniques less attractive for practical implementation where low cost, simplicity, and reliability are paramount. Of all stabilisation techniques, external optical

feedback is the simplest and most cost-effective demonstrated to date both experimentally and numerically, which suppresses instabilities and filters noise by establishing one or more compound cavities with external reflectors or resonators. It is clear that stabilisation using conventional single-loop feedback is very sensitive to small delay adjustments, with optimum performance being limited to one narrow regime. In practice, MLLs require a reduced sensitivity of RF linewidth and timing jitter to detuning and drift in the delay phase. In this regard, the first area of interest is to maintain the stability of our SML QDash laser over the widest delay range using external optical feedback. Besides improvement in timing jitter with single-loop feedback, the existence of extra mirror(s) generates side-bands resonant with the round-trip time of the external cavities which affect RMS timing jitter and quality of the pulse trains, as measured by RF spectra. Recently, dual-loop feedback [109, 110] with the second loop shorter than the main one has been demonstrated to suppress external cavity side-bands but produces additional noise peaks resonant with the delay in the second cavity which is undesirable in many applications where low noise and flat spectra are required, as in optical frequency comb generation. Most recently, the influence of the various length of second feedback delay on side-mode suppression [112] and timing jitter [113] has been studied numerically. However, a thorough experimental investigation is desired to explore the relation of side-mode suppression with precise alignment of the length of the second loop delay.

In order to deal with general issues mentioned above, a series of experimental studies have been performed, and reported in this thesis.

1.6 Thesis Outline

This thesis is organised as follows:

Chapter 1 has discussed a basic overview of semiconductor lasers and mode-locking mechanisms along with a literature review on InP based semiconductor QDash MLLs and stabilisation techniques (optical feedback and optical injection). The motivation for this work including the outline of thesis was given.

Chapter 2 provides basic structure and fabrication details of our SML QDash lasers. In addition, measurement techniques carried out to study the basic characteristics of free-running InP QDash MLLs are discussed.

Chapter 3 explains the influence of symmetric dual-loop optical feedback (equal feedback loops) on the RF linewidth and timing jitter of SML QDash lasers versus delay tuning. Various feedback schemes are investigated and optimum levels were determined for the narrowest RF linewidth and reduced timing jitter, for single-loop and symmetric dual-loop feedback. Two symmetric dual-loop configurations, with balanced and unbalanced feedback ratios, were studied and compared to results with single-loop feedback and free-running conditions. We demonstrated that unbalanced SDL feedback provides the best stability, maintaining stable RF spectra with narrow linewidth and low timing jitter over a range of delay detuning. In addition, for symmetric dual-loop feedback, the influence of different power split ratios through the external feedback loops was determined.

Chapter 4 presents the variation in RF linewidth versus delay tuning followed by different power split ratios through the symmetric dual-loop feedback configuration. RF linewidth narrowing and broadening over a broad range of delay phase was demonstrated when each cavity was set to integer resonance and the second cavity was fine-tuned. We further observed that RF linewidth reduction over a broad range of phase delay was achieved by setting the stronger cavity to an integer resonance then fine-tuning the weaker cavity.

Chapter 5 focuses on the influence of asymmetric dual-loop feedback (second loop shorter than the main one) on timing stability of SML QDash laser as a function of delay tuning. Various feedback conditions were investigated and optimum levels determined for the narrowest linewidth and reduced timing jitter for both single-loop and asymmetric dual-loop configurations. We demonstrated that asymmetric dual-loop feedback, with the shorter feedback cavity tuned to be fully resonant, followed by fine-tuning of the phase of the longer feedback cavity, gives stable narrow RF spectra across the widest delay range, unlike single-loop feedback. Moreover, the influence of asymmetric dual-loop feedback scheme on suppression of external cavity side-modes was further discussed.

Chapter 6 presents a novel asymmetric dual-loop feedback method to suppress external cavity side-modes induced in a SML QDash laser with conventional single-loop and asymmetric dual-loop feedback. The best combination of the lengths of the two feedback cavities, to eliminate the external cavity side-modes and modal overlaps in the RF spectra was determined. In addition, we determined optimum conditions for stabilisation and timing jitter reduction by vary-

ing the length of the second feedback cavity. Measured experimental results were compared with recently published numerical simulations.

Chapter 7 explains the influence of simultaneous external optical feedback and CW optical injection on the timing stability of the SML QDash laser, and compared to results with external optical feedback alone. Wavelength ranges which yield narrow RF linewidth and reduced timing jitter under full resonance were identified. In addition, variation in RF linewidth and pulse repetition frequency as functions of the master laser wavelength were investigated.

Finally, a conclusive summary of the contributions of this research work followed by suggested future work is given in **Chapter 8**.

Chapter 2

Basic Characteristics of SML QDash MLLs

2.1 Introduction

In this chapter, the basic structure and fabrication details of two-section SML QDash lasers are presented. After introducing the devices, the main measurement techniques of optical power, free-running optical/electrical spectra and timing jitter will be briefly introduced.

This chapter is organised as follows: In Section 2.2, the basic structure of SML QDash lasers is described, then in Section 2.3 device fabrication details are given. In Section 2.4, techniques used to measure optical power, free-running optical/electrical spectra and integrated timing jitter of SML QDash lasers are described.

2.2 Device Structure

Devices under investigation were two-section InAs/InP QDash MLLs with active regions consisting of nine InAs QDash monolayers grown by gas source molecular beam epitaxy (GSMBE) embedded within two barrier layers, and separate confinement heterostructure (SCH) layers of InGaAsP, emitting at $\sim$ 1550 nm [31]. Both the barriers and SCH layers consisted of $In_{0.8}Ga_{0.2}As_{0.4}P_{0.6}$ quaternary materials with λ_g = 1.55 μm. In the DBARR (dash-in-barrier) type, QDash

mono layers were embedded directly into the barriers and SCH layers as shown in Fig. 2.1.

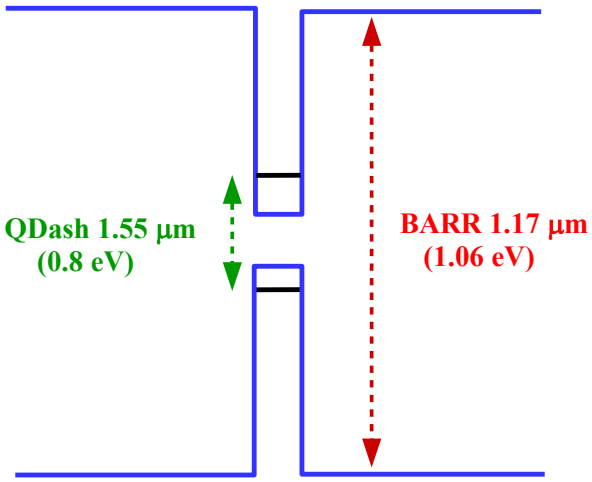

Figure 2.1: Active region structure of the device and resonant wavelengths of the device, Acronyms: QDash: Quantum-Dash, BARR: barrier layer.

In DBARR type, the barrier and SCH were undoped. Cavity length was 2030 μm, 11.8% (240 μm) of which formed the absorber section, giving pulsed repetition frequency $\sim$ 20.7 GHz. These devices had two sections along the direction of light propagation: one was the gain section and the other was the absorber section, with the same active layers. The gain and absorber sections were electrically isolated by 9 kΩ. The lasers were mounted p-side up (substrate down) on an AlN submount and a copper block with active temperature control. Electrical contacts were formed by wire bonding, and heat sink temperature was fixed at 19^0C. The schematic of the cavity structure of our two-section devices is shown in Fig. 2.2.

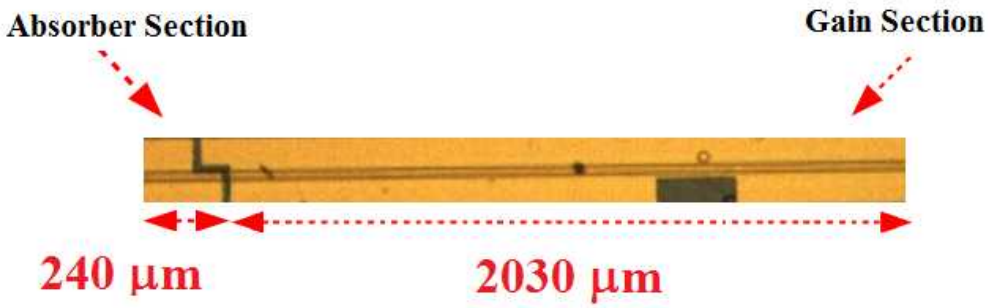

Figure 2.2: Schematic of absorber and gain sections of two-section QDash devices.

One important difference between our two-section devices with other saturable-absorber mode-locking (SAML) devices is that the two-section QDash MLLs still

operate as MLLs when the absorber is left open or is slightly forward biased. In this work, mode-locking of the devices under test was obtained without reverse bias applied to the absorber section. This was a two-section device but was packaged similarly to a single-section self-mode-locked lasers since the absorber was unbiased: its minimal absorption does not affect the self-mode-locking mechanism [107]. Recently, 1550 nm InAs/InP based QDash single-section self-mode-locked lasers have demonstrated promising high speeds, narrow pulse generation, specifically GHz pulse repetition rate and very low RF linewidth [54, 55] with low timing jitter. The absence of any obvious active/passive mode-locking scheme in these devices looks surprising at first glance. However, self-phase modulation (SPM), cross-phase modulation (XPM) and four-wave-mixing (FWM) in the cavity has been proposed as the reason for this coherent self-pulsing behavior [31].

2.3 Device Fabrication

Growth of our QDash structures was carried out using gas-source molecular beam epitaxy (GSMBE) on a Silicon-doped InP substrate with (100) crystal direction using the Stransky-Krastanow growth method [31]. The QDash layer growth is based on deposition of a very thin layer (about 1 nm thick) of InAs on InGaAsP; the mismatch between the lattice constants of the two layers causes the formation of QDot islands [31]. However, due to the GSMBE growth conditions and surface anisotropy of InGaAsP layer, the formation of QDots is usually modified to form nanostructures elongated in the direction perpendicular to the growth direction. These nanostructures are called quantum-dashes and have typical thickness $\sim$ 2 nm, width $\sim$ 15-20 nm and length $\sim$ 40-300 nm, depending on growth conditions [31] (shown in Fig. 2.3).

The DBARR structure was processed into waveguides with either shallow ridge or buried ridge structures with well-established InP processing technology for InP based quantum-well or bulk devices [31]. For buried ridge stripe structures, waveguides were defined using contact lithography. Metal Organic Vapour Phase Epitaxy (MOVPE) was used to grow the p-doped InP cladding layer and GaInAs contact layers. For lateral confinement of carriers, proton implantation was utilized. P and n type electrical contact pads were realized by ion beam sputtering of Ti/Pt/Au films [114]. For the two-section devices, interruption of the metal mask, etching of the ternary contact layer and ion implantation forms

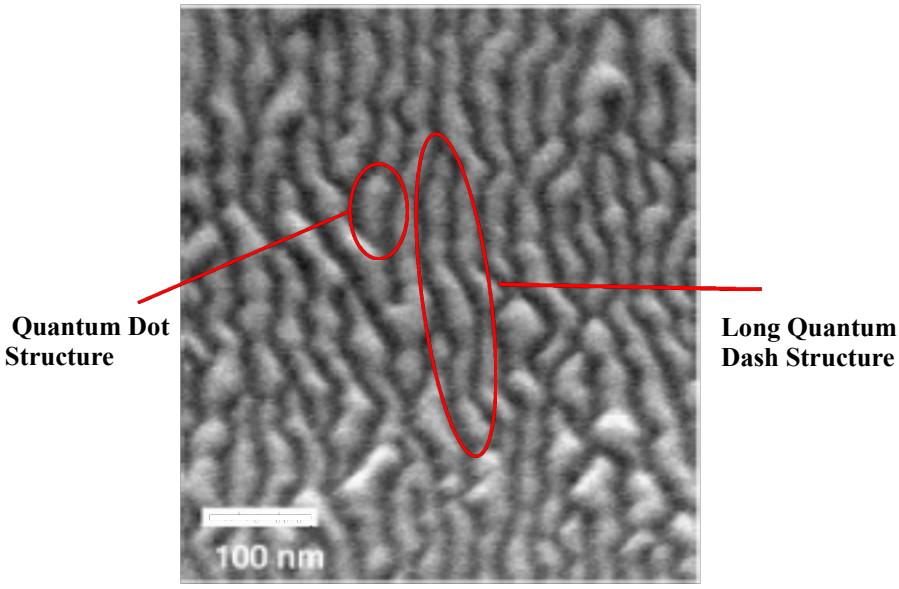

Figure 2.3: View of the active layer using transmission electron microscopy (TEM).

two isolated sections used as the gain and absorber sections with the desired length ratios. Growth and processing of the devices were performed at III-V lab, a joint ventures of Alcatel Lucent Bell Labs, Thales Research Technology and CEA-LETI, France [114]. The devices were cleaved to the required lengths at the Laboratory for Photonics and Nanostructures (LPN), CNRS, France. The layer schematic of the DBARR device is shown in Fig. 2.4.

The singulation of devices, mounting and wire-bonding were carried out at UCC/Tyndall. The devices were mounted on AlN submounts using silver epoxy as the bond material, followed by electrical connections to the devices using standard wire bonding. The submount was mounted on a copper block for active temperature control. A picture of a mounted device is shown in Fig. 2.5.

2.4 Measurement Techniques

In this section, we will discuss the measurement techniques used in the course of this work to determine the following parameters of the device under test (DUT): optical power, optical/electrical spectra and measurement of integrated timing jitter.

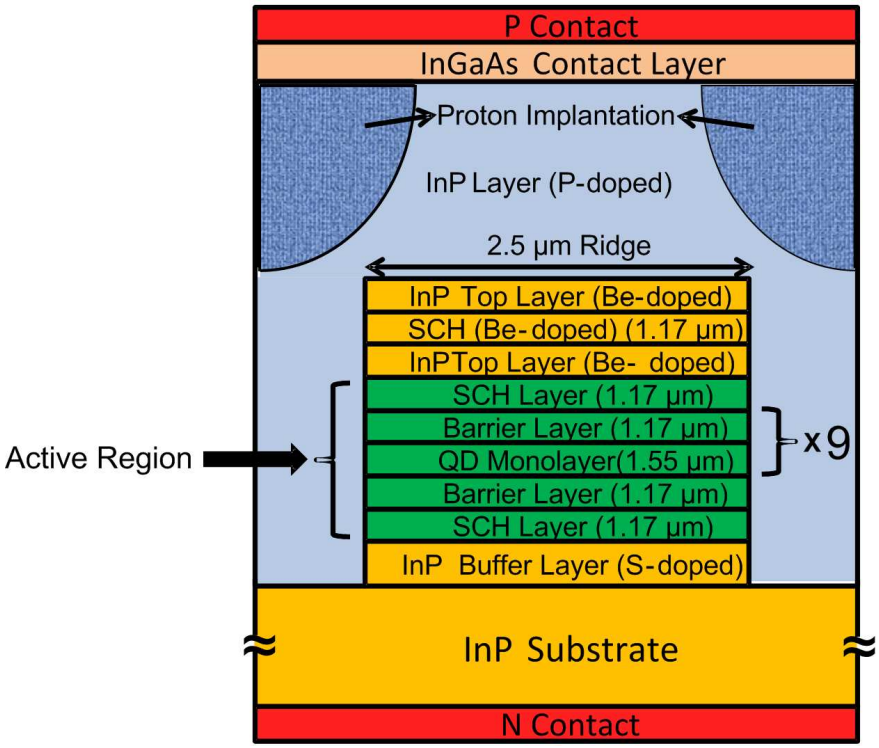

Figure 2.4: Layer structures of the DBARR laser device.

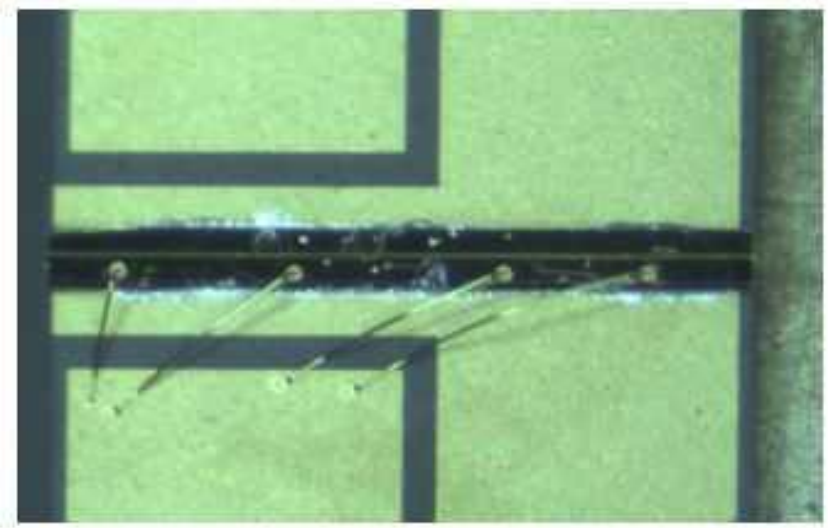

Figure 2.5: Photo of a mounted device on an AlN submount with electrical contacts using ball-type wire bonding.

2.4.1 Optical Power Versus Bias Current Characterisation

The schematic of the experimental arrangement for power measurement is shown in Fig. 2.6. Light from the laser was collected and collimated using lenses and a free space isolator, and was shone onto a photodetector with large

detection area connected to a power meter (Thorlabs Germanium PIN photodetector, model S122B with PM30 console system). The free space isolator was used to prevent any possible feedback from the photodetector to the laser. The photodetector was so slow that it could be assumed that it always measured the time-averaged power. This term will be used from now on for any correspondence about the emitted power, and the injection ratio used to evaluate the strength of external injection.

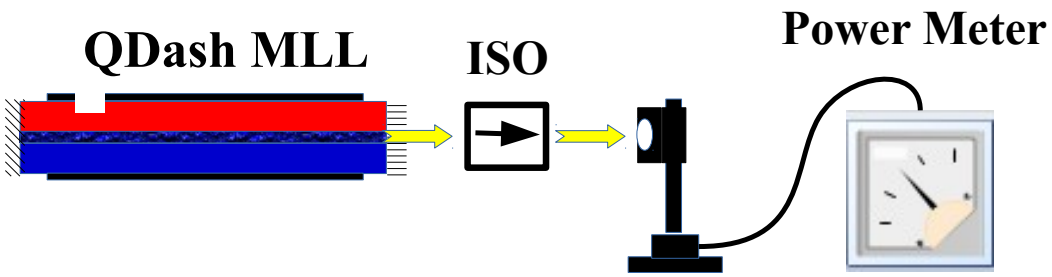

Figure 2.6: Schematic of measurement setup for (L-I) and optical measurement, Acronyms– QDash MLL: Quantum-Dash mode-locked laser, ISO: Optical Isolator.

For the L-I measurement, LabView® was run on a computer connected to the power meter and current source to automatically change the current of the laser and read measurements from the power meter in a loop. Fig. 2.7 shows the resulting light-current (L-I) characteristics.

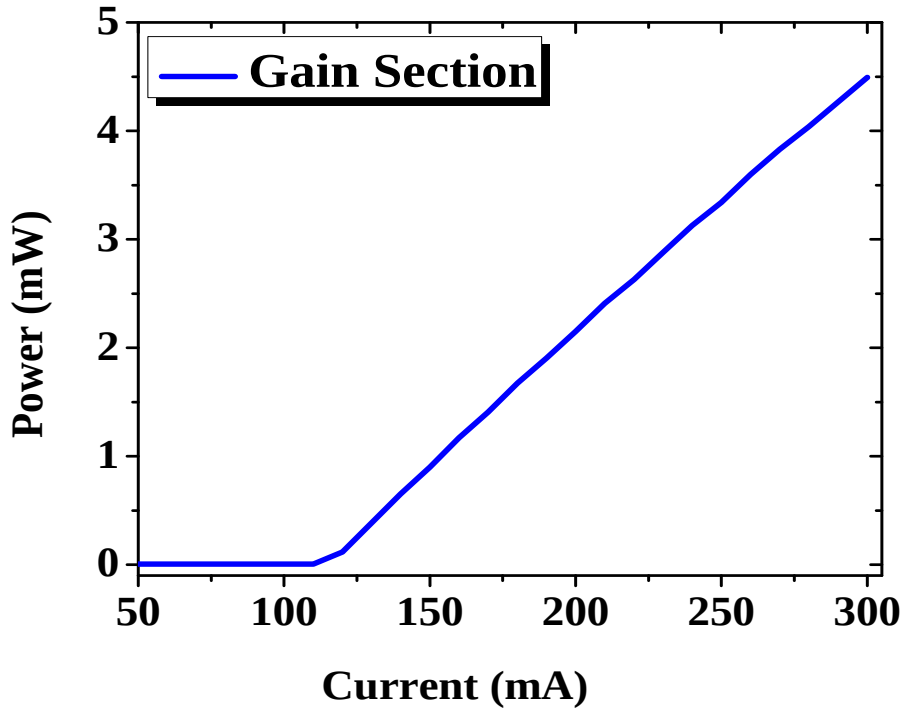

Figure 2.7: Light-Current (L-I) characteristics of SML QDash laser.

2.4.2 Optical Spectrum Analysis

The schematic of an experimental arrangement for the analysis of optical spectra is shown in Fig. 2.8. Light from the laser was collected from port 2 of an optical circulator and then the output of the circulator was sent to a semiconductor optical amplifier (SOA, gain 9.8 dB). Optical coupling loss between adjacent ports was -0.64 dB. For automatic measurements (for example the evolution of optical/RF spectra versus bias current), a computer was used to control instruments via LabView®. The optical spectrum of the laser was measured using a diffraction-grating based commercial optical spectrum analysers (Ando AQ6317B and Advantest Q8384) covering the infrared wavelength range up to 1700 nm with a minimum resolution bandwidth of 0.01 nm. The measured

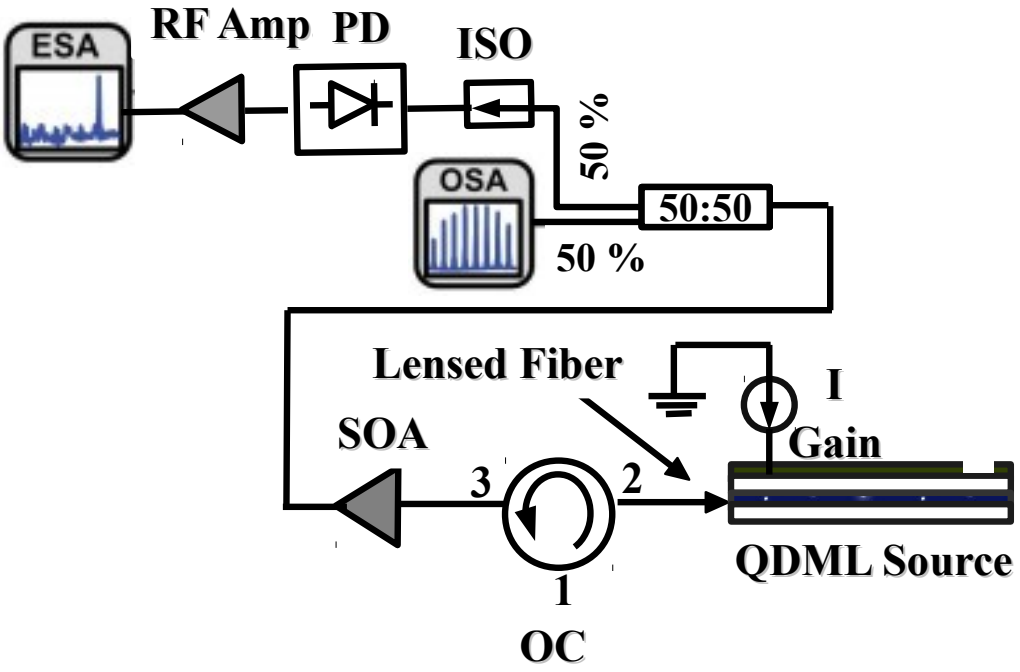

Figure 2.8: Schematic of measurement setup for optical and RF spectra, Acronyms- OC: Optical Circulator, SOA: Semiconductor Optical Amplifier, OSA: Optical Spectrum Analyser, ESA: Electrical Spectrum Analyser, ISO: Optical Isolator, PD: High-speed Photodetector, RF Amp.: RF Amplifier, QDML: Quantum-Dash mode-locked laser.

optical spectrum of our QDash, mode-locked under free-running condition, is shown in Fig. 2.9. The spectrum was centered at 1570 nm with a 3 dB bandwidth spanning 12 nm and containing $\sim$ 68 longitudinal modes, with 0.18 nm free spectral range (FSR).

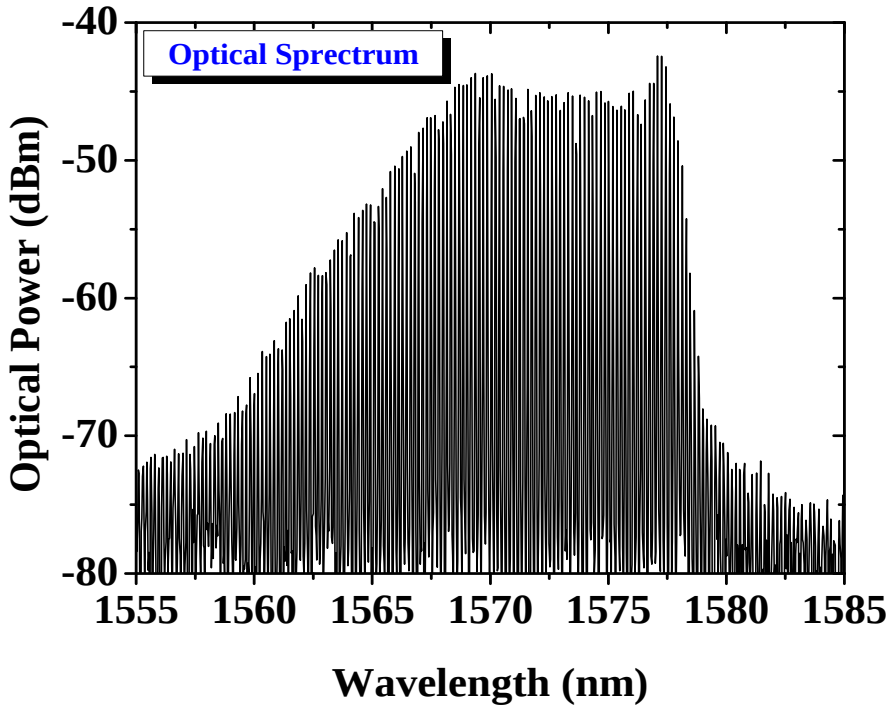

Figure 2.9: Optical spectra of free-running SML QDash laser measured for a bias condition of 300 mA and temperature controlled at 19^{o}C.

2.4.3 RF Spectrum Analysis

The power spectrum in the radio-frequency (RF) domain provides useful information about the stability of MLL. For example, the RF spectrum gives information on the laser's repetition frequency, its frequency purity (phase-noise information), effective RF power, amplitude noise, and other nonlinear effects such as Q-switching. In the frequency domain, a Dirac-comb spaced by the repetition rate is expected. However, in a real mode-locked, the Dirac-delta functions are broadened due to unavoidable timing jitter. A schematic of an experimental arrangement for the analysis of RF spectra is shown in Fig. 2.8. To measure RF spectra, an optical signal from the laser was collected from port 2 of an optical circulator and then the output of the circulator was sent to a semiconductor optical amplifier (SOA, gain 9.8 dB). Finally, the amplified signal went to an RF spectrum analyser (Agilent, E-series, E4407B model) with a minimum resolution bandwidth of 1 kHz and a frequency range of 9 kHz - 26.5 GHz. The RF spectrum of the free-running QDash mode-locked over the full frequency span [0-26 GHz] is shown in Fig. 2.10. For the free-running laser, the minimum RF linewidth was measured to be 100 kHz. The RF spectrum and its Lorentzian fit are shown in Fig. 2.11.

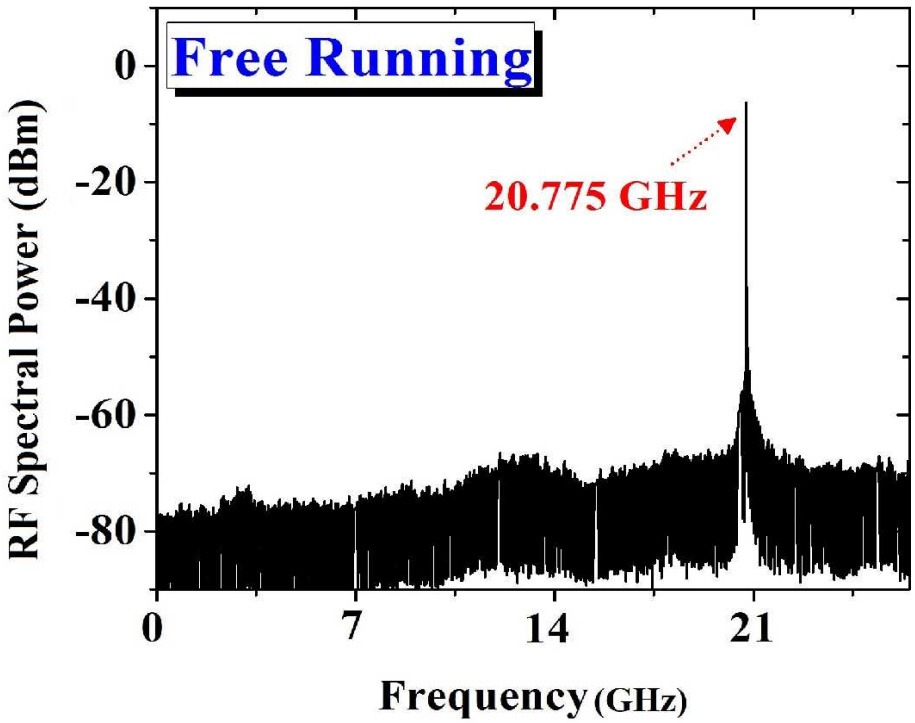

Figure 2.10: RF spectra of free-running QDash MLLs across the full frequency span [0 - 26 GHz] for a bias condition of 300 mA and temperature controlled at 19°C.

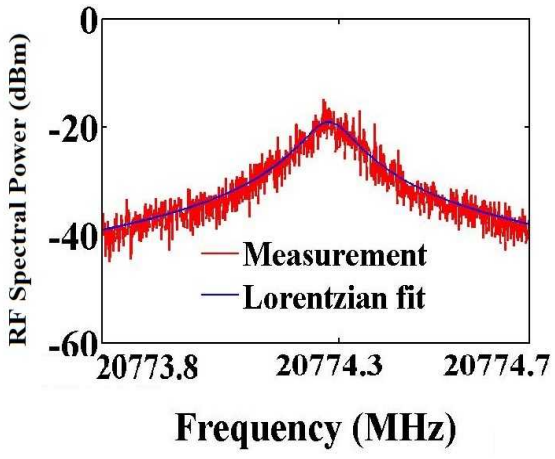

Figure 2.11: RF spectra of free-running SML QDash laser and its Lorentzian fit using frequency span 1 MHz (resolution bandwidth 1 kHz and video bandwidth 100 Hz). [Note: The Lorentzian fit was made over a 5 MHz frequency span but only the zoom is shown here so as to better demonstrate the excellence of the fit at the peak.]

2.4.4 Integrated Timing Jitter

Pulse trains generated by MLLs exhibit some deviations of the temporal pulse positions from those in a perfectly periodic pulse train, and this is refereed

to as timing jitter. The fundamental origin of timing jitter in MLLs arises due to spontaneous emission of the gain medium coupled into resonator modes, and to intra-cavity losses [116]. The spontaneous emission essentially generates photons with random phase and polarisation, unlike the desired stimulated emission which generates photons with the same polarisation in phase as those already in the laser cavity. In addition, there can be technical noise influences, vibrations of the cavity mirrors and temperature fluctuations.

We calculated the root mean square (RMS) timing jitter from single sideband (SSB) phase-noise spectra measured at the fundamental RF pulse repetition frequency (20.7 GHz) using [116]:

$$\sigma_{RMS} = \frac{1}{2\pi f_{ML}} \sqrt{2 \int_{f_d}^{f_u} L(f)\, df} \tag{2.1}$$

where f_{ML} is the pulse repetition rate and f_u and f_d are the upper and lower integration limits. *L(f)* is the single sideband (SSB) power due to phase fluctuations relative to the total power and is given by:

$$Ł(f) = \frac{Noise\ power\ in\ 1\ Hz\ bandwidth}{Total\ signal\ power} \tag{2.2}$$

To measure the RMS timing jitter of the laser, single-sideband (SSB) noise spectra for the fundamental harmonic repetition frequency were measured. RF spectra at several spans around the repetition frequency were measured from small (finest) to large (coarse) resolution bandwidths. The corresponding ranges for frequency offsets were then extracted from each spectrum and superimposed to obtain SSB spectra normalized for power and per unit frequency bandwidth. The higher frequency bound was 100 MHz (instrument limited).

Using this method, the timing jitter of our QDash mode-locked was observed to be 3.9 ps for the free-running condition [integration: 10 kHz to 100 MHz]. Measured phase-noise trace for free-running laser (black line) as functions of frequency offset from fundamental mode-locked frequency are depicted in Fig. 2.12.

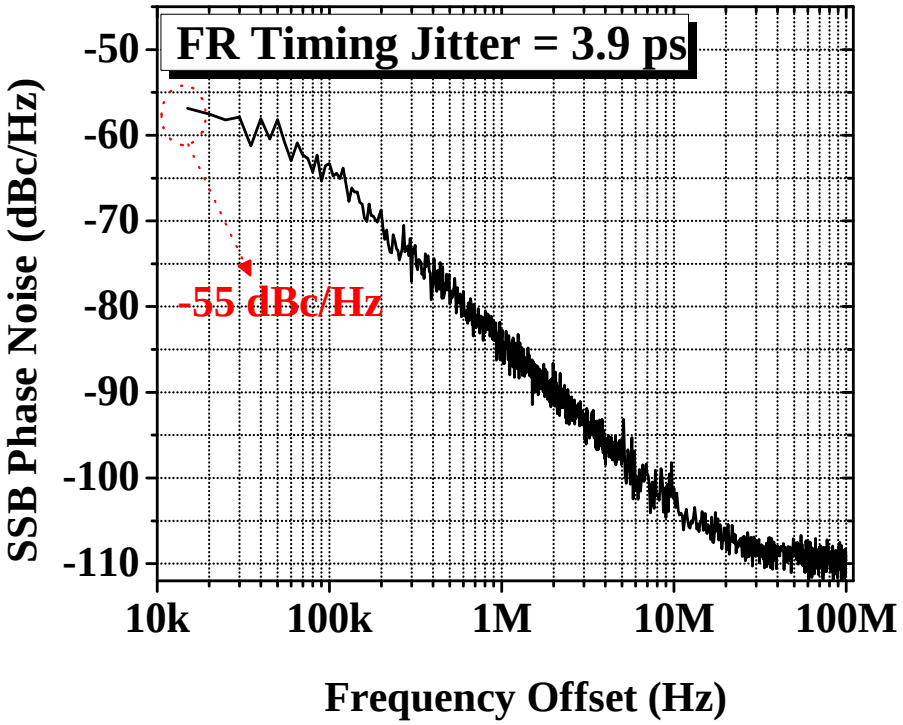

Figure 2.12: SSB phase-noise trace of free-running laser using integration limits 10 kHz to 100 MHz.

2.5 Summary

In this chapter, a detailed discussion on the basic structure and fabrication of the SML QDash laser was presented. The measurement techniques are described for the optical power, optical/electrical spectra and integrated timing jitter of the device under test. Our QDash mode-locked laser generated optical spectra centered at 1570 nm with a 3 dB bandwidth spanning 12 nm and containing approximately 68 optical modes. The RF linewidth was 100 kHz at 300 mA gain current. In addition, it was observed that under free-running conditions the timing jitter of our SML QDash laser was 3.9 ps. Low jitter achieved by the QDash SML indicates the potential for applications such as microwave and terahertz generation.

Chapter 3

Stabilisation of SML QDash Lasers by Symmetric Dual-Loop Optical Feedback

3.1 Introduction

In this chapter, we report on experimental studies of the influence of symmetric dual-loop optical feedback on the RF linewidth and timing jitter of SML two-section QDash lasers emitting at 1550 nm. Various feedback schemes were investigated and optimum levels were determined for the narrowest RF linewidth and low timing jitter, for single and symmetric dual-loop feedback. Two symmetric dual-loop configurations, with balanced and unbalanced feedback ratios, were studied. We demonstrated that unbalanced symmetric dual-loop feedback, with the inner cavity resonant and fine delay tuning of the outer loop, produced the narrowest RF linewidth and reduced timing jitter over a wide range of delay, unlike single and balanced symmetric dual-loop configurations. For symmetric dual-loop feedback, the influence of different power split ratios through the feedback loops was further determined. Our results show that symmetric dual-loop feedback is markedly more effective than single-loop feedback in reducing RF linewidth and timing jitter, and is much less sensitive to delay phase, making it ideal for applications where robustness and alignment tolerance are essential.

This chapter is structured as follows. In the next section, Mach-Zehnder interferometer based symmetric dual-loop feedback will be presented. The experimental setup will be introduced in Section 3.3 and analysis of experimental

results will be given in Section 3.4. In Subsections (3.4.1, 3.4.2 and 3.4.3), the effects of optical delay length, external feedback levels, and optical delay phase tuning are described on the RF linewidth and timing jitter of QDash mode-locked laser using single-loop optical feedback. In Subsection 3.4.4, we shall then discuss the influence of balanced symmetric dual-loop feedback on the timing stability of SML QDash lasers versus the widest delay phase tuning. Under the double resonance condition, RF linewidth versus power split ratio through symmetric dual-loop feedback will be presented in Subsection 3.4.5. In Subsection 3.4.6, we will then discuss the influence of unbalanced symmetric dual-loop feedback versus full delay phase tuning on the timing stability of the SML QDash laser. Finally, comparison of balanced and unbalanced symmetric dual-loop configuration with longer delay lengths will be presented in Subsection 3.4.7.

3.2 Mach-Zehnder Interferometer Based Symmetric Dual-Loop Feedback

The Mach-Zehnder interferometer is used to determine the relative phase shift between collimated beams by splitting from a single light source and then recombining them. An optical signal is equally (50:50) split into two phase shifting arms of the interferometer by a 3-dB coupler and then recombined to produce the output. The lengths of the phase shifting arms are equal as shown in Fig. 3.1. If the optical path in the two arms of the interferometer is an integral number of optical wavelengths, the two waves will arrive at the output coupler in phase and interfere constructively to produce high intensity. If an electric field is used to create a relative phase difference between the two optical signals, as in Mach-Zehnder modulators (MZMs), the intensity can be reduced. In MZMs, each of the phase shifters can also be manipulated individually and the phase difference between the two arms can be varied from 0^o to 180^o. For this particular configuration, 0^o phase difference between two arms results in constructive interference and 180^o phase difference results in destructive interference.

Symmetric dual-loop feedback can be regarded as a superposition of two single feedback loops at the 3-dB coupler. Fig. 3.2 shows the two fibre paths between 3-dB couplers forming a Mach-Zehnder (M-Z) interferometer. The path differ-

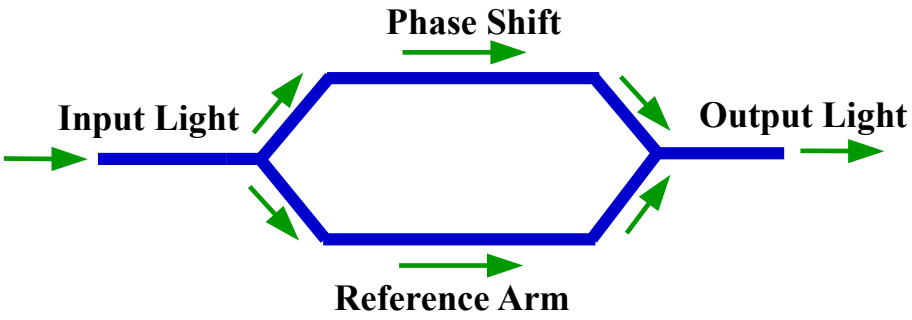

Figure 3.1: Schematic of a general Mach-Zehnder interferometer.

ence in this interferometer can be finely tuned using optical delay lines (ODL-I and ODL-II) attached to the two external feedback loops. When modes in the outer and inner feedback loops were aligned, then optical pulses in either feedback loop overlapped and constructive interference was formed in the M-Z fibre interferometer to stabilise the optical pulses. The superposition of RF spectra in either feedback loop makes the RF spectrum with symmetric dual-loop feedback much narrower and sharper relative to single-loop feedback.

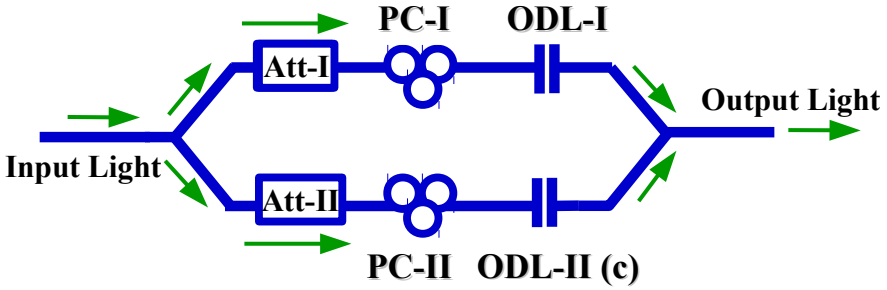

Figure 3.2: Superposition effect of RF spectra in M-Z interferometer formed by symmetric dual-loop optical feedback, Acronyms– ODL: Optical delay line; Att: Optical attenuator; PC: polarisation controller.

3.3 Experimental Arrangement

A schematic of the single-loop and symmetric dual-loop feedback experiments is depicted in Fig. 3.3. For single and dual-loop feedback, a calibrated fraction of light was fed back through port 1 of an optical circulator, then injected into the laser cavity via port 2. Optical coupling loss from port 2 to port 3 was -0.64 dB. The output of the circulator was sent to a semiconductor optical amplifier (SOA) with gain 9.8 dB then split into two arms by a 50/50 coupler. Half the amplified signal went to an RF spectrum analyser (Keysight, E4407B)

via a 21 GHz photodiode, and also to two optical spectrum analysers (Ando AQ6317B and Advantest Q8384). The other half of the power was directed to the feedback arrangement. For a single feedback loop, all power passed through loop-I in Fig. 3.3. For symmetric dual-loop configurations, power was split into equal two parts via a 3-dB splitter, each loop containing an optical delay line plus a variable optical attenuator and a polarisation controller. For symmetric dual-loop configurations, two combinations of feedback ratios were studied. For symmetric dual-loop with balanced feedback ratios, equal power was coupled to both external cavities. However, for unbalanced symmetric dual-loops feedback more power (-20 dB), was coupled to loop-I than to loop-II (-26 dB). The lengths of the fibre loops were fine-tuned by optical delay lines based on stepper-controlled stages with delay resolution 1.67 ps. polarisation controllers in each loop and one polarisation controller before port 1 of the circulator ensured the light from both loops matched the emitted light polarisations to maximise feedback effectiveness.

3.4 Analysis of Results

In this section, we described the effects of three key parameters: optical loop length, optical feedback level, and optical delay phase tuning, on the timing stability of our QDash mode-locked laser. The laser was subjected to single and symmetric dual-loop (balanced and unbalanced power ratios) feedback into the gain section.

3.4.1 Effects of Fibre Delay Length on RF Linewidth and Integrated Timing Jitter using Single-Loop Feedback

To achieve improved stability and spectral purity, optical feedback with a high-quality-factor (Q-factor) resonator is the most practical approach to reduce the phase-noise and RF linewidth of MLLs. It has been previously demonstrated, both analytically and experimentally [104], that the length of the fibre determines the phase-noise and is inversely proportional to the loop length [110]. In the following section, we explored the relationship between the RF linewidth and timing jitter versus fibre delay length using single-loop feedback.

To study the effects of various fibre delay lengths on the RF linewidth and timing

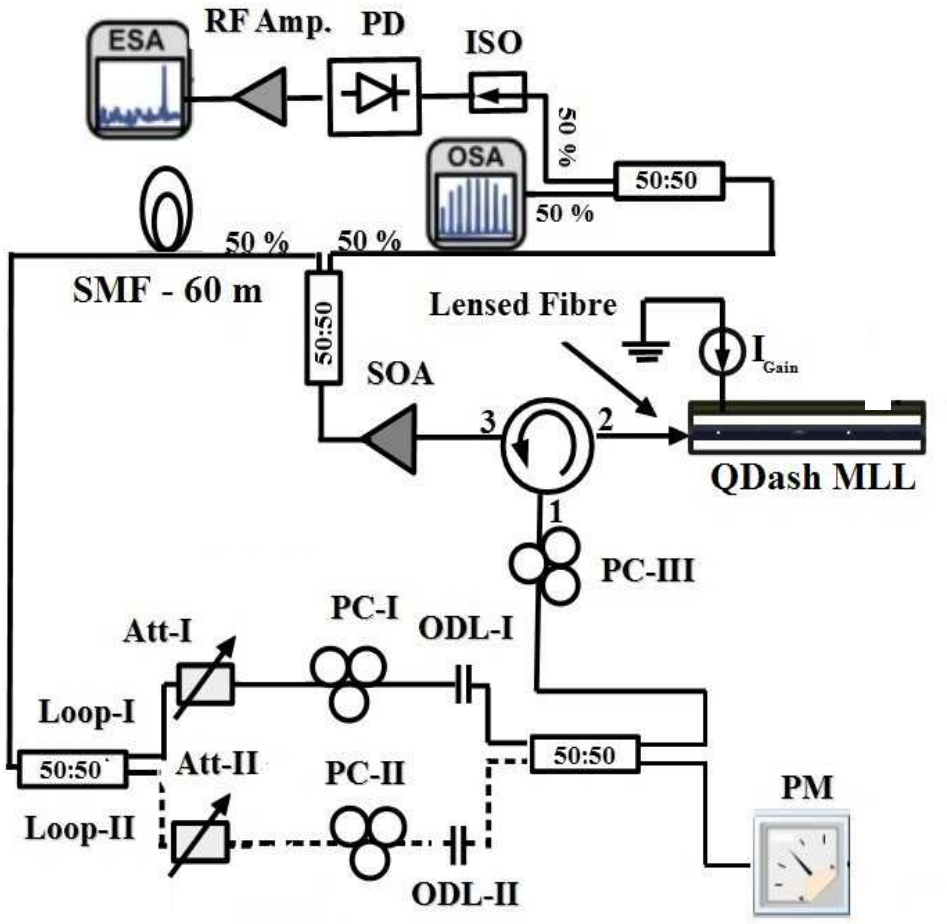

Figure 3.3: Schematic of the experimental arrangement for a single (excluding dashed portion) and dual-loop configurations (with dashed portion). Acronyms– SOA: Semiconductor Optical Amplifier; ISO: Optical isolator; PD: Photodiode; RF Amp.: RF Amplifier; ODL: Optical delay line; Att: Optical attenuator; PC: polarisation controller; ESA: Electrical spectral analyser; OSA: Optical spectrum analyser; SMF: Single mode fibre; PM: Power Meter; QDash MLL: Quantum-dash mode-locked laser.

jitter of the laser, loop-II was disconnected and the maximum feedback to the gain section was -22 dB, as shown in Fig. 3.3. Single 20, 48, 80 and 140 m fibre spans were used, the stable resonant condition being achieved by optimising optical delay line ODL-I which was adjustable from 0-84 ps in steps of 1.67 ps. The exact condition of integer resonance is obtained when the optical length of the external cavity is an integral multiple of that of the internal cavity.

$$\tau_{FB} = n\tau_{ML} \qquad n = 1, 2, 3, ... \tag{3.1}$$

where τ_{FB} is the round trip time inside the feedback loop and τ_{ML} is the round

trip time inside the laser cavity.

Upon detuning of the optical delay line (ODL-I), RF linewidth narrowing and broadening occur at various delay settings. Under full resonance, the RF linewidth decreased from 100 kHz free-running to 15 kHz for loop length 20 m, 13 kHz for loop length 48 m, 3 kHz for loop length 80 m and 4 kHz for loop length 140 m. Under similar conditions, the RF spectrum is shown in Fig. 3.4 for loop length 20 m (black line), 48 m (red line), 80 m (blue line) and 140 m (green line).

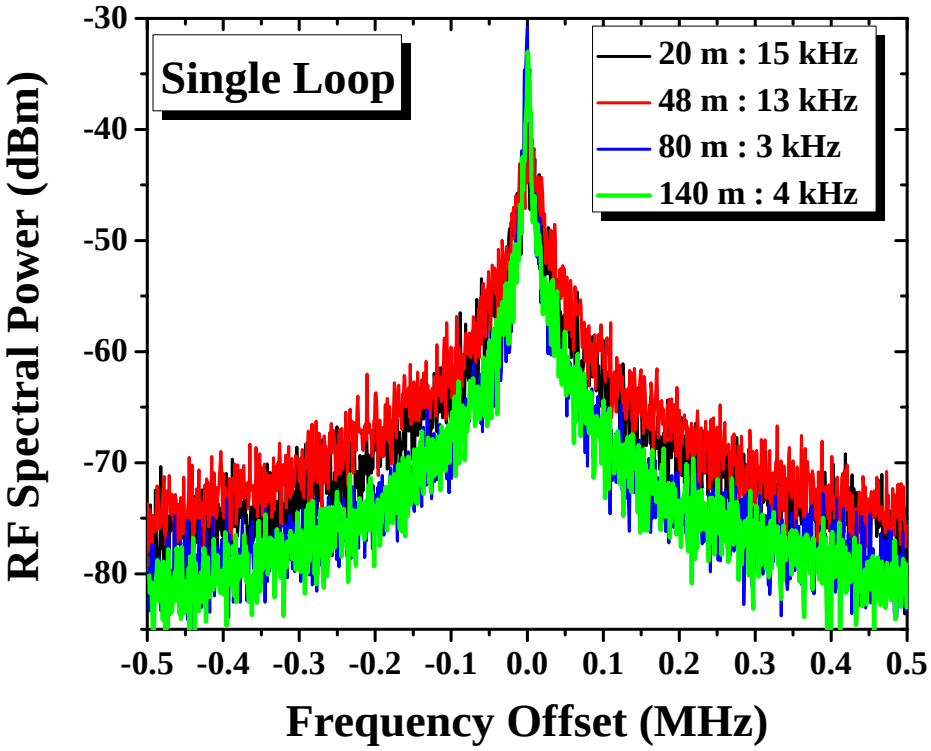

Figure 3.4: Measured RF spectra under fully resonant condition for loop lengths 20 m (black line), 48 m (red line), 80 m (blue line) and 140 m (green line).

As detuning of the optical delay line varies the RF linewidth considerably, therefore integrated timing jitter also varies as a function of optical delay tuning. The RF linewidth, which directly influences the phase-noise spectral density, is directly related to the integrated RMS timing jitter in semiconductor passive MLLs [116]. When the optical delay line was fully resonant, the integrated timing jitter was reduced from 3.9 ps for free-running to 1.2 ps for loop length 20 m, 0.8 ps for loop length 48 m, 0.6 ps for loop length 80 m and 0.65 ps for loop length 140 m. It should be noted that integrated timing jitter was measured using integration limits 10 kHz - 100 MHz. Measured phase-noise traces as a function of frequency offset under fully resonant condition are shown in Fig.

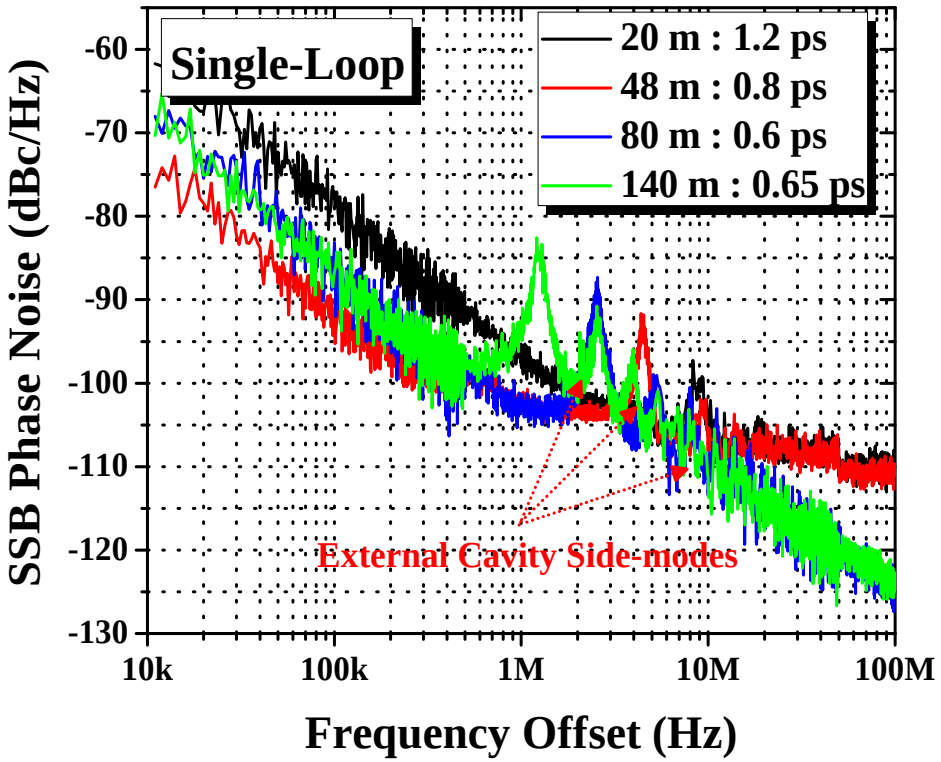

Figure 3.5: Measured phase-noise traces under fully resonant condition for loop length 20 m (black line), 48 m (red line), 80 m (blue line) and 140 m (green line) using single-loop optical feedback with integration limits 10 kHz - 100 MHz.

3.5 for loop length 20 m (black line), 48 m (red line), 80 m (blue line) and 140 m (green line).

Measured RF linewidth and integrated timing jitter data as functions of external cavity loop length are shown in Fig. 3.6 using single-loop feedback. It can be seen from measured experimental results that RF linewidth and integrated timing jitter decrease with increasing external cavity loop length. These results agree well with the model presented in [116].

In addition, measured RF spectra are shown in Fig. 3.7 for the four chosen feedback lengths. Strong external cavity side-modes were noticed a few MHz away from the fundamental mode-locked frequency. The frequency spacing of these external cavity side-modes was 4.3 MHz, 2.53 MHz, and 1.45 MHz in accordance with the 48, 80 and 140 m nominal length of each loop, respectively.

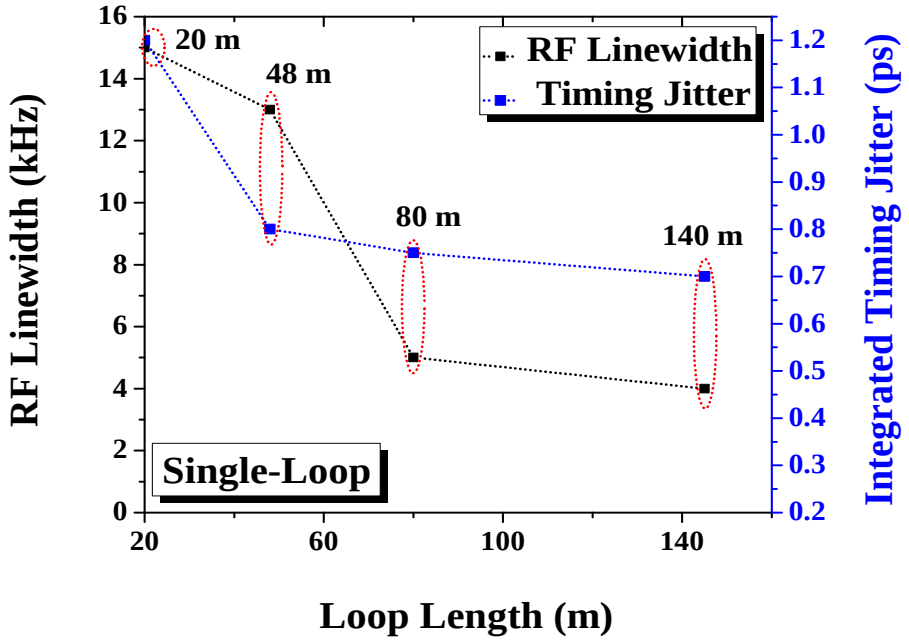

Figure 3.6: Measured RF linewidth and integrated timing jitter under fully resonant condition for loop length 20 m (black square), 48 m (red square), 80 m (green square) and 140 m (blue square) using single-loop feedback.

3.4.2 Effects of Feedback Strength on RF Linewidth and Integrated Timing Jitter Subject to Single-Loop Feedback

A number of experimental [77-81] and numerical investigations [81-85] have been performed to evaluate the influence of MLLs under external optical feedback. The effects of small amounts of external optical feedback with proper phase matching can be highly beneficial for the characteristics of semiconductor lasers, and considerable reduction in RF linewidth and timing jitter can be obtained. On the other hand, slightly higher levels of optical feedback result in coherence collapse and low-frequency fluctuation regimes [78, 79] leading to a sharp increase in RF linewidth and timing jitter. It is therefore essential to identify the most favorable amount of optical feedback for stable mode-locked operation.

In this section, the impact of external optical feedback from single-loop and symmetric dual-loop on the RF linewidth and integrated timing jitter was investigated. The attenuation in the feedback loop was varied from the minimum achievable feedback ratio -46 dB up to a maximum -22 dB after which laser exhibits unstable behavior. The feedback ratio into the gain section was subjected to nine chosen attenuations (-46 dB, -39 dB, -36 dB, -31 dB, -29 dB, -26 dB, -24 dB, -21 dB and -22 dB). For single-loop feedback, all the power was passed

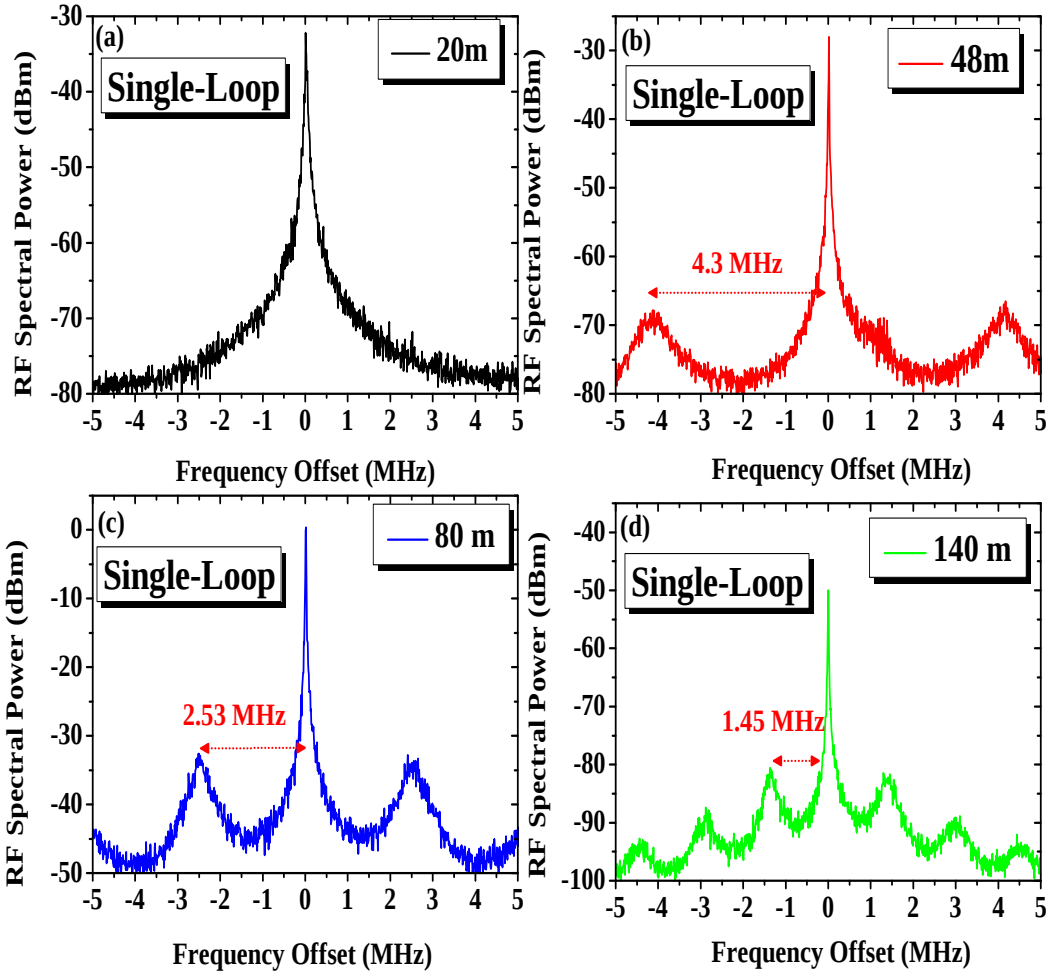

Figure 3.7: RF spectrum of loop length (a) 20 m, (b) 48 m (c) 80 m and (d) 140 m subject to single-loop feedback using frequency span 10 MHz (resolution bandwidth 10 kHz and video bandwidth 1 kHz).

through loop-I. However, for symmetric dual-loop configuration, the feedback ratio was equally split into two parts as shown in Fig. 3.3. It can be seen that at feedback level -46 dB, the RF linewidth was 73 kHz for single-loop, 69 kHz for unbalanced symmetric dual-loop and 75 kHz for balanced symmetric dual-loop feedback configuration, with corresponding timing jitter 3, 2.9 and 3.1 ps, respectively (integration from 10 kHz-100 MHz). Under weak feedback (-46 dB, -39 dB and -36 dB), upon tuning of the optical delay line, no deviation in the position of the fundamental frequency occurred, so that no major reduction in RF linewidth and timing jitter was seen relative to free-running. With a slight increase in feedback level to -29 dB, a gradual decrease in RF linewidth and timing jitter was observed. At this feedback condition, the RF linewidth was reduced to 28.7 kHz for single-loop, 21.5 kHz for unbalanced symmetric dual-loop and 29 kHz for balanced symmetric dual-loop configuration. As a result,

RMS timing jitter was decreased to 1.75 ps for single-loop, 1.6 ps for unbalanced symmetric dual-loop and 1.8 ps for balanced symmetric dual-loop feedback scheme. Further increase in feedback level to -22 dB results in optimum reduction in RF linewidth and timing jitter for single and symmetric dual-loop feedback configurations (subject to balanced and unbalanced feedback ratios).

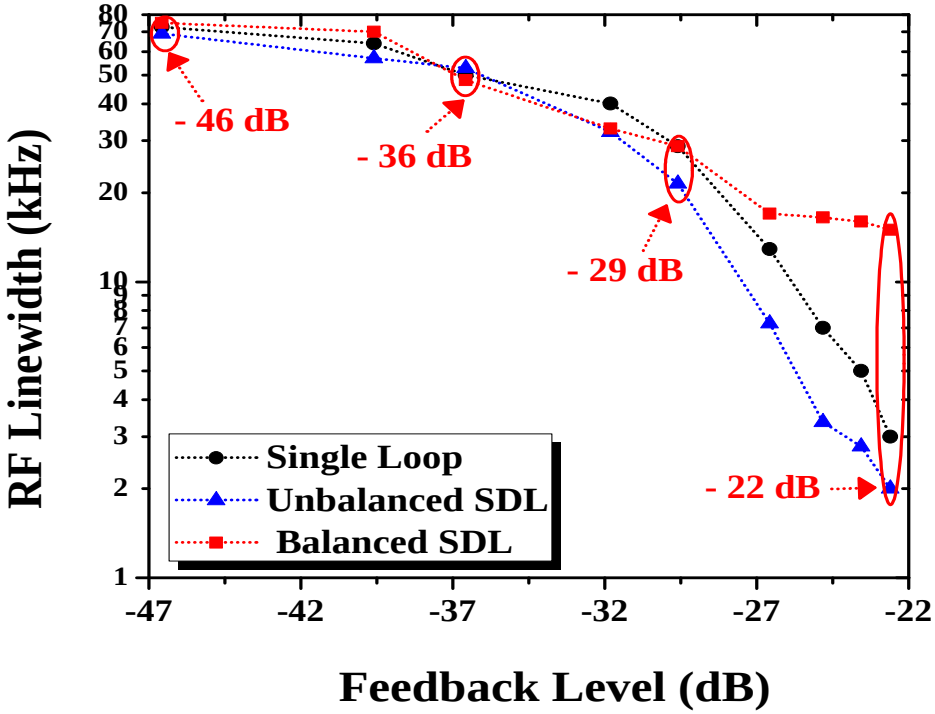

Figure 3.8: 3-dB RF linewidth under resonant condition for single-loop (black circles), unbalanced symmetric dual-loop (blue triangles) and balanced symmetric dual-loop (red squares) feedback configurations as a function of external feedback ratio at 300 mA gain current.

The minimum achieved RF linewidth and timing jitter for single and symmetric dual-loop configurations as functions of feedback level are depicted in Figs. 3.8 and 3.9, respectively, under integer resonance. From this data, we have identified the optimal feedback ratio to be -22 dB for single and symmetric dual-loop feedback, limited by self-pulsation above this level. Our results demonstrate that for practical applications, the relatively flat characteristics of the plot of RF linewidth versus feedback ratio (-26 dB, -24 dB, -23-dB and -22 dB) are more favourable. Other studies [77, 80] also depict the variation in RF linewidth as a function of feedback level, with behaviour corresponding well with our studies. Furthermore, variation in RF linewidth and timing jitter in all feedback schemes (single, balanced/unbalanced symmetric dual-loop feedback configurations) follows a similar trend when the feedback level approaches the optimal value (- 22 dB). A theoretical expression was suggested to measure RF

linewidth and corresponding integrated timing jitter, instead of calculating the RF phase-noise power spectral density (PSD) from the photocurrent [116]. Our experimental measurements agree well with the reported analytical expression (square root dependence of the RF linewidth on integrated timing jitter) [116]. Recently, for a QDot mode-locked laser operating at a 5.1 GHz repetition rate, the minimum RF linewidth was obtained at relatively low feedback level -36 dB [79]. On the other hand, for a passively mode-locked QDash laser emitting at 1580 nm and operating at 17 GHz repetition rate, a marked reduction in RF linewidth occurs at a significantly stronger feedback (-22 dB) [80], in agreement with our studies. These differences are explicable by the likelihood that the anti-guiding (phase-amplitude coupling) factor is lower in QDashes.

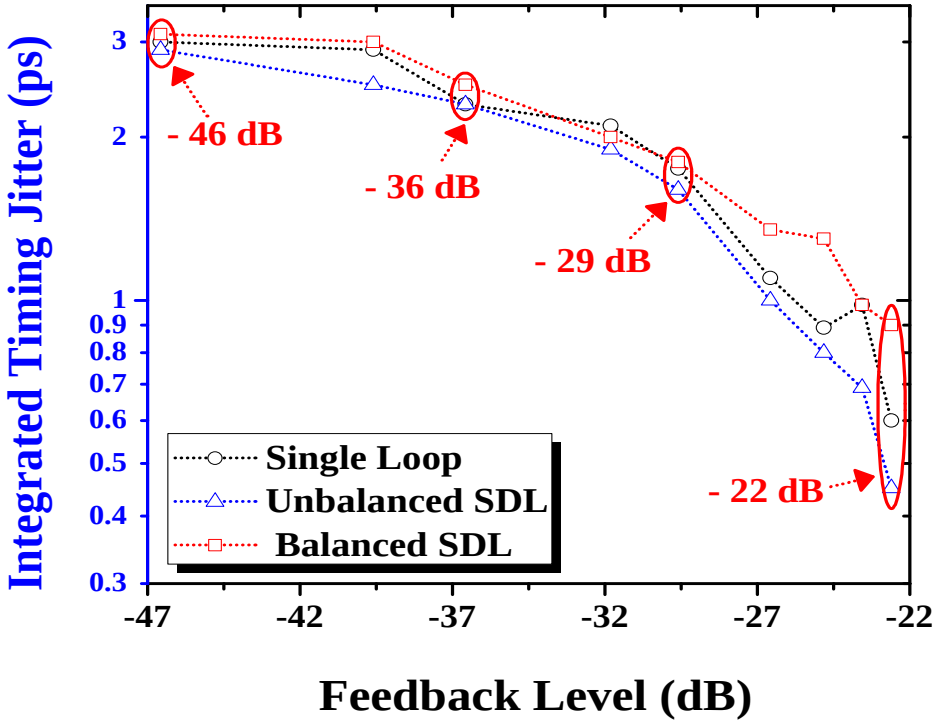

Figure 3.9: Integrated timing jitter under resonant condition subjected to single-loop (black circles), unbalanced symmetric dual-loop (blue triangles) and balanced symmetric dual-loop (red squares) feedback configurations as functions of external feedback ratio at 300 mA gain current.

As discussed above, by optimisation of the optical delay to the fully resonant condition and varying the feedback ratio, significant reduction in RF linewidth and corresponding timing jitter was noted, for both single- and symmetric dual-loop configurations. Measured RF spectra for single- and symmetric dual-loop configurations under three chosen feedback attenuations (-46 dB, -29 dB, and -22 dB) is shown in Figs. 3.10 (a) and (b), respectively.

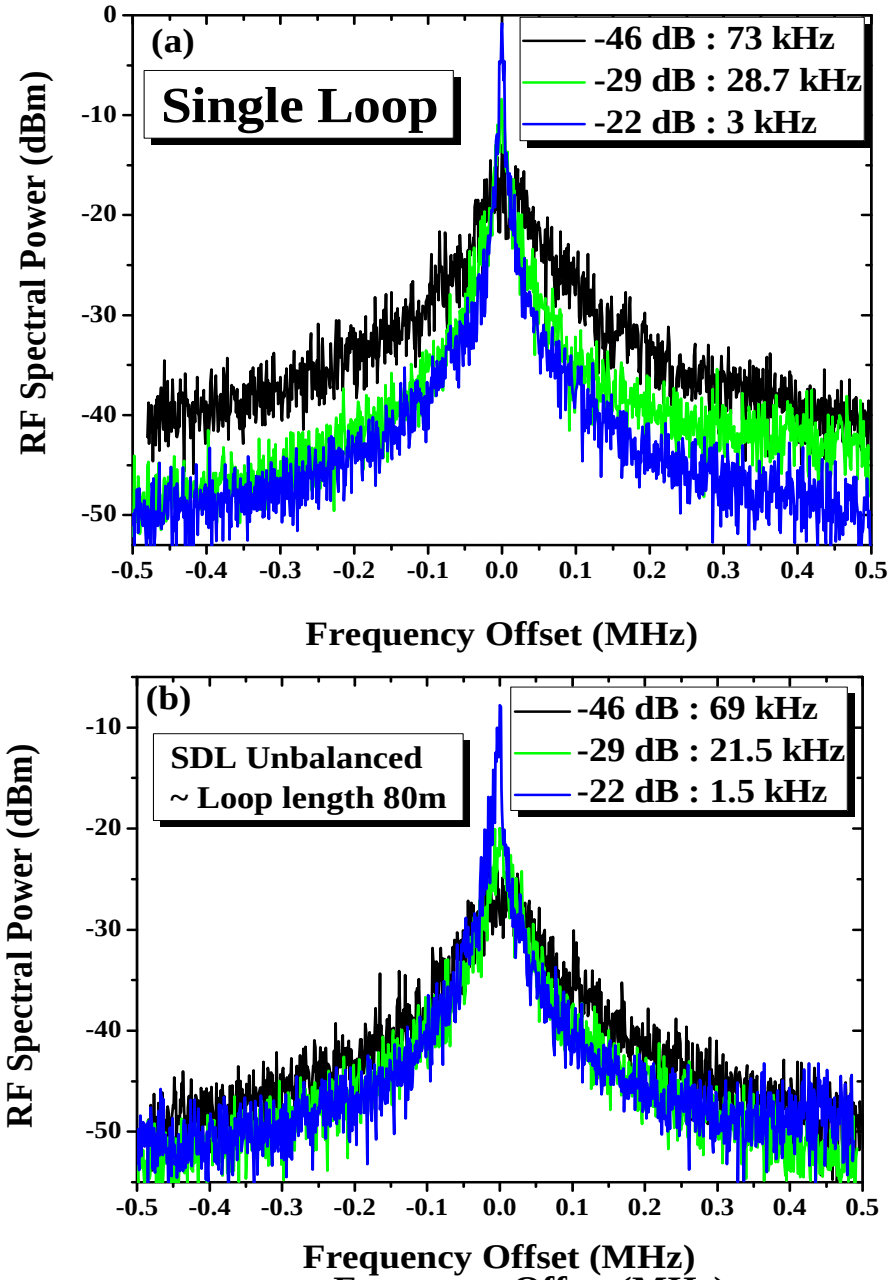

Figure 3.10: RF spectra under stable resonant condition with frequency span 1 MHz (resolution bandwidth 1 kHz and video bandwidth 100 Hz) using (a) single- and (b) symmetric dual-loop feedback configurations under three chosen feedback attenuations (-46 dB, -29 dB and -22 dB).

3.4.3 RF Linewidth and Integrated Timing Jitter Versus Delay Tuning for Single-Loop Feedback

From the above measured results, the optimal feedback level and fibre delay length yielding the narrowest RF linewidth and reduced timing jitter were determined to be -22 dB and 80 m, respectively. Our next experimental measure-

ments were performed at these fixed feedback levels and fibre delay length.

To study the effects of single-loop feedback on RF linewidth and timing jitter over a wide delay range (0-84 ps), loop-II was disconnected and the maximum feedback to the gain section was set (-22 dB) via a single 60 m fibre span using a variable optical attenuator (Att-I). The schematic of this single-loop optical feedback is shown in Fig. 3.11.

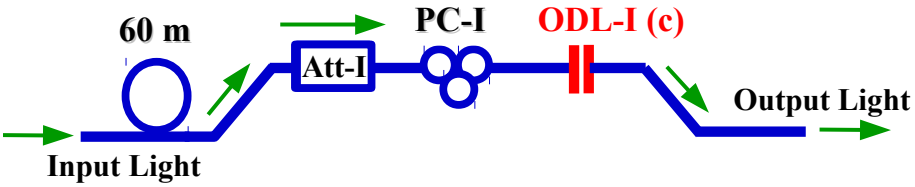

Figure 3.11: Schematic of single-loop optical feedback scheme; Acronyms–ODL: Optical delay line; Att: Optical attenuator; PC: polarisation controller.

Stable resonance was achieved by optimising optical delay line ODL-I, adjustable from 0-84 ps in steps of 1.67 ps. The resulting RF linewidth (black squares) and timing jitter (blue triangles) versus delay are shown in Fig. 3.12. Clearly, stabilisation effectiveness depends strongly on feedback delay, most likely because detuning of the optical delay from exact resonance changes synchronization conditions between pulses in the laser cavity and feedback loops [112]. The periodicity in RF linewidth versus delay tuning is 48 ps, in agreement with the fundamental mode-locked frequency (20.7 GHz) of our laser. Furthermore, this optimisation of the single-loop delay reduced the RF linewidth and corresponding timing jitter considerably, as in other reported experiments [77, 79] and theoretical predictions [85].

Effective stable mode-locking occurs when the external cavity optical length is close to an integer multiple of that of the laser cavity. When fully resonant, the RF linewidth decreased from 100 kHz free-running to 3 kHz, and integrated timing jitter from 3.9 ps to 0.6 ps (10 kHz-100 MHz). Measured RF spectra and phase-noise traces at this feedback delay with single-loop feedback (blue line) and free-running (gray line) are shown in Figs. 3.13 (a) and (b), respectively. Upon tuning of the loop delay by 6-54 ps, synchronization of the optical pulses between the laser cavity and external cavity did not occur, the RF spectra became highly deformed and non-resonant feedback was observed. Experimental results for a single-loop feedback show that for practical use of QDash MLLs the most stable, delay-insensitive ranges are near 5 and 53 ps. Optimum stabilisation using conventional single-loop feedback is very sensitive to phase adjustment and limits the region of optimum performance to a narrow

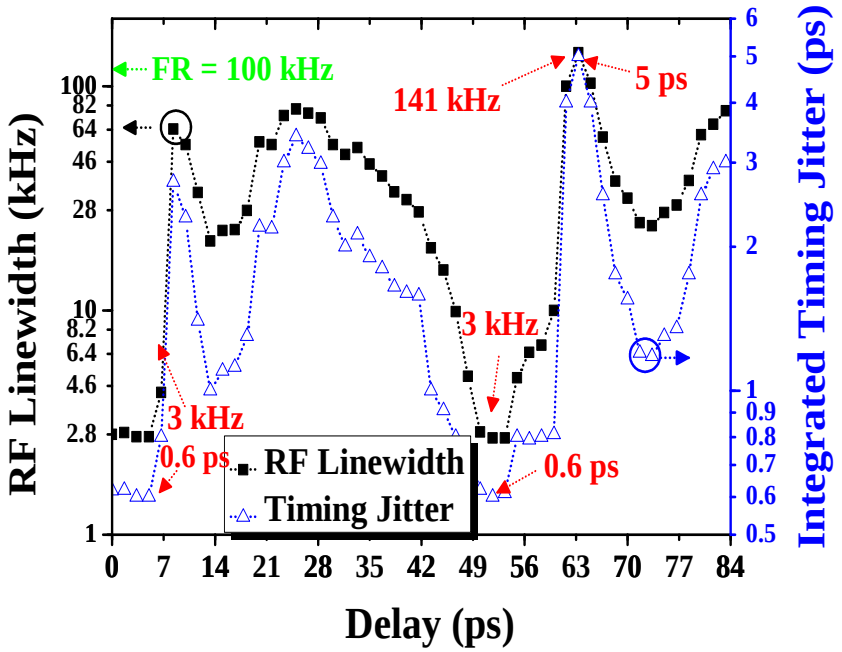

Figure 3.12: RF linewidth (black squares) and integrated timing jitter (blue triangles) as a functions of full delay range [0-84 ps], for single-loop optical feedback.

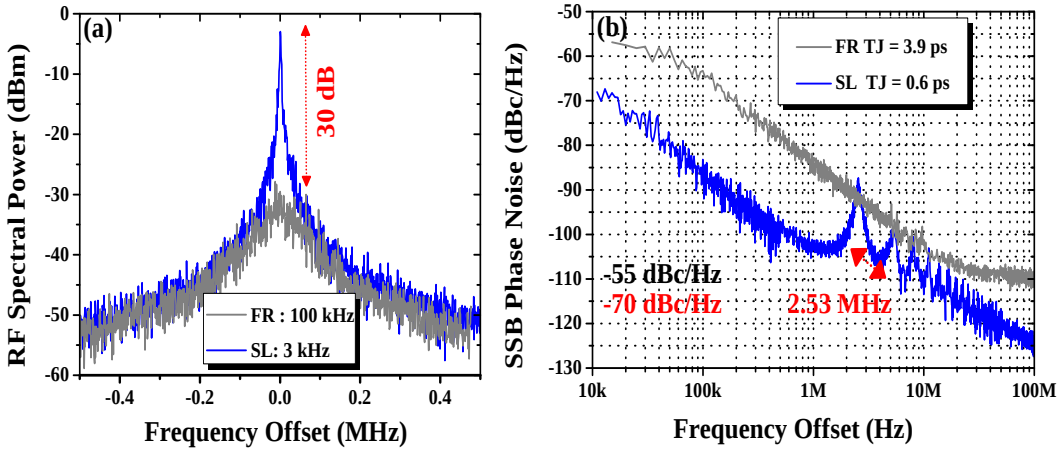

Figure 3.13: (a) Comparison of RF spectra measured using single-loop feedback (blue line) and free-running condition (gray line) with frequency span 1 MHz (resolution bandwidth 1 kHz and video bandwidth 100 Hz) (b) Comparison of phase-noise traces measured using single-loop feedback (blue line) and free-running (gray line) with integration limits 10 kHz -100 MHz.

parameter space. For practical applications of MLLs, it is desirable to extend the range of resonant feedback over a much wider range of delay times, such that environmental changes maintain stable pulse trains with narrow linewidth and low timing jitter.

3.4.4 RF Linewidth and Integrated Timing Jitter Versus Delay Tuning for Balanced Symmetric Dual-Loop Configuration

For dual-loop experiments, the optical feedback was split into two fibre cavities whose lengths were calibrated by measurement of RF spectra with each loop unblocked separately. A schematic of single cavity feedback for each loop is shown in Fig. 3.14.

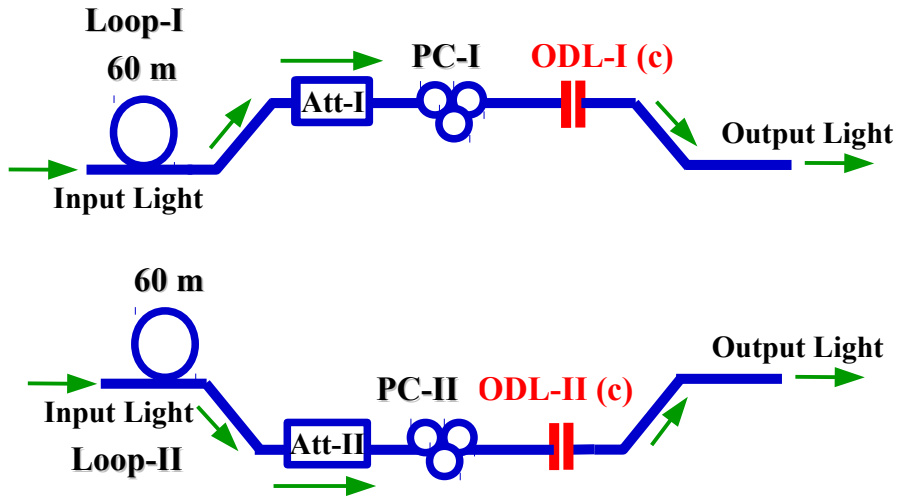

Figure 3.14: Schematic of single-loop feedback with loop-I and loop-II; Acronyms– ODL: Optical delay line; Att: Optical attenuator; PC: polarisation controller.

For the first set, loop-II was disconnected and RF spectra were measured. Similarly, for the second set, loop-I was blocked and RF spectra were measured. For each loop, the cavity spacing was 2.53 MHz, consistent with 80 m nominal length of both equal loops. RF spectral measurements with this arrangement are shown in Fig. 3.15.

To study the effects of symmetric dual-loop feedback on laser stability, fine adjustment of the optical attenuator (Att-I) and polarisation controller (PC-I) was made with equal feedback power (-22 dB) coupled to both loops. Optical delay line ODL-I was set to full resonance (integer number of times the laser cavity delay) and ODL-II tuned over its entire available delay range. The schematic of symmetric dual-loop feedback is shown in Fig. 3.16.

The RF linewidth and integrated timing jitter are presented as functions of delay in Fig. 3.17. We see that symmetric dual-loop feedback yields results comparable to those using a single-loop, and is similarly sensitive to delay. In the liter-

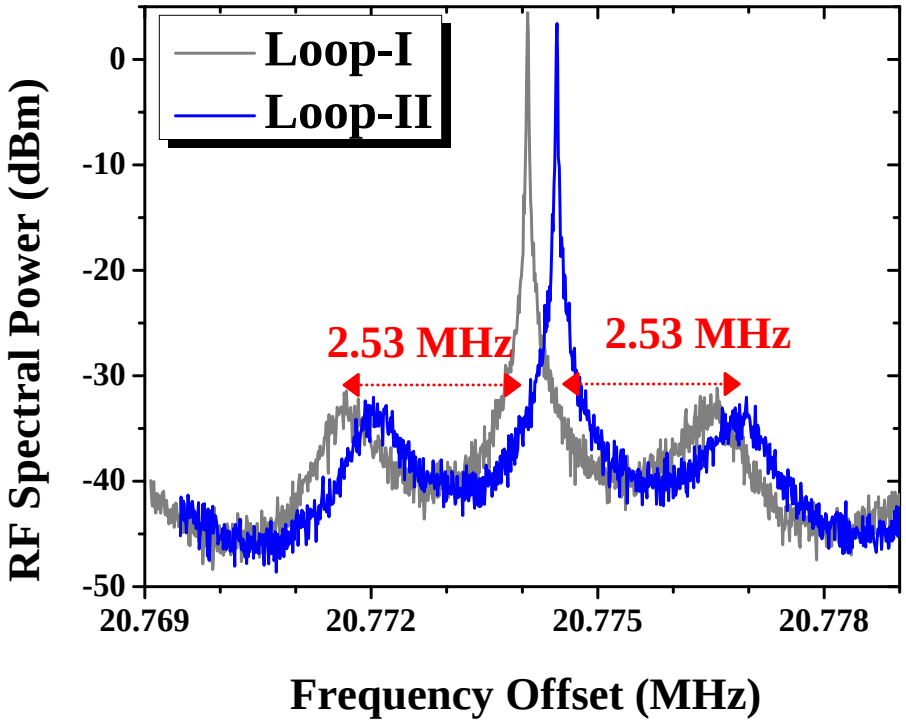

Figure 3.15: Separate measurement of RF spectra of single-loop feedback from loop-I (gray line) and loop-II (blue line) using frequency span 10 MHz (resolution bandwidth 10 kHz and video bandwidth 1 kHz).

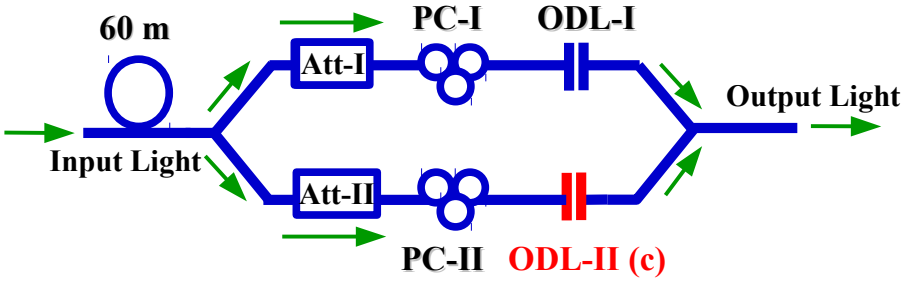

Figure 3.16: Schematic of symmetric dual-loop optical feedback scheme; Acronyms– ODL: Optical delay line; Att: Optical attenuator; PC: polarisation controller.

ature [77, 79], it was observed that the pulse repetition frequency shifts with feedback delay; in our experiments, we used the fully resonant Loop-I to set the fundamental repetition frequency, then tuned pulse trains from Loop-II through these by varying the delay. For most settings of Loop-II delay, pulses from both loops overlapped at the edges rather than the center (see Fig. 3.18(a)), broadening RF linewidth and increasing timing jitter, so that measured RF spectra were worse than for single-loop feedback. Only with both loops resonant does stability improve, giving RF linewidth 12 kHz and timing jitter 0.85 ps, versus 3 kHz and 0.6 ps for optimized single-loop feedback. The measured RF spectrum

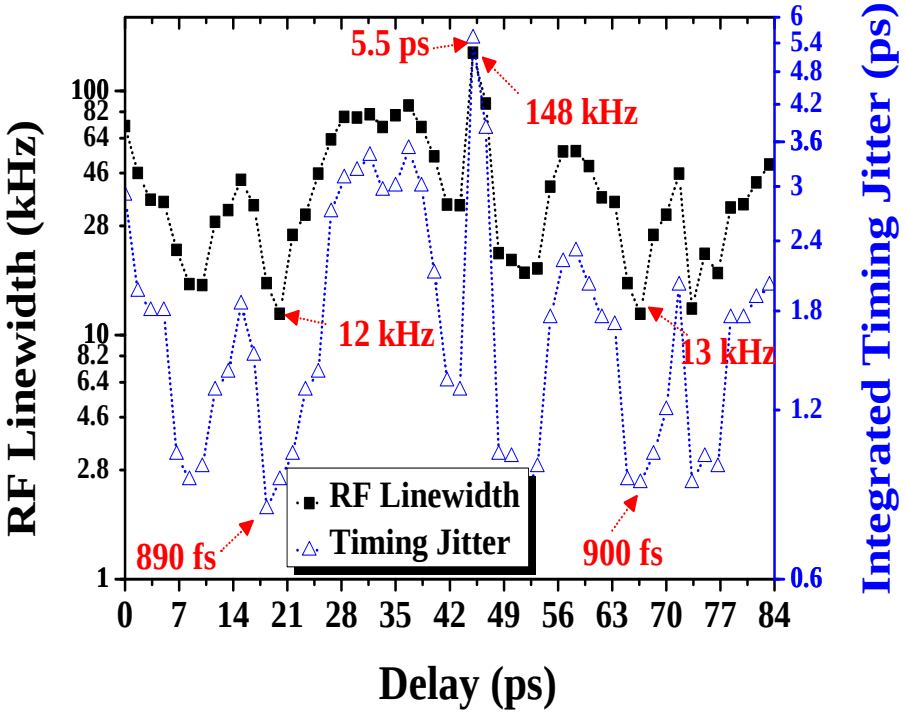

Figure 3.17: RF linewidth (black squares) and Integrated timing jitter (blue triangles) as a function of full delay phase subjected to balanced symmetric dual-loop feedback.

(blue line) is shown in Fig. 3.18 (b) for balanced feedback ratio symmetric dual-loop.

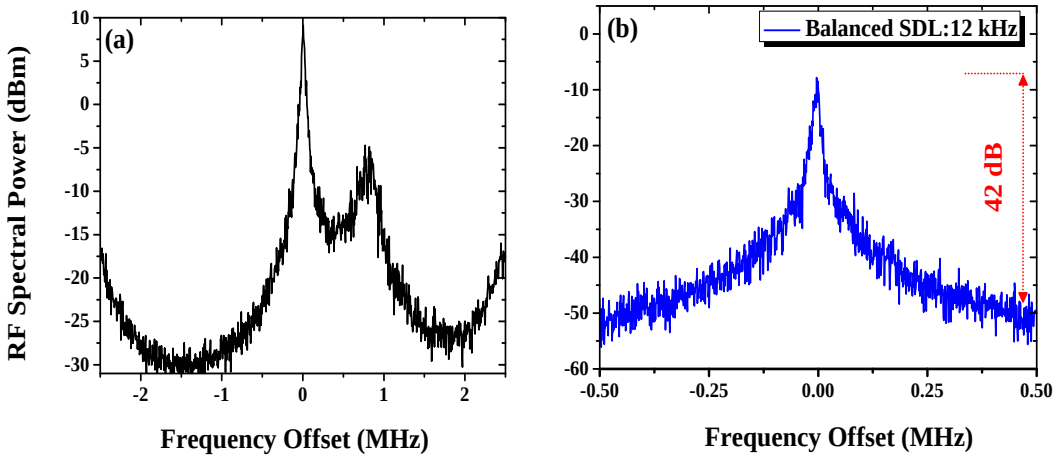

Figure 3.18: (a) Broadening of RF spectra under non resonant condition using frequency span 5 MHz (resolution bandwidth 3 kHz and video bandwidth 1 kHz) (b) RF spectra under resonant condition for balanced symmetric dual-loop feedback using frequency span 1 MHz (resolution bandwidth 1 kHz and video bandwidth 100 Hz).

Recently, in a separate series of experiments, we achieved 0.97 kHz linewidth (instrument limited) and timing jitter 0.45 ps with both cavities resonant [118],

confirming balanced symmetric dual-loop feedback produces effective stabilisation, but only at a specific delay with tolerance $\sim$ 1 ps, a very stringent requirement in practice.

3.4.5 RF Linewidth Versus Power Split for Symmetric Dual-Loop Feedback

Next, we explored unbalanced dual-loop feedback, in which the power split between the two cavities was varied. In these experiments, the inner feedback cavity (loop-I) was fully resonant and the outer feedback cavity fine-tuned around resonance. The schematic of this setup is shown in Fig. 3.19.

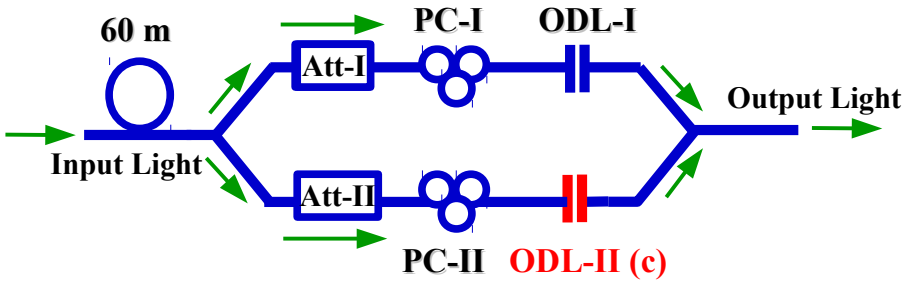

Figure 3.19: Schematic of symmetric dual-loop with ODL-I at integer resonance and fine-tuning of ODL-II (c); Acronyms– ODL: Optical delay line; Att: Optical attenuator; PC: polarisation controller.

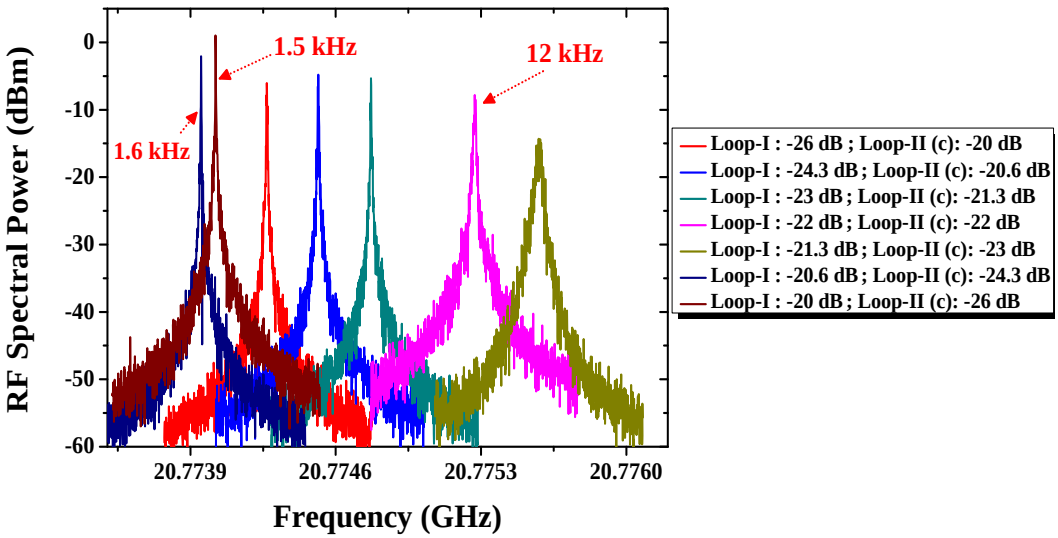

Figure 3.20: Measured RF spectra as a function of different feedback ratios through two external feedback cavities for symmetric dual-loop feedback. Frequency span was 1 MHz (resolution bandwidth 1 kHz and video bandwidth 100 Hz).

Measured RF spectra at different loop power splits are shown in Fig. 3.20, with corresponding RF linewidths in Table 3.1.

Table 3.1: Calculated RF linewidth as a function of power split ratio (in dB) through two external feedback loops using the asymmetric dual-loop feedback configuration

Loop-I	Loop-II (c)	Total Feedback at Gain Facet	RF-Linewidth
-26 dB	-20 dB	-22 dB	4.1 kHz
-24.3 dB	-20.6 dB	-22 dB	3.4 kHz
-21 dB	-21 dB	-22 dB	2.1 kHz
-22 dB	-22 dB	-22 dB	12 kHz
-21 dB	-21 dB	-22 dB	30 kHz
-20.6 dB	-24.3 dB	-22 dB	1.6 kHz
-20 dB	-26 dB	-22 dB	1.5 kHz

Minimum RF linewidth occurred when both external cavities were fully resonant, as expected. Values of 1.6 and 1.5 kHz were achieved when resonant loop-I had feedback -20.6 and -20 dB, and fine-tuned loop-II had -24.3 and -26 dB, respectively. This combination of feedback ratios was particularly effective and was investigated further.

3.4.6 RF Linewidth and Timing Jitter Versus Delay for Unbalanced Symmetric Dual-Loop Feedback

The next experiments concerned the effects of unbalanced symmetric dual-loop feedback on timing stability of the laser: feedback strengths in loop-I and loop-II were set at -20 and -26 dB, a ratio of 4:1 resulting in overall feedback -22 dB to the gain section. Delay in loop-I was then fine-tuned to full resonance, and loop-II tuned over its entire available delay ranged 0-84 ps. This yielded much more stable dynamics: narrow RF spectra and reduced timing jitter were maintained over the full delay range, unlike single-loop and balanced symmetric dual-loop feedback. This dual-loop scheme with 4:1 power ratio between loops was most successful, reducing RF linewidth by up to two orders of magnitude (70x) compared to free-running, 2-5x over single-loop and 5-8x relative to balanced symmetric dual-loop feedback. Measured RF linewidths (black squares) and timing jitter (blue triangles) for this unbalanced symmetric dual-loop scheme are given in Fig. 3.21. Furthermore, with this feedback configuration, measured RF linewidth and integrated timing jitter on full delay range ranged from as high as 28 kHz and 1.5 ps to as low as 1.5 kHz and 0.45 ps

(free-running values are 100 kHz and 3.9 ps). Again the most effective and robust linewidth narrowing and lowest timing jitter occurred when both external cavities were fully resonant. The RF spectrum under double resonance is shown in Fig. 3.22 (blue line). Recently, it was theoretically predicted that dual-loop optoelectronic oscillators could be optimized by controlling the phase delay and power split ratio [118].

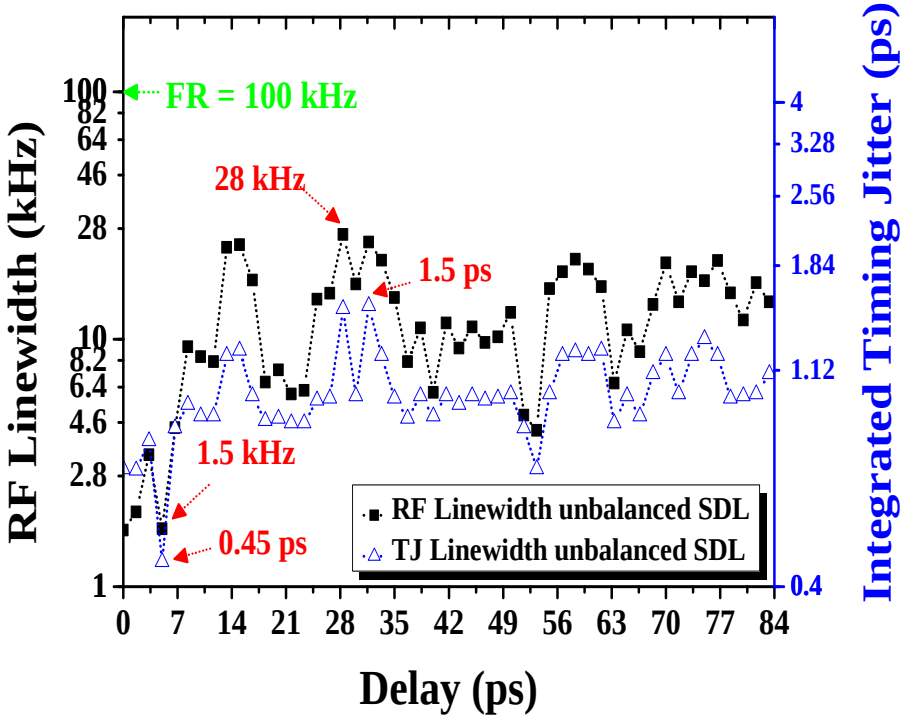

Figure 3.21: RF linewidth (black squares) and integrated timing jitter (blue triangles) as a function of full delay phase subject to unbalanced symmetric dual-loop feedback.

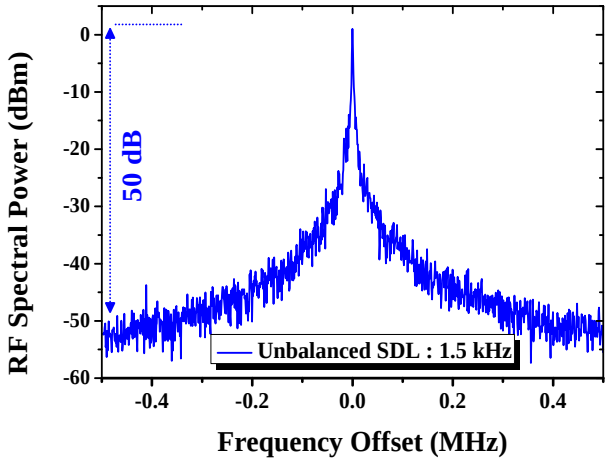

Figure 3.22: RF spectra under double resonance condition using unbalanced symmetric dual-loop feedback.

In addition, when optical delay line ODL-I was adjusted to full resonance, and loop-II tuned over its entire available delay range 0-84 ps, it was observed that stable RF linewidth could be achieved versus delay when the attenuation in the laser gain section is varied in three chosen feedback levels (-46 dB, -29 dB and -22 dB), as shown in Fig. 3.23. These results demonstrate that at feedback level -46 dB, across the full delay range, no significant reduction in RF linewidth occurs and results were comparable to the free-running condition. Under double resonance, the RF linewidth narrows to 68 kHz. This attenuation level agrees well with previously reported measurements [78]. It has been shown, that with further increase in feedback level up to -29 dB, the RF linewidth narrows down to 2.5-5x, across the widest delay range, compared to free-running. However, under double resonance it lowers to 20 kHz. With a slight increase in feedback level to -22 dB, extreme suppression of RF linewidth and corresponding reduced timing jitter occurs versus full delay tuning and RF linewidth narrows down to 3.6-67x compared to free-running. The influences of three chosen feedback attenuations (-46 dB, -29 dB and -22 dB) on the laser performance are presented in Fig. 3.23. These experimental results suggest that stability of MLLs on widest delay ranges could be achieved even at low feedback ratios.

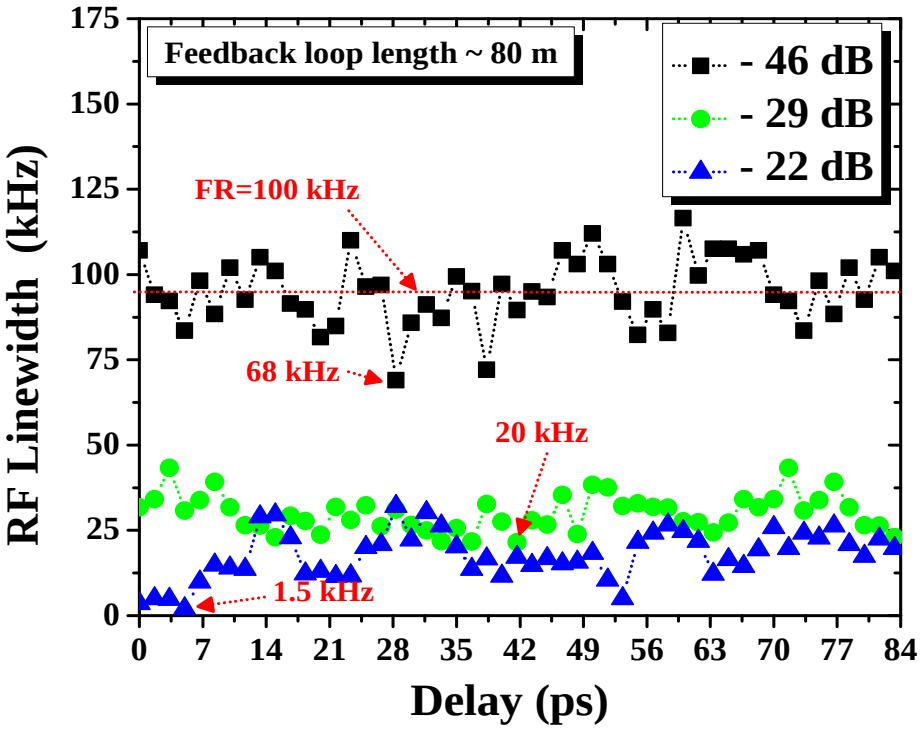

Figure 3.23: RF Linewidth as a function of maximum available optical delay range [0 – 84 ps] for unbalanced symmetric dual-loop feedback configurations under three chosen feedback attenuations (-46 dB (black squares), -29 dB (green circles) and -22 dB (blue triangles)).

Furthermore, when free-running the peak power of RF noise spectra is -20 dB. For single-loop and unbalanced symmetric dual-loop feedback, the noise peak is 30 dB higher (see Fig. 3.13(a)) due to the reduced RF linewidth and also lower threshold current with feedback, increasing the optical power emitted at fixed bias. This increase in the amplitude of RF spectra of single-loop feedback and unbalanced symmetric dual-loop configuration compared to the free-running condition are shown in Figs. 3.13(a) and 3.22, respectively. Comparison of RF spectra and measured phase-noise traces for unbalanced symmetric dual-loop feedback versus frequency offset with the free-running condition are given in Figs. 3.24(a) and 3.24(b), respectively.

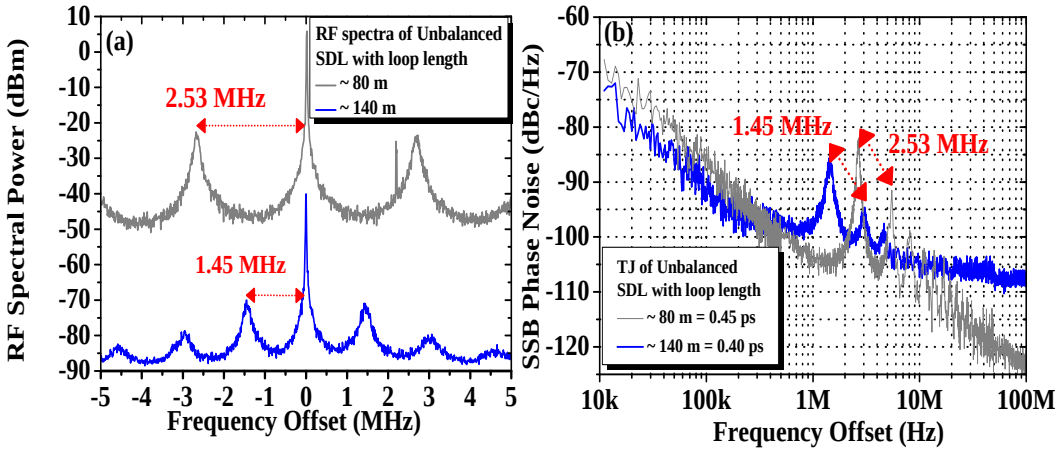

Figure 3.24: (a) Measured RF spectra with loop length 140 m (blue line) and free-running (gray line) under frequency span 10 MHz (resolution bandwidth 10 kHz and video bandwidth 1 kHz) (b) Comparison of phase-noise trace of symmetric dual-loop with loop length 140 m (blue line) and free-running laser (gray line) with integration limit 10 kHz-100 MHz.

Measured RF linewidths versus delay for a single-loop, with -20 dB feedback through loop-I (blue triangles), are shown in Fig. 3.25(a) for comparison. At stable resonance, single-loop feedback at -20 and -26 dB narrows the linewidth to 8 kHz and 68 kHz, respectively. When dual-loops were unbalanced, measured RF linewidth as a function of the delay was as in Fig. 3.25(b), showing that unbalanced dual-loops are more effective in stabilizing the linewidth. Here optimisation of ODL-II yields better linewidth stabilisation (blue triangles) than optimisation of ODL-I (black squares) (see Fig. 3.25(b)). For symmetric dual-loop feedback, fine-tuning of ODL-I yields narrow RF linewidth at an integer resonance, but the linewidth broadens significantly when the delay is tuned away from this point. Our results show that the most effective algorithm for stable linewidth reduction over a broad range of phase delay is to set the

stronger cavity to an integer resonance then fine-tune the weaker cavity. Optimising loop-II in symmetric dual-loop feedback (blue triangles in Fig. 3.25(b)), changes the linewidth similarly to single-loop feedback (black squares in Fig. 3.25(a)) but almost 1-2 orders of magnitude (6-64x) narrower.

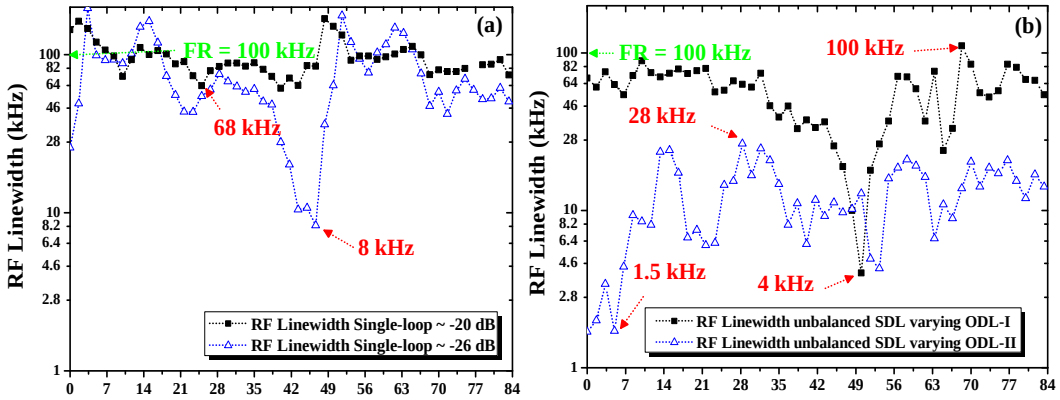

Figure 3.25: (a) RF linewidth as a function of maximum delay [0 - 84 ps] using single-loop feedback with feedback strength -20 (blue triangles) and -26 dB (black squares) (b) RF linewidth versus delay [0 - 84 ps] for unbalanced symmetric dual-loop configuration with optimisation of ODL-I (black squares) and ODL-II (blue triangles).

3.4.7 Comparison of Balanced and Unbalanced Symmetric Dual-Loop Feedback with Longer Delay Times

Effects of longer delay times on RF linewidth were also investigated for both balanced and unbalanced symmetric dual-loop feedback. For this purpose, the 60 m fibre loop was replaced with 120 m of fibre. The basic schematic for this feedback configuration is depicted in Fig. 3.26.

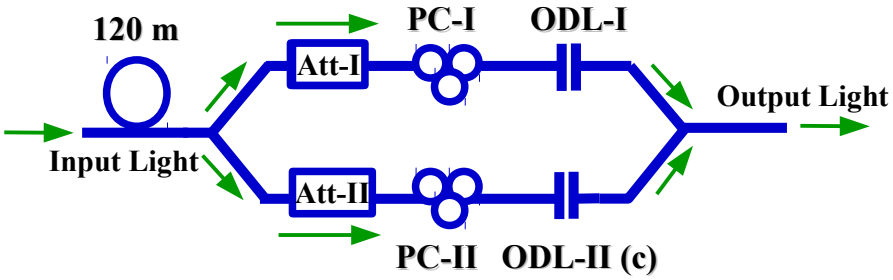

Figure 3.26: Schematic of symmetric dual-loop with ODL-I at integer resonance and full delay tuning of ODL-II (c); Acronyms– ODL: Optical delay line; Att: Optical attenuator; PC: polarisation controller.

Measured RF linewidth versus phase tuning is shown in Fig. 3.27 for symmetric dual-loops with balanced (black squares) and unbalanced (blue triangles) feedback ratios. Unbalanced symmetric dual-loop feedback again reduced the RF linewidth by 10-100x across a broader range of delay than the free-running laser. However, balanced symmetric dual-loop feedback was less sensitive to delay, though the linewidth was 8-16x broader than unbalanced symmetric dual-loop (Fig. 3.27). Narrowest linewidth obtained was 1 kHz under full resonance (25 ps delay in Fig. 3.28) which is the limit of resolution of our spectrum analyser. Timing jitter was also minimized at 0.4 ps and timing jitter versus widest delay range for unbalanced symmetric dual-loop optical feedback is shown in Fig. 3.28.

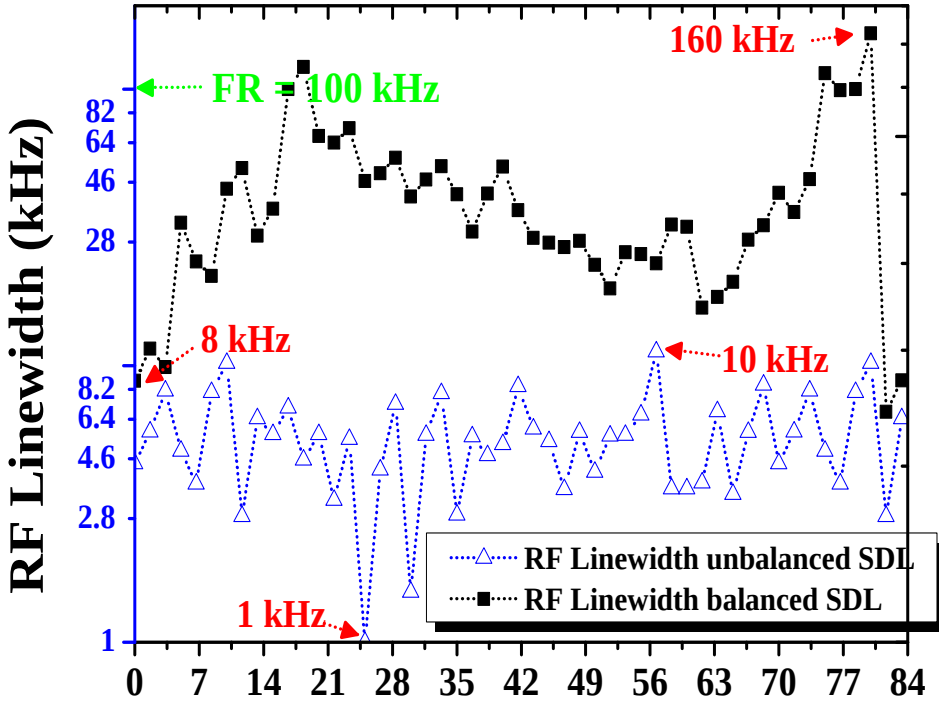

Figure 3.27: RF linewidth subjected to balanced (red squares) and unbalanced symmetric dual-loop feedback configuration (blue triangles) as a function of maximum available delay tuning [0 - 84 ps].

The RF spectrum under these conditions is shown in Fig. 3.29(a) (blue line). We observed 1.45 MHz external cavity mode spacing as expected for a 140 m loop. Measured phase-noise versus frequency offset from the fundamental mode-locked frequency is shown in Fig. 3.29(b) (blue line). RF linewidth and timing jitter were lower over a wider delay range with the longer cavity, due to its higher quality factor (Q). The Q-factor is commonly used to describe the sharpness of the resonance of a resonator. The higher the Q-factor, the narrower the linewidth and corresponding integrated timing jitter.

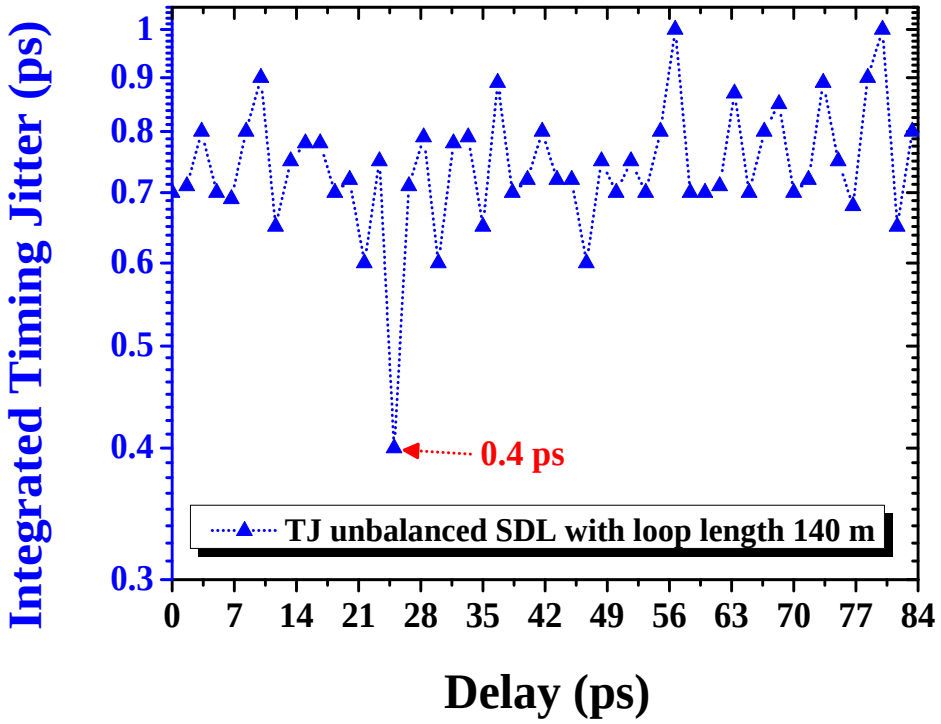

Figure 3.28: Integrated timing jitter subjected to unbalanced symmetric dual-loop feedback configuration (blue triangles) as a function of maximum available delay tuning [0 - 84 ps].

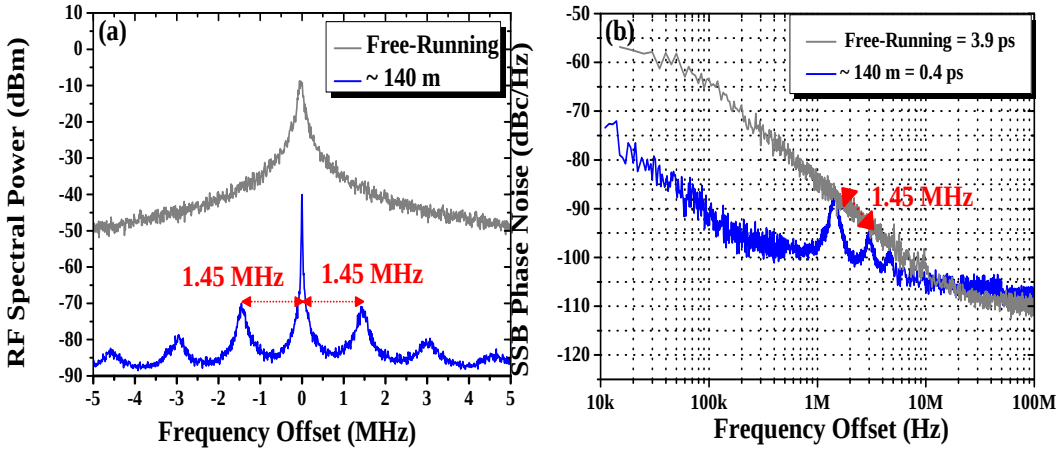

Figure 3.29: (a) Comparison of RF spectra subjected to unbalanced symmetric dual-loop feedback (blue triangles) and free-running condition (gray line) under frequency span 10 MHz (resolution bandwidth 10 kHz and video bandwidth 1 kHz) (b) Comparison of phase-noise trace of unbalanced symmetric dual-loop feedback (blue triangles) and free-running condition (gray line) with integration limit 10 kHz-100 MHz.

3.5 Summary

This chapter has highlighted the effects of external optical feedback level, maximum effective optical delay phase tuning (0-84 ps), optical delay lengths (80

and 140 m), and external optical feedback scheme on the timing jitter and stability of the 21 GHz SML QDash laser. Two symmetric dual-loop configurations, subject to balanced and unbalanced feedback ratios were demonstrated, and results were compared with single-loop feedback and free-running condition.

First, effects of different lengths of fibre delays on the RF linewidth and timing jitter were investigated using a single-loop feedback scheme. It was found that increased fibre delay length leads to significant reduction in RF linewidth and timing jitter, mainly due to the quality factor (Q) of the feedback loop determined by the round-trip time (optical length) of the external cavity. In addition, the influence of external optical feedback on the RF linewidth and integrated timing jitter was investigated for single and symmetric dual-loop feedback (with balanced and unbalanced feedback ratios). Initially a gradual decrease in RF linewidth and integrated timing jitter was observed, however after a certain value of feedback ratio, saturation in RF linewidth and timing jitter was achieved. From this analysis, we have identified the optimal feedback ratio (-22 dB) for single and symmetric dual-loop feedback, which leads to significant reduction in RF linewidth and timing jitter. It is reported in the literature that RF linewidth narrowing and reduced timing jitter versus delay phase tuning depend strongly on feedback delay. For single-loop feedback, RF linewidth and timing jitter were shown to be very sensitive to small delay adjustments, with optimum performance being limited to a narrow range of delay (0 - 5 ps). For practical applications of MLLs, it is desirable to extend the range of resonant feedback condition to the full range of delay phase, such that changes in delay maintain stable RF spectra with narrow linewidth and minimal timing jitter even in the most demanding applications.

After investigating the influence of single-loop feedback on the RF linewidth and timing jitter of the QDash mode-locked laser, a second cavity was added which made a significant contribution to the timing jitter over the full delay tuning. The lengths of both external feedback loops were kept similar and two feedback schemes were studied: balanced and unbalanced symmetric dual-loop feedback. For symmetric dual-loop with balanced feedback ratio, equal power was fed through both external feedback loops. We see that balanced symmetric dual-loop feedback yields results comparable to those using a single-loop, and is similarly sensitive to delay, producing effective stabilisation only at a specific delay value. For unbalanced symmetric dual-loop feedback configuration, higher feedback ratio (-20 dB) was passed through loop-I relative to the other (-26 dB). We found that unbalanced symmetric dual-loops, with the in-

ner cavity fully resonant (at higher feedback intensity) and fine delay tuning of the outer loop (at lower feedback intensity), gave narrow RF linewidth and reduced timing jitter over a wide range of delay detuning [0-84 ps], unlike single and balanced symmetric dual-loop configurations. In this proposed symmetric dual-loop configuration, reduced sensitivity of RF linewidth and timing jitter was observed over a wider delay range because changing delay does not cause switching into unstable or unwanted dynamical regimes. In addition, the influence of longer feedback delay times (140 m) on the RF linewidth narrowing and reduced timing jitter on wider delay range tuning [0-84 ps] were further studied. It was found that with long feedback delay times (140 m), the RF linewidth and timing jitter on the full delay range was much narrower than that with the shorter feedback delay time (80m) which is mainly due to the higher quality factor (Q) of the external cavity.

In summary, we have demonstrated that unbalanced symmetric dual-loop feedback provides best overall stability, maintaining stable RF spectra with narrow linewidth and low timing jitter over a range of delay detuning $\sim$ 80 ps, which means it would be relatively insensitive to temperature, vibration and other common environmental variations. Unbalanced symmetric dual-loop feedback is significantly better than conventional single-loop feedback and balanced symmetric dual-loop feedback, producing up to two orders of magnitude reduction in RF linewidth to 1 kHz (instrument limited) and RMS timing jitter 0.4 ps, compared to free-running. Longer (140 m) fibre loops are more effective than shorter (80 m) loops. For symmetric dual-loop feedback, we have studied the effects of varying the power split between the loops. We demonstrated a novel unbalanced symmetric dual-loop feedback scheme with feedback lengths of 80 and 140 m, which narrowed the RF linewidth by $\sim$ 4-67x and $\sim$ 10-100x, respectively, across the widest delay range, compared to free-running. The proposed scheme is effective in overcoming the primary drawback of mode-locked diode laser their lack of dynamical stability and robustness in practical applications such as frequency comb generation, optical sampling, signal timing and regeneration, metrology, lidar and many others.

Chapter 4

stabilisation of SML QDash Lasers using Symmetric Dual-Loop Optical Feedback

4.1 Introduction

In Chapter 3, we described investigation of the RF linewidth versus power split through symmetric dual-loop feedback configurations under double resonance. However, for unbalanced symmetric dual-loop feedback, the influence of variation in optical delay of either feedback loop on stability of the QDash mode-locked laser was neglected. In this chapter, we are primarily interested in observing the variation in RF linewidth versus a wide range of delay tuning [0-84 ps] followed by varying the power split between the feedback loops. RF linewidth narrowing/broadening over a broad range of delay phase was obtained when one cavity was set to an integer resonance, the second cavity was fine-tuned. Later we will see that RF linewidth reduction over a broad range of phase delay can be achieved by setting the stronger cavity to an integer resonance then fine-tuning the weaker cavity.

This chapter is structured as follows. In Section 4.2, two different feedback approaches were studied to investigate stabilisation versus power split ratio for symmetric dual-loop optical feedback. A comprehensive analysis of the RF linewidth as a function of full delay range tuning will be presented in Subsections 4.2.1 and 4.2.2, when the first feedback cavity (stronger) was set to an integer resonance and fine-tuned the second cavity (weaker). Finally, in Sec-

tion 4.3, the RF linewidth versus delay for balanced and unbalanced symmetric dual-loop optical feedback will be presented.

4.2 Stabilisation of SML QDash Lasers Versus Power Split Ratio for Symmetric Dual-Loop Optical Feedback

In this section, we conducted an experimental analysis of the RF linewidth with dual-loop optical feedback as a function of the power split ratio and separate fine tuning of the optical delay phase in either feedback loop. Thus, two dual-loop feedback configurations, symmetric (equal arms of external loops) and asymmetric (unequal arms of external loops) were presented. Both feedback schemes with following optical delay phase settings have been studied.

1. RF linewidth versus full phase delay with the weaker cavity (ODL-II) set to an integer resonance, the stronger cavity fine-tunes (ODL-I (c))
2. RF linewidth versus full phase delay with the stronger cavity (ODL-I) set to an integer resonance, then weaker cavity fine-tunes (ODL-II (c))

A comprehensive analysis of RF linewidth versus the widest range of delay tuning for both symmetric and asymmetric dual-loop feedback mentioned above is presented in the following sections.

4.2.1 RF Linewidth Versus Phase Delay with Weaker Cavity (ODL-II) set to an Integer Resonance, the Stronger Cavity Fine-Tunes (ODL-I (c))

The experimental arrangement for this symmetric dual-loop setup remained the same as in Fig. 3.3 except for replacing the 80 m fibre with 200 m. To study the effects of optical delay phase tuning on the RF linewidth of our QDash mode-locked laser, fine adjustment of PC-I and PC-II were made: optical delay line ODL-II was set to full resonance (integer number of times the laser cavity delay), then we fine-tuned the ODL-I. A higher feedback ratio of loop-I relative to loop-II was fixed using the variable optical attenuators (Att-I and Att-II),

with overall feedback ratio -22 dB back into the gain section. A schematic of the symmetric dual-loop optical feedback setup is shown in Fig. 4.1.

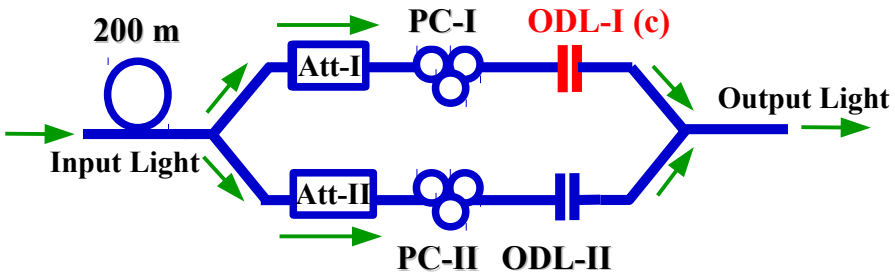

Figure 4.1: Schematic of symmetric dual-loop with ODL-II at integer resonance and full delay tuning of ODL-I (c); Acronyms– ODL: Optical delay line; Att: Optical attenuator; PC: polarisation controller

Four chosen combinations of feedback ratios (in units of percentage and dB) investigated in this work are presented in Table. 4.1. The percentage of feedback ratio through either external feedback loop can be converted into dB using the following formula:

$$feedback\ into\ dB = 10 * log_{10} \frac{(\%\ loop - I) + (\%\ loop - II)}{2 * 100} \tag{4.1}$$

Table 4.1: Four chosen combinations of feedback ratio through either feedback loop, and the resulting overall feedback strength into the gain section.

Loop-I(c)	Loop-II	Total Feedback at Gain Facet
-19.5 dB (1.13%)	-29.03 dB (0.12%)	-22 dB (0.625%)
-20.6 dB (1%)	-24.3 dB (0.25%)	-22 dB (0.625%)
-21 dB (0.88%)	-22.7 dB (0.3%)	-22 dB (0.625%)
-21.3 dB (0.75%)	-23 dB (0.5%)	-22 dB (0.625%)

- **Loop-I (c) = -19.5 dB and Loop-II = -29.03 dB**

In order to study the effects of -19.5 dB feedback ratio through loop-I and -29.03 dB feedback ratio through loop-II, ODL-II was adjusted to integer resonance and ODL-I was tuned over its entire available delay range 0-84 ps. Measured RF linewidth data versus full delay range tuning are shown in Fig. 4.2(a). From these experimental results, it was observed that under integer resonance the RF linewidth narrowed to 11 kHz from 100 kHz for the free-running laser. Measured RF spectra (black line) are shown in Fig. 4.3. These results show that, with this selective combination of feedback ratios (loop-I=-19.5 dB and loop-II=-29.03 dB) effective stabilisation can be achieved at only one particular delay setting ($\sim$ 50 ps), but over a wider delay range (0-30 ps and 56-84 ps) the RF linewidth was relatively broad and was comparable to free-running.

- **Loop-I (c) = -20.6 dB and Loop-II = -24.3 dB**

In this case, -20.6 dB feedback was passed through loop-I and -24.3 dB was fed through loop-II. Measured RF linewidth versus delay is shown in Fig. 4.2(b). When both feedback cavities were fully resonant, the measured RF linewidth was as low as 3 kHz from 100 kHz, which is 33x lower than free-running. RF spectra under double resonance are shown in Fig. 4.3 (green line). In addition, with full delay phase tuning, the results were much better than measured with the previous combination of feedback ratios (loop-I=-19.5 dB and loop-II=-29.03 dB).

- **Loop-I (c) = -21 dB and Loop-II = -22.7 dB**

In the following, the feedback ratios in loop-I and loop-II were fixed at -21 dB and -22.7 dB, respectively. Measured RF linewidth data as a function of full delay range tuning (ODL-I) are shown in Fig. 4.2(c). When both feedback loops were fully resonant, the RF linewidth was reduced from 100 kHz for free-running to as low as 3 kHz, which was 33x lower than the free-running. A 33x reduction in RF linewidth also occurs under double resonance in the above combination of feedback ratio (loop-I=-20.6 dB and loop-II=-24.3 dB). However on full delay phase tuning, significant suppression in RF linewidth was noticed, across a broad delay range 8 to 84 ps. Measured RF spectra under the double resonance are shown in Fig. 4.3 (red line).

- **Loop-I (c) = -21.3 dB and Loop-II = -23 dB**

When -21.3 dB feedback was passed through loop-I and -23 dB through loop-II, the RF linewidth narrowed from 100 kHz free-running to as low as 10 kHz. On the other hand, under non-resonant conditions, the RF linewidth broadened to 55 kHz which is only $\sim$ 1.9x lower than free-running. In addition, the RF linewidth versus full delay range tuning (0 - 84 ps) was only 5-10x lower than free-running. Measured RF linewidth versus delay is shown in Fig. 4.2(d). In comparison to previous combinations of feedback ratios, this combination (loop-I=-21.3 dB and loop-II=-23 dB) through either feedback loop shows stable behaviour in RF linewidth over a broad range of delay (0 to 84 ps). This comprehensive analysis confirms that to achieve effective stabilisation on full delay phase tuning, -21 dB feedback through loop-I and -21 dB through loop-II is desirable when the optical delay line (ODL-I) on the first (stronger) feedback loop is fine-tuned. Measured RF spectra under double resonance are shown in Fig. 4.3 (blue line).

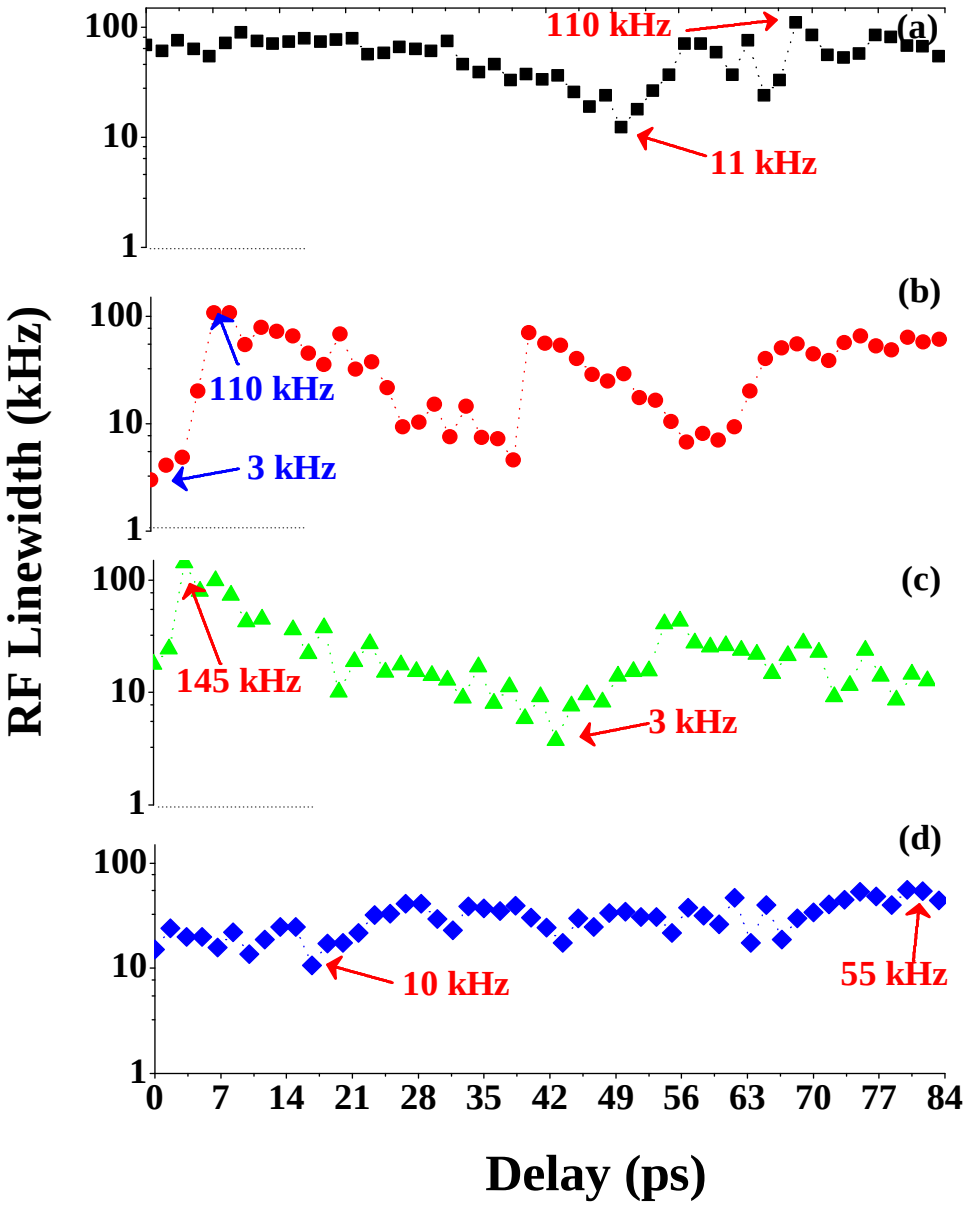

Figure 4.2: Measured RF as a function of full delay phase (ODL-I(c)) subjected to following combinations of feedback ratio through either external feedback loop (a) loop-I:-19.5 dB; loop-II:-29.03 dB (b) loop-I:-20.6; loop-II:-24.3 dB (c) loop-I:-21 dB; loop-II:-22.7 dB (d) loop-I:-21.3 dB; loop-II:-23 dB.

Comprehensive analysis of RF linewidth versus delay demonstrates that for symmetric dual-loop feedback, fine-tuning of ODL-I yields narrow RF linewidth at an integer resonance [see in Table 4.3], but the linewidth broadens significantly when the delay is tuned away from this point. In the literature [77, 79], it was observed that the pulse repetition frequency shifts with feedback delay; in our experiments, we have used the fully resonant loop-II to set the fundamental repetition frequency, then tuned pulse trains from loop-I through

these by varying the delay. With a higher feedback ratio through loop-I, the first feedback loop was more sensitive to frequency pulling than the other. For most settings of loop-II delay, pulses from both loops overlapped at the edges rather than the center, broadening RF linewidth and increasing timing jitter, so that measured RF spectra are worse and corresponding timing jitter values are higher.

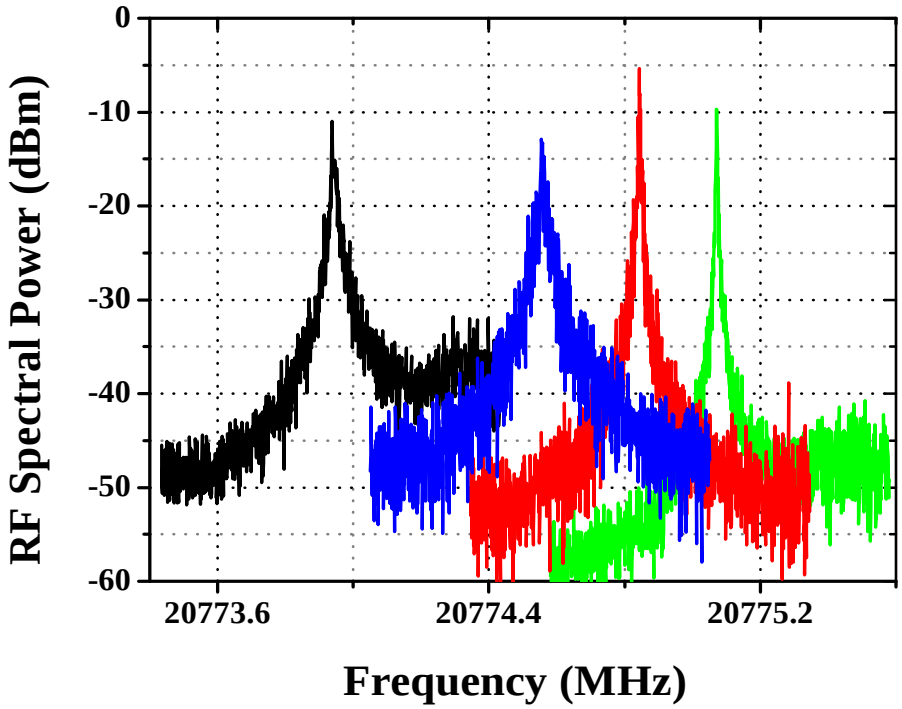

Figure 4.3: Measured RF spectra using frequency span 1 MHz (resolution bandwidth 1 kHz, video bandwidth 100 Hz) as functions of power split ratio (a) loop-I:-19.5 dB; loop-II:-29.03 dB (black line) (b) loop-I:-20.6; loop-II:-24.3 dB (green line) (c) loop-I:-21 dB; loop-II:-22.7 dB (red line) (d) loop-I:-21.3 dB; loop-II:-23 dB (blue line).

The minimum RF linewidth, measured for four chosen combinations of feedback ratios is summarised in Table. 4.2 under double resonance.

Table 4.2: Four chosen combinations of feedback ratio through either feedback loop using symmetric dual-loop optical feedback and measured minimum and maximum RF linewidth for each case.

Loop-I(c)	Loop-II	Minimum RF	Maximum RF
-19.5 dB	-29.03 dB	11 kHz	110 kHz
-20.6 dB	-24.3 dB	3 kHz	110 kHz
-21 dB	-22.7 dB	3 kHz	145 kHz
-21.3 dB	-23 dB	10 kHz	55 kHz

4.2.2 RF Linewidth Versus Phase Delay with Stronger Cavity (ODL-I) set to an Integer Resonance then Weaker Cavity Fine-Tunes (ODL-II (c))

In the second feedback approach, the phase delay in the strong cavity (ODL-I) is set to integer resonance, then we fine-tuned the weaker cavity (ODL-II (c)). A schematic of this symmetric dual-loop configurations is depicted in Fig. 4.4.

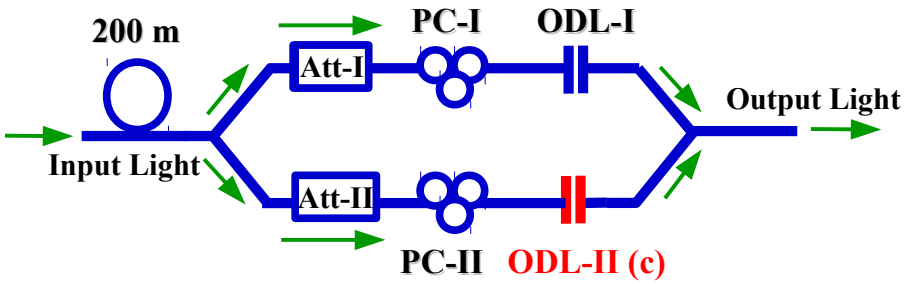

Figure 4.4: Schematic of symmetric dual-loop feedback with ODL-I at integer resonance and full delay tuning of ODL-II (c); Acronyms– ODL: Optical delay line; Att: Optical attenuator; PC: polarisation controller.

The combinations of feedback ratio passed through the two feedback loops in various symmetric dual-loop feedback configurations are presented in Table. 4.3.

Table 4.3: Four chosen combinations of feedback ratios through either feedback loop and overall feedback strength into gain section.

Loop-I	Loop-II (c)	Total Feedback at Gain Facet
-19.5 dB (1.13%)	-29.03 dB (0.12%)	-22 dB (0.625%)
-20.6 dB (1%)	-24.3 dB (0.25%)	-22 dB (0.625%)
-21 dB (0.88%)	-22.7 dB (0.3%)	-22 dB (0.625%)
-21.3 dB (0.75%)	-23 dB (0.5%)	-22 dB (0.625%)

- **Loop-I = -21.3 dB and Loop-II (c) = -23 dB**

This experiment concerned the effects of unbalanced symmetric dual-loop feedback on timing stability of the laser: fine adjustment of the polarisation controllers (PC-I and PC-II), variable optical attenuators (Att-I and Att-II) and one optical delay line (ODL-I) was done. Higher feedback strength was passed through loop-I relative to loop-II. The feedback ratio from loop-I was fixed to -21.3 dB, while from loop-II it was adjusted to -23 dB giving overall feedback ratio -22 dB back into the gain section. In this symmetric dual-loop feedback approach, maximum available delay range tuning (0 to 84 ps) was tuned on

the second (weaker coupled) cavity. Optical delay line ODL-II and optical delay line ODL-I were held at integer resonant condition. Measured RF linewidth data versus delay are shown in Fig. 4.5(a). From these experimental results, it was observed that under double resonance, the RF linewidth narrowed to 8 kHz from 100 kHz, $\sim$ 14x lower than the free-running. Measured RF spectra (black line)are shown in Fig. 4.6.

- **Loop-I = -21 dB and Loop-II (c)= -22.7 dB**

In this section, -21 dB feedback was passed through loop-I and -22.7 dB through loop-II. When both feedback cavities were fully resonant, this configuration narrowed the RF linewidth from 100 kHz free-running to as low as 15 kHz. Measured RF linewidth data as a function of full delay range tuning are shown in Fig. 4.5(b). In comparison to previous combinations of feedback ratios, this combination of feedback ratios (loop-I=-21.3 dB and loop-II=-23 dB) yield several instabilities at a few delay settings (24, 49 and 72 ps). Measured RF spectra are shown in Fig. 4.6 (red line).

- **Loop-I = -20.6 dB and Loop-II (c)= -24.3 dB**

In this case, -20.6 dB feedback ratio was passed through loop-I and -24.3 dB through loop-II. In this case, RF linewidth narrowing to as low as 5 kHz was observed under full resonance. Measured RF linewidth versus delay is shown in Fig. 4.5(c). In addition, under delay settings (7, 28, 58 and 80 ps) the RF linewidth was much broader then free-running. Measured RF spectra are shown in Fig. 4.6 (green line).

- **Loop-I = -19.5 dB and Loop-II (c)= -29.03 dB**

Unbalanced symmetric dual-loop feedback, with -19.5 dB feedback ratio through loop-I and -29.03 dB through loop-II, yielded much more stable dynamics: narrow RF spectra and reduced timing jitter were maintained over the full delay range, unlike the first three combinations of feedback ratios discussed above. Measured RF linewidth data as a function of full delay range tuning (ODL-II) are shown in Fig. 4.5(d). Under full resonance, the RF linewidth, in this case, was reduced from 100 kHz free-running to as low as 1.5 kHz. RF spectra are shown in Fig. 4.6 (blue line). Our measurements show that to achieve RF linewidth stabilisation over a broad delay range, -19.5 dB feedback ratio through loop-I and -29.03 dB feedback ratio through loop-II is desirable when the optical delay line (ODL-I) in the second feedback loop (lower feedback intensity) is varied. These experimental results demonstrate that different percentages of feedback

ratio through the two external feedback cavities have a significant influence on the timing stability of the laser. In this feedback configuration, the fundamental mode spacing frequency from one feedback cavity was fixed and the other one was fine-tuned. As weak feedback was passed through the second feedback cavity, the repetition frequency as a function of optical delay range (ODL-II) is not changing too much. Hence frequency shifting as a function of optical delay length (ODL-II) from loop-II lies within the range of mode-locked frequency from loop-I which leads to jitter stabilisation over full delay range followed by optimisation of the weaker cavity (optical delay line (ODL-II)).

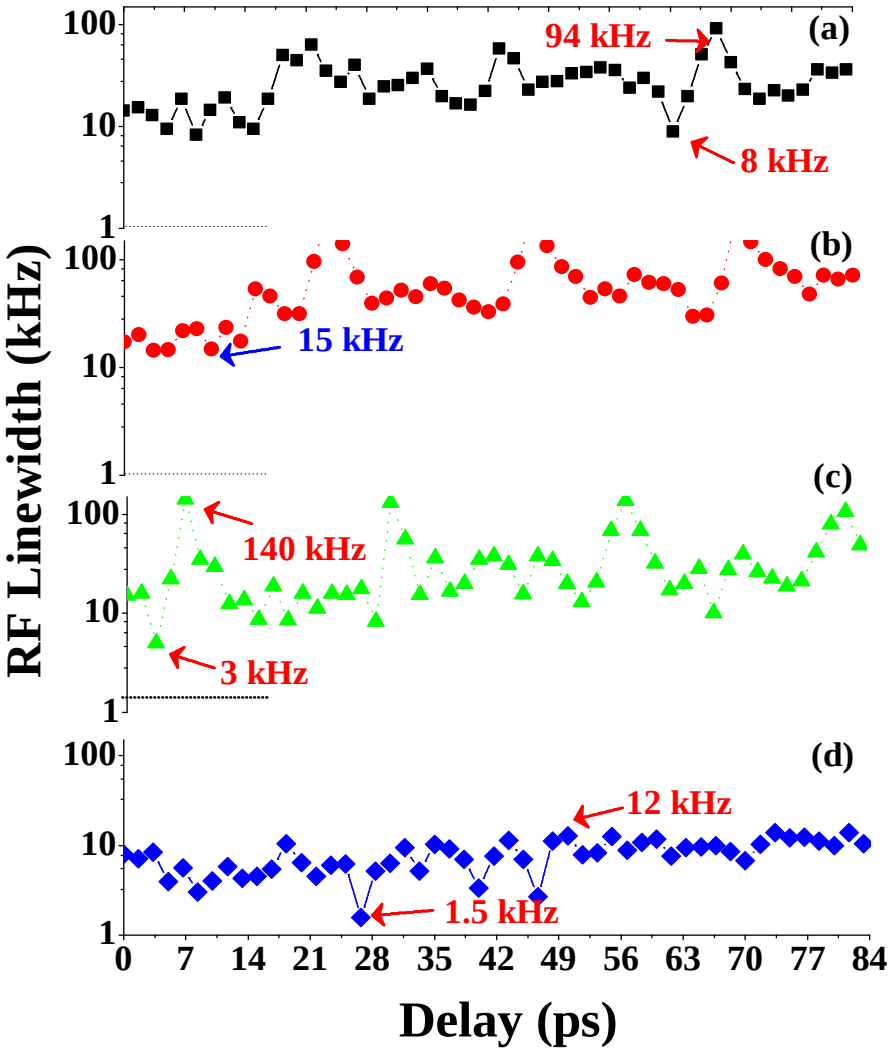

Figure 4.5: Measured RF linewidth as a function of full delay phase (ODL-II(c)) subjected to following combinations of feedback ratio through either external feedback loop (a) loop-I:-21.3 dB; loop-II:-23 dB (b) loop-I:-21 dB; loop-II:-22.7 dB (c) loop-I:-20.6; loop-II:-24.3 dB (d) loop-I:-19.5 dB; loop-II:-29.03 dB.

Minimum and maximum RF linewidth, measured for four chosen combinations of feedback ratio is summarised in Table. 4.4 under double resonance.

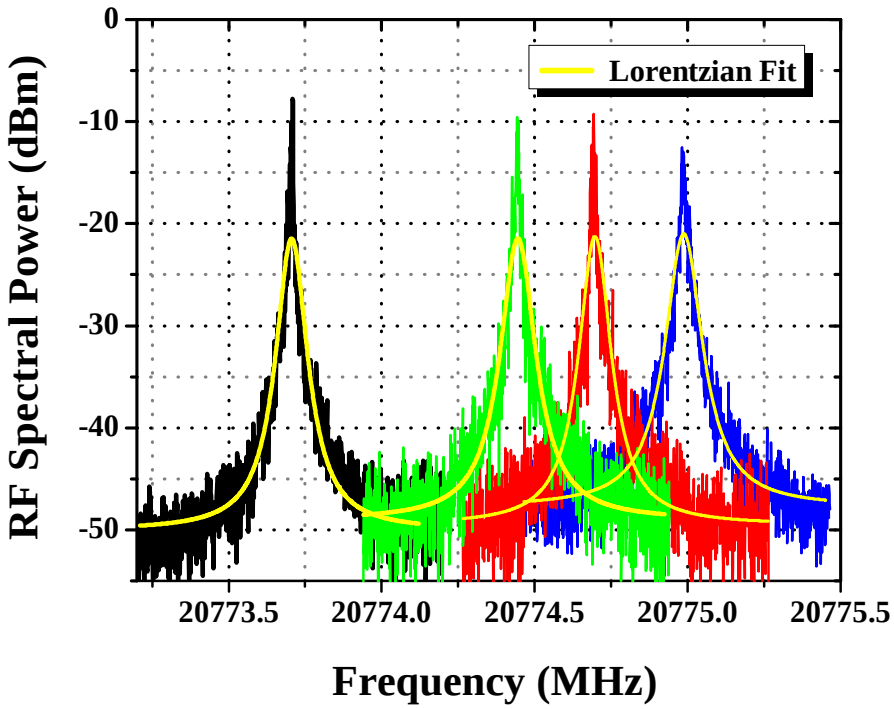

Figure 4.6: Measured RF spectra using frequency span 1 MHz (resolution bandwidth 1 kHz and video bandwidth 100 Hz) as a function of power split ratio (a) loop-I:-21.3 dB; loop-II:-23 dB (black line)(b) loop-I:-21 dB; loop-II:-22.7 dB (red line) (c) loop-I:-20.6; loop-II:-24.3 dB (green line) (d) loop-I:-19.5 dB; loop-II:-29.03 dB (blue line).

Table 4.4: Four chosen combinations of feedback ratio through either feedback loop with measured minimum and maximum RF linewidth for each case.

Loop-I	Loop-II(c)	Minimum RF	Maximum RF
-19.5 dB	-29.03 dB	1.5 kHz	12 kHz
-20.6 dB	-24.3 dB	3 kHz	140 kHz
-21 dB	-22.7 dB	14 kHz	150 kHz
-21.3 dB	-23 dB	7 kHz	94 kHz

4.3 RF Linewidth Versus Delay using Balanced and Unbalanced Symmetric Dual-Loop Feedback

In this section, the effects of balanced and unbalanced symmetric dual-loop feedback, on the RF linewidth and timing jitter of our QDash mode-locked laser are described. For balanced symmetric dual-loop feedback, equal ratios were coupled to the two external feedback cavities, while for unbalanced symmetric dual-loops, the feedback ratios in the two loops were fixed to -19.5 dB and -29.03 dB. The measured RF linewidth as a function of maximum available phase tuning (0 - 84 ps) is given in Fig. 4.7 for symmetric dual-loops with bal-

anced (black squares) and unbalanced (blue triangles) feedback. It was further confirmed that for unbalanced symmetric dual-loop feedback, the RF linewidth narrowed to 8-40x over the full delay phase relative to free-running. However, balanced symmetric dual-loop feedback yields broadened RF linewidth over a wider delay range. It can be seen for unbalanced symmetric dual-loop feedback, the RF linewidth was 2-14x lower than with balanced symmetric dual-loops over the full delay range. For unbalanced symmetric dual-loop feedback, under fully resonant conditions (tunable delay set to $\sim$ 28 ps), the RF linewidth narrows to 1.5 kHz, versus 4 kHz for balanced symmetric dual-loop feedback.

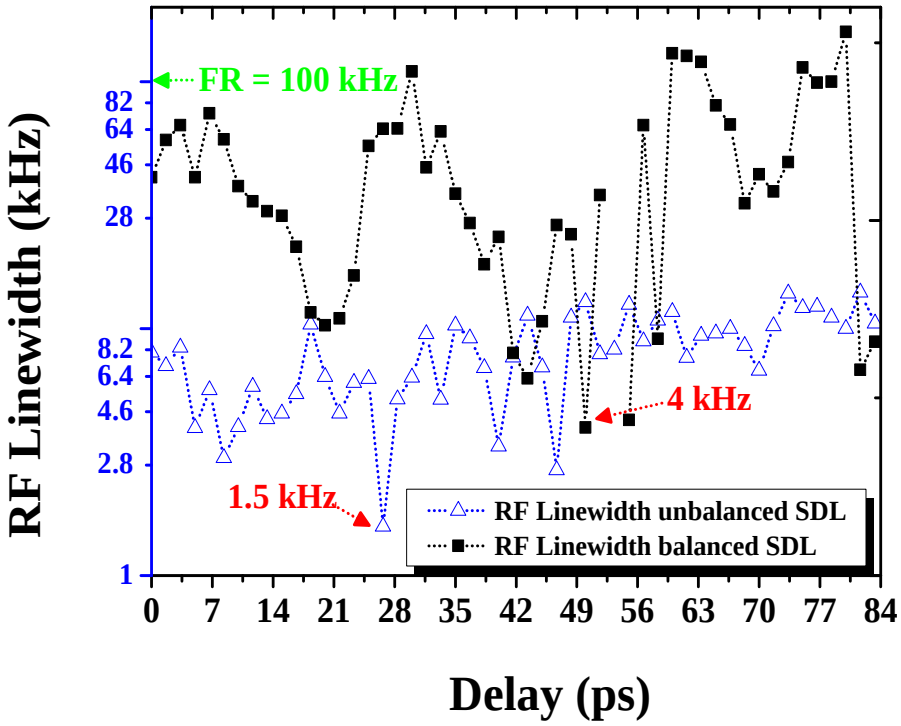

Figure 4.7: RF linewidth subjected to balanced (black squares) and unbalanced symmetric dual-loop feedback configuration (blue triangles) as a function of maximum available delay tuning [0 - 84 ps].

Comparison of measured RF spectra under stable resonance is shown in Fig. 4.8(a) for a feedback loop of length 220 m (blue line). Here, we observed 0.92 MHz spacing of external cavity side-modes from the fundamental mode-locked frequency, consistent with the 220 m loop length. The measured phase-noise trace as a function of the frequency offset from the fundamental mode-locked frequency is shown in Fig. 4.8(b) (blue line).

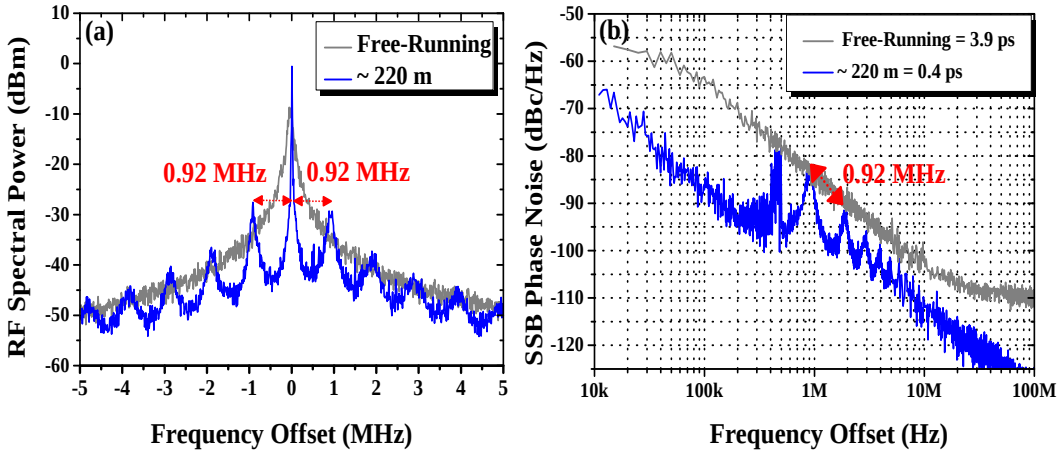

Figure 4.8: (a) Measured RF spectra with loop length 220 m (blue line) with free-running RF spectra using frequency span 10 MHz (resolution bandwidth 10 kHz and video bandwidth 1 kHz) (b) Comparison of phase-noise trace of loop length 220 m (blue line) with free-running laser (gray line) using integration limit 10 kHz-100 MHz.

4.4 Summary

In this chapter, we have investigated the effectiveness of unbalanced symmetric dual-loop optical feedback as a means of robust stabilisation of SML QDash lasers. We demonstrated that symmetric dual-loop optical feedback provides the best stability, maintaining stable RF spectra with narrow linewidth over a broad range of delay detuning by controlling the power split-ratio and separate fine-tuning of the optical delay phase. For symmetric dual-loop feedback, better RF linewidth stabilisation ($\sim$ 9-100x compared to free-running) versus delay was achieved when the feedback strengths in loop-I and loop-II were -19.5 and -29.03 dB and the delay phase in the weaker cavity was fine-tuned. A study of the feedback ratio controlled dual-loop feedback scheme further suggests that dual-loop optical feedback can be implemented for greater stabilisation and improvement of ultrashort optical pulse dynamics.

Chapter 5

Optimum stabilisation of SML QDash Lasers using Asymmetric Dual-Loop Feedback

5.1 Introduction

In this chapter, we experimentally investigated the RF linewidth and timing jitter over a wide range of delay tuning in the SML two-section QDash laser subject to single- and asymmetric dual-loop optical feedback back into the gain section. Various configurations were investigated and optimum feedback levels determined to obtain the narrowest linewidth and lowest timing jitter for both single- and dual-loop arrangements. We will demonstrate that dual-loop feedback, with the shorter cavity tuned to be fully resonant, followed by fine-tuning of the phase of the longer cavity, gave stable narrow RF spectra across the widest delay range, far superior to single-loop feedback. Moreover, we will show the influence of asymmetric dual-loop feedback on the side-mode suppression ratio (SMSR).

The chapter is organised as follows: In the next section, we will introduce the experimental setup. Various feedback scenarios will be investigated and described in Section 5.3 and optimum levels determined for the narrowest RF linewidth and reduced timing jitter for single- and asymmetric dual-loop feedback schemes. In Section 5.4, RF linewidth and integrated timing jitter as functions of delay tuning [0-84 ps] using single-loop optical feedback will be presented. In Section 5.5, we discuss the influence of balanced and unbalanced

asymmetric dual-loop feedback on the RF linewidth and integrated timing jitter versus delay, and results will be compared to single-loop and free-running conditions. Finally, the influence of asymmetric dual-loop feedback on SMSR will be presented in Section 5.6.

5.2 Asymmetric Dual-Loop Feedback

The optical fibre is essentially the energy-storage component in the feedback loop, the length of which determines the Q-factor of the resonator [110]. In addition, the pulse train stability of mode-locked QDot laser can be improved using passive auxiliary optical fiber cavity [111] which reduced the timing jitter of the pulse train. The reduction of the timing jitter for resonant single cavity feedback can be directly related to the increase in the memory of the systems. Besides an improvement in timing jitter, single-cavity optical feedback induces adverse frequency fluctuations around the fundamental frequency in the power spectrum [78]. In Chapters 3 and 4, we have proposed unbalanced symmetric dual-loop feedback and demonstrated its efficacy over a much wider delay range. However, a major disadvantage of symmetric dual-loop feedback is external cavity side-modes which arise due to the equal lengths of the external feedback loops. These side-modes contribute significantly to timing jitter, particularly for longer cavities when they are close to the main peak and are less suppressed.

To deal with these issues, an asymmetric dual-loop feedback configuration has been demonstrated, with the shorter feedback cavity tuned to be fully resonant (ODL-II), followed by fine-tuning of the phase of the longer feedback cavity (ODL-I (c)). A schematic of this asymmetric dual-loop feedback is depicted in Fig. 5.1.

A schematic of our feedback experiment is depicted in Fig. 5.2. For single- and dual-loop feedback, a calibrated fraction of light was fed back through port 1 of an optical circulator, then injected into the laser cavity via port 2. Optical coupling loss from port 2 to port 3 was -0.64 dB. The output of the circulator was sent to a semiconductor optical amplifier (SOA) with a gain of 9.8 dB, then split into two arms by a 50/50 coupler. 50% went to an RF spectrum analyser (Keysight, E4407B) via a 21 GHz photodiode, and to two optical spectrum analysers (Ando AQ6317B and Advantest Q8384). The other 50% of

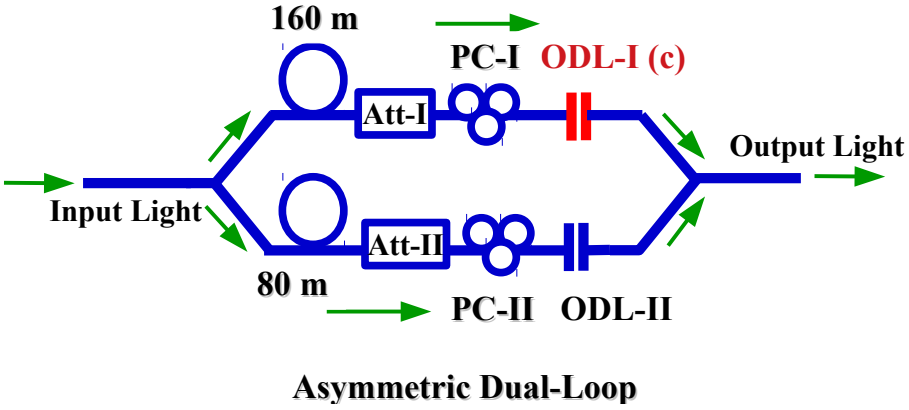

Figure 5.1: Schematic of asymmetric dual-loop feedback (red line indicates that ODL-I is varied); Acronyms– ODL: Optical delay line; Att: Optical attenuator; PC: polarisation controller.

power was directed to the feedback arrangements. For a single feedback loop, all power passed through loop-I. For dual-loop configurations the power was split into two equal parts (feedback loops-I and-II) via a 3-dB splitter. Each feedback loop contained an optical delay line combined with a variable optical attenuator and a polarisation controller. Loop lengths were 160 m and 80 m corresponding to pulse round-trip frequencies 1.28 MHz and 2.60 MHz, respectively. Feedback strengths in both loops were controlled by variable optical attenuators and monitored using a power meter. Equal feedback was received from both external feedback cavities. The microscopic lengths of the fibre loops were optimized by optical delay lines based on stepper-controlled stages with resolution 1.67 ps, covering a range of 0-84 ps. polarisation controllers in each loop plus a polarisation controller before port 1 of the circulator ensured the light fed back through both loops matched the emitted light polarisations to maximise feedback effectiveness.

5.3 Effects of Feedback Strength on the RF Linewidth and Integrated Timing Jitter Using Single and Asymmetric Dual-Loop Feedback

To investigate the effects of external optical feedback on RF linewidth and integrated timing jitter using single-loop feedback, the attenuation in the gain section was varied from the minimum achievable feedback level -46 dB to the maximum feedback -22 dB before the laser became unstable. The feedback ra-

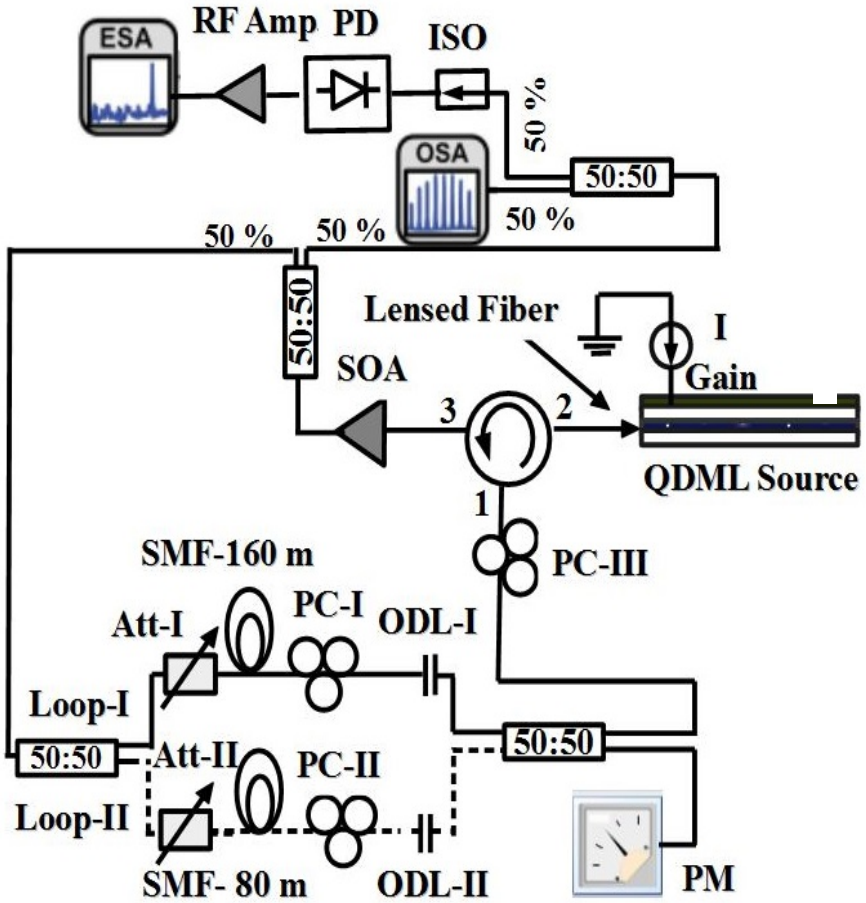

Figure 5.2: Schematic of the experimental arrangement for a single (excluding dashed portion) and asymmetric dual-loop configurations (with dashed portion). *Acronyms*; SOA: Semiconductor optical amplifier; ISO: Optical isolator; PD: Photodiode; RF Amp.: RF Amplifier; ODL: Optical delay line; Att: Optical attenuator; PC: polarisation controller; ESA: Electrical spectral analyser; OSA: Optical spectrum analyser; SMF: Single mode fibre; PM: Power meter.

tio in the gain section was set to one of nine chosen values (-46 dB, -39 dB, -36 dB, -31 dB, -29 dB, -26 dB, -24 dB, -23-dB and -22 dB). These results demonstrate that at -46 dB, -39 dB and -36 dB, the RF linewidth was 80 kHz, 61.3 kHz, and 60 kHz respectively for single-loop feedback. Under feedback attenuations -46 dB, -39 dB and -36 dB, the corresponding RMS timing jitter was reduced to 3, 2.7 and 2.6 ps, respectively (integrated from 10 kHz to 100 MHz). At this low feedback attenuation (-46 dB, -39 dB and -36 dB), the effects of external optical feedback were very small, so that no major reduction in RF linewidth and timing jitter was seen relative to free-running (100 kHz). With increased feedback ratio to -29 dB, gradual decreases in the RF linewidth and RMS jitter were observed. This feedback level (-29 dB) gave RF linewidth as low as 11 kHz, with RMS timing jitter as low as 1.38 ps. Further, increase in feedback level to -22

dB resulted in saturation of the RF linewidth and timing jitter. The minimum achieved RF linewidth and integrated timing jitter as functions of feedback ratio for integer resonant cases are depicted in Fig. 5.3. Furthermore, measured RF spectra and phase-noise traces using single-loop feedback are shown in Figs. 5.4(a) and (b), respectively, for three chosen feedback attenuations (-46 dB, -29 dB and -22 dB).

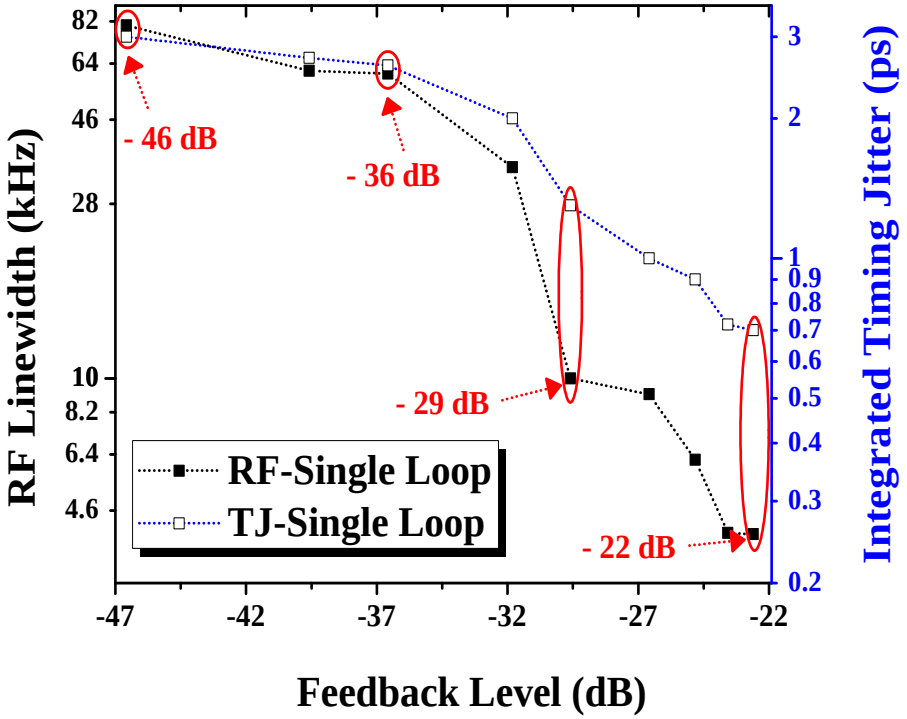

Figure 5.3: 3-dB RF linewidth (solid black squares) and integrated timing jitter (hollow blue squares) as a function of external feedback ratio at 300 mA gain current for single-loop feedback.

To study the influence of external optical feedback on RF linewidth and integrated timing jitter using asymmetric dual-loop feedback, the optical power was split into two equal parts via a 3-dB coupler. The resulting feedback ratio into the gain section was set to -22 dB. To achieve stable resonant conditions for dual-loop feedback, the first optical delay line (ODL-I) was tuned to full resonance while the second optical delay line (ODL-II) was fine-tuned. When both feedback cavities were fully resonant, RF linewidth narrowing and reduced timing jitter were achieved. The feedback ratio in the gain section was set to one of nine chosen values (-46 dB, -39 dB, -36 dB, -31 dB, -29 dB, -26 dB, -24 dB, -23-dB and -22 dB). The measured experimental results reveal that at -46 dB, -39 dB and -36 dB, the RF linewidth was 70 kHz, 60 kHz, and 58 kHz respectively for dual-loop feedback. Under feedback attenuations -46 dB, -39 dB and -36 dB, the corresponding RMS timing jitter was reduced to 3, 2.9 and 2.8 ps,

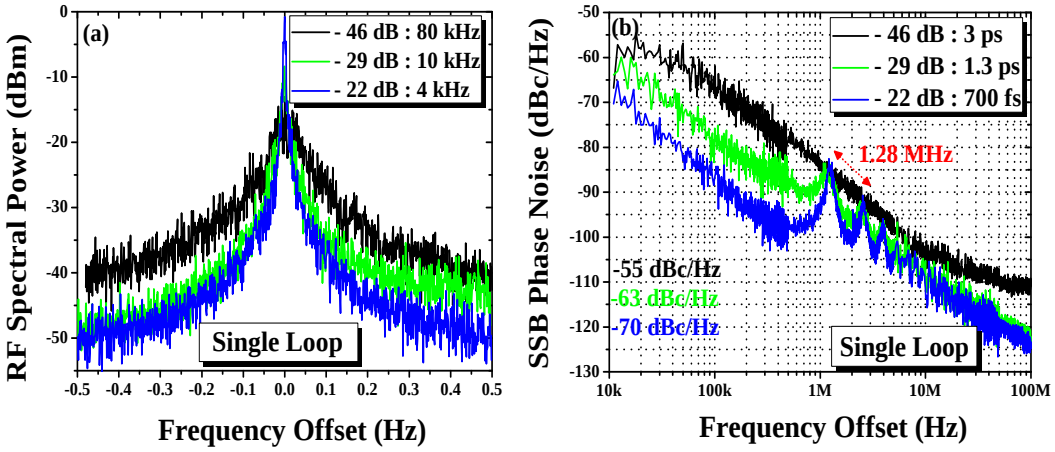

Figure 5.4: (a) Measured RF spectra using frequency span 1 MHz (resolution bandwidth 1 kHz and video bandwidth 100 Hz) under fully resonant condition as a function of three chosen feedback attenuations (-46 dB, -29 dB and -22 dB) using single-loop feedback configuration (b) Measured SSB Phase-noise traces under fully resonant condition as a function of three chosen feedback attenuations (-46 dB, -29 dB and -22 dB) using single-loop feedback configuration with integration limits 10 kHz - 100 MHz.

respectively (integrated from 10 kHz to 100 MHz). Similar to single-loop feedback, at low feedback attenuations (-46 dB, -39 dB and -36 dB), the effects of external optical feedback were very small, so that no significant reduction in RF linewidth and timing jitter was observed relative to free-running and single-loop feedback. However, with increased feedback ratio to -29 dB, a gradual decrease in the RF linewidth and RMS timing jitter was noted. This feedback level (-29 dB) gives RF linewidth as low as 10 kHz, with RMS timing jitter as low as 1.38 ps. Further increase in feedback ratio to -22 dB yielded saturated RF linewidth and timing jitter. The minimum achieved RF linewidth and timing jitter, as functions of feedback ratio for integer resonant cases, are depicted in Fig. 5.5. Furthermore, measured RF spectra and phase-noise traces using asymmetric dual-loop feedback are shown in Figs. 5.6(a) and (b), respectively for three chosen feedback attenuations (-46 dB, -29 dB and -22 dB). From this detailed experimental analysis of RF linewidth versus feedback strength, we have identified optimal parameters for single and asymmetric dual-loop configurations, with a strong reduction in RF linewidth and timing jitter. Our results demonstrate that for practical applications, the relatively flat characteristics of RF linewidth versus feedback ratio (-24 dB, -23-dB and -22 dB) are more favorable. Variation in RF linewidth and timing jitter in both single and asymmetric dual-loop feedback follows similar trends when feedback approaches the optimal value, which agrees well with reported square root dependence of RF

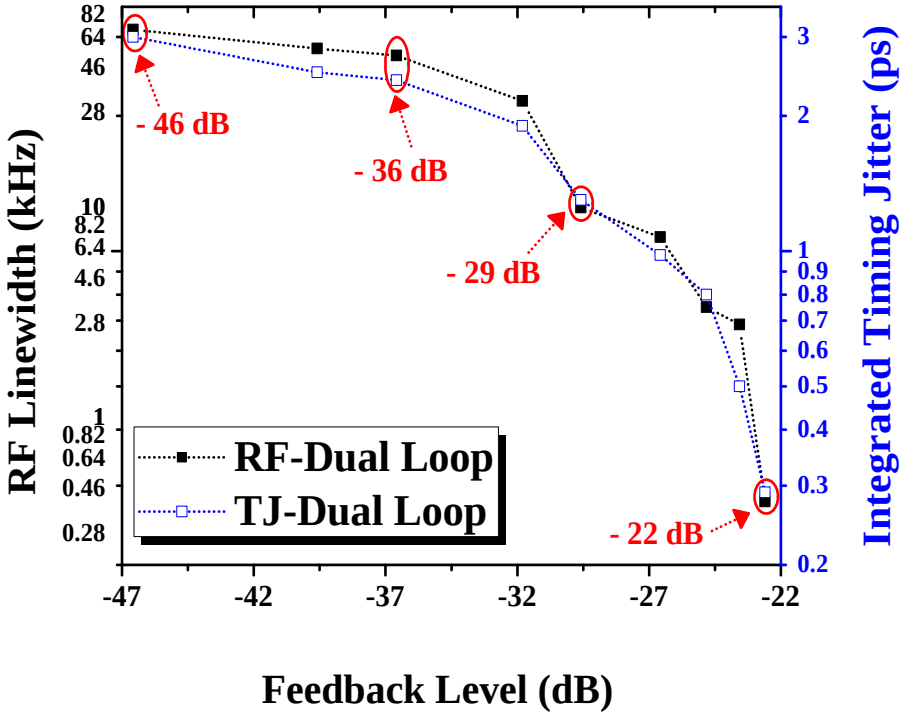

Figure 5.5: RF linewidth (solid black squares)and integrated timing jitter (hollow blue squares) as a function of external feedback ratio at 300 mA gain current for asymmetric dual-loop feedback.

linewidth on integrated timing jitter [116].

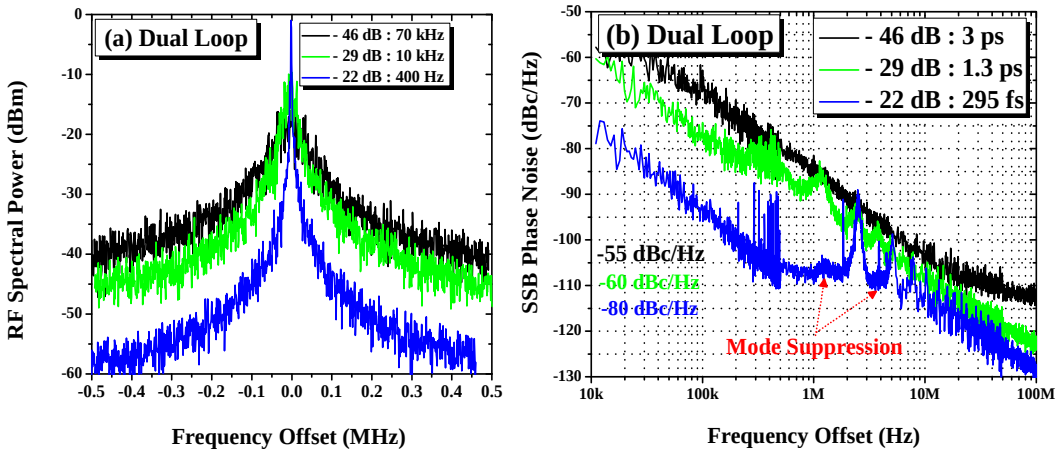

Figure 5.6: (a) Measured RF spectra using frequency span 1 MHz (resolution bandwidth 1 kHz and video bandwidth 100 Hz) under fully resonant condition as a function of three chosen feedback attenuations (-46 dB, -29 dB and -22 dB) using asymmetric dual-loop feedback (b) Measured SSB phase-noise traces under fully resonant condition as a function of three chosen feedback attenuations (-46 dB, -29 dB and -22 dB) using asymmetric dual-loop feedback with integration limits 10 kHz - 100 MHz.

5.4 RF Linewidth and Integrated Timing Jitter Versus Delay for Single-Loop Feedback

To study the dynamic effects of single-loop feedback on RF linewidth and noise properties of MLLs, fine-tuning of one polarisation controller (PC-I) was done and maximum feedback to the gain section was limited to -22 dB using the variable optical attenuator (Att-I). A schematic of the single-loop optical feedback setup is shown in Fig. 5.7.

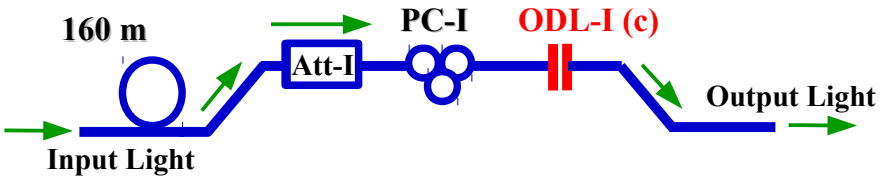

Figure 5.7: Basic schematic of single-loop optical feedback setup; Acronyms– ODL: Optical delay line; Att: Optical attenuator; PC: polarisation controller.

To achieve stable resonant conditions for the single-loop, the microscopic length of the feedback cavity was optimized using an optical delay line (ODL-I), adjustable from 0 to 84 ps in steps of 1.67 ps. This optimisation of the single feedback loop delay reduced the RF linewidth considerably, as with reported experiments [77, 79] and theoretical predictions [85]. Resulting RF linewidth (black squares) and timing jitter (blue triangles) are shown in Fig. 5.8 versus delay tuned from 0-84 ps; clearly, the efficacy of single-loop feedback is highly dependent on feedback delay. As the feedback delay phase was tuned, the system adapted such that the pulses in the laser cavity are synchronised with the pulses in the feedback cavity. Under this situation, significant reduction in RF linewidth and reduced timing jitter was observed. It can be seen from measured experimental results (see Fig. 5.8), over delay ranges 0-13 and 60-78 ps that effective stabilisation is achieved, as the external cavity length was close to an integer multiple of that of the solitary laser.

When fully resonant (13 and 63 ps delay), the RF linewidth decreased from 100 kHz free-running to 4 kHz. In addition, SSB phase-noise - 70 dBc/Hz at a frequency offset 10 kHz was measured. Due to this decrease in phase-noise, the timing jitter reduced from 3.9 ps free-running to 700 fs [10 kHz – 100 MHz]. Measured RF spectra is shown in Fig. 5.9(a). The measured phase-noise traces for the free-running laser (gray line) and single-loop feedback (blue line) as

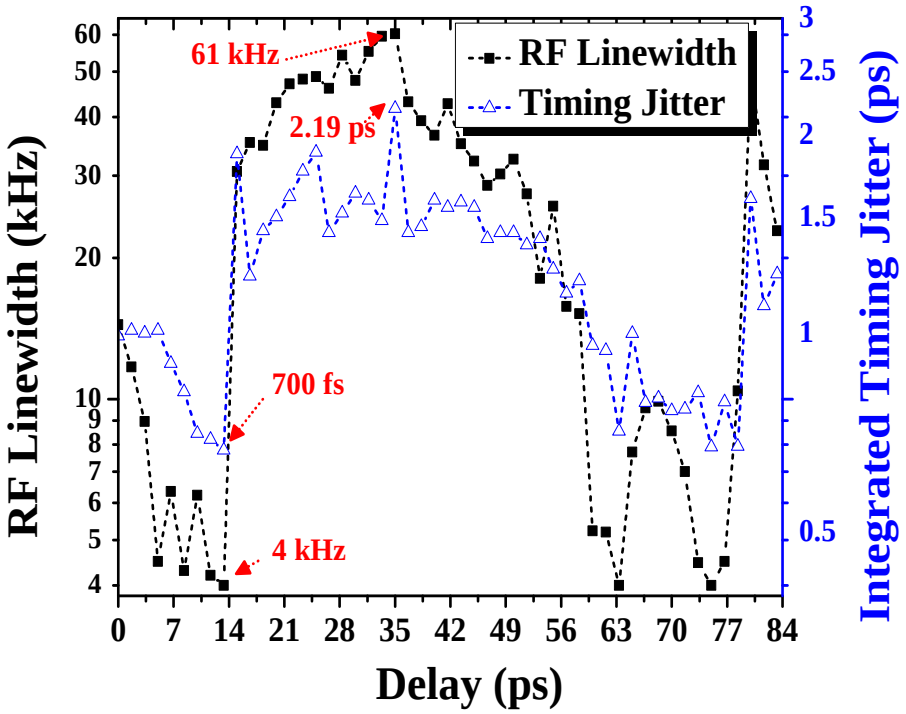

Figure 5.8: RF linewidth (black squares) and integrated timing jitters (blue triangles) of mode-locked pulse trains as a function of full delay phase tuning [0 – 84 ps] for single-loop optical feedback.

functions of frequency offset from the fundamental mode-locked frequency are depicted in Fig. 5.9(b).

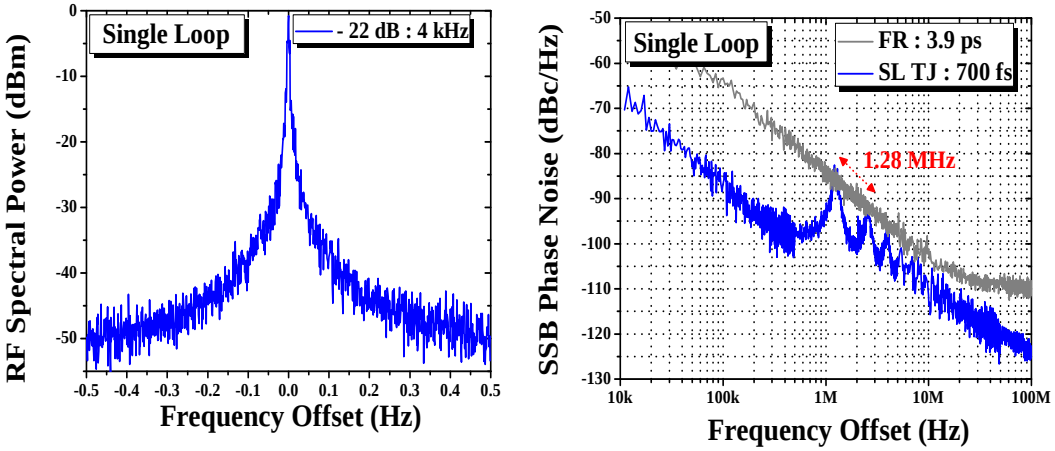

Figure 5.9: Measured RF spectrum for asymmetric dual-loop configurations using 1 MHz frequency span (resolution bandwidth 1 kHz and video bandwidth 100 Hz (b) Comparison of SSB phase-noise traces of single-loop feedback (blue line) with free-running condition (gray line) using integration limits 10 kHz - 100 MHz).

In addition, under fully resonant condition (delay 13 ps), strong side-modes

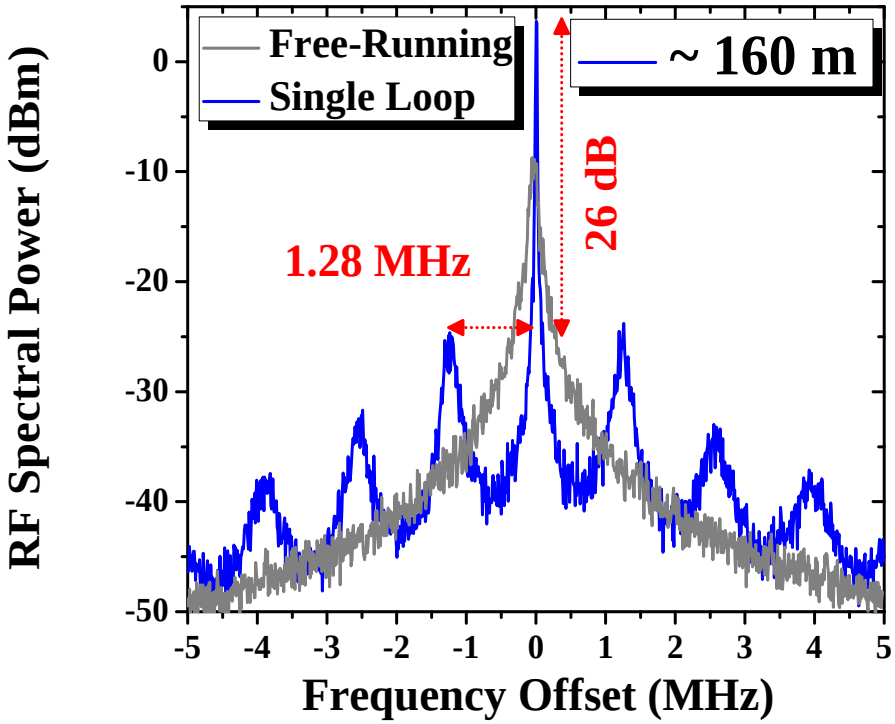

Figure 5.10: Comparison of RF Spectra of single-loop feedback (blue line) with length 160 m and free-running laser (gray line) using frequency span 10 MHz (resolution bandwidth 10 kHz and video bandwidth 1 kHz).

appeared at frequency spacing 1.28 MHz, corresponding to the length of the feedback loop (160 m). The external cavity modes can be seen in the SSB phase-noise trace and are more prominent under optimal feedback level (-22 dB). Comparison of the free-running RF spectrum (gray line) with RF spectra measured with single-loop optical feedback (blue line) is shown in Fig. 5.10. Frequency resonances a few MHz from the fundamental mode-locked frequency make significant contributions to integrated timing jitter. Most recently, an asymmetric dual-loop feedback scheme with the second loop shorter than the main loop has been demonstrated [109, 110] to suppress these external cavity side-modes. We will discuss such suppression in Section 5.6.

Under the fully resonant condition (delay 13 ps) the peak power of the RF spectrum rose by 52 dB. However, for the free-running condition, the peak power of the RF spectrum was observed to be 20 dB. For single-loop feedback, this 32 dB increase in peak spectral power is a result of reduced RF linewidth which contributes to increase in optical power. The peak power of the RF spectrum was measured at each delay length and is shown in Fig. 5.11 as a function of full delay phase tuning.

From measured RF linewidth, integrated timing jitter and RF peak power as

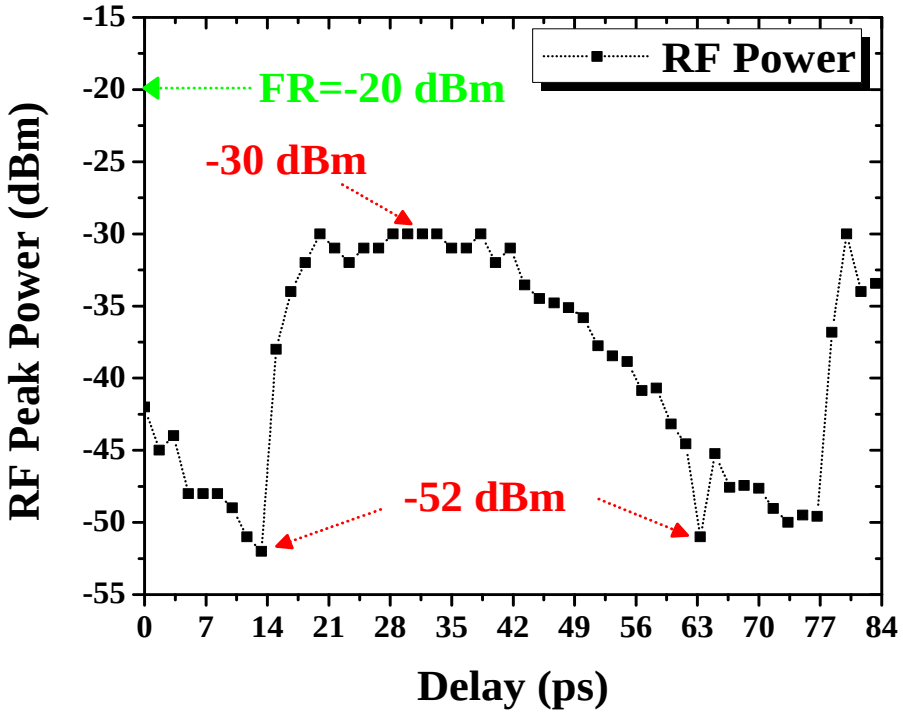

Figure 5.11: Peak power of RF spectra of mode-locked pulse trains as a function of full delay phase tuning [0 – 84 ps] for single-loop optical feedback and its comparison with free-running situation.

functions of delay, we observed that, at delay settings from 15-58 ps and 80-83 ps, the laser became highly unstable in its noise emission: RF linewidth broadened to 61 kHz and RMS timing jitter to 2.2 ps at delay 35 ps. This occurs because the delay time is tuned too far from the fundamental mode-locked frequency, the system cannot adapt its periodicity and the pulses become highly deformed. Experimental results on single-loop feedback show that for practical use of MLLs, the most suitable and stable delay ranges are close to resonant regimes (0-13 ps and 60-78 ps). However, this is still quite sensitive to packaging and production. In the next section, we describe how to reduce the sensitivity of resonant single-loop feedback using a stable and efficient asymmetric dual-loop feedback scheme which is practical, robust and cost-effective.

5.5 RF Linewidth and Integrated Timing Jitter Versus Delay for Balanced Asymmetric Dual-Loop Feedback Configurations

In asymmetric dual-loop feedback, simultaneous optical feedback from two external cavities was applied to the gain section at -22 dB, using the setup shown in Fig. 5.2. Feedback from both cavities was kept equal using the variable optical attenuators (Att-I and Att-II) plus fine adjustment of the polarisation controllers (PC-I and PC-II) in both feedback loops. The first optical delay (ODL-II) was adjusted to full resonance and the length of the second optical delay line (ODL-I) was tuned from 0-84 ps, the maximum range available. This arrangement yielded much better dynamics: stable narrow RF spectra were maintained across the full delay range, unlike single-loop feedback. This asymmetric dual-loop scheme reduced the RF linewidth 2.5-4x compared to single-loop, and 4-100x relative to free-running. Measured RF linewidth (black squares) and timing jitters data (blue triangles) versus delay are shown in Fig. 5.12.

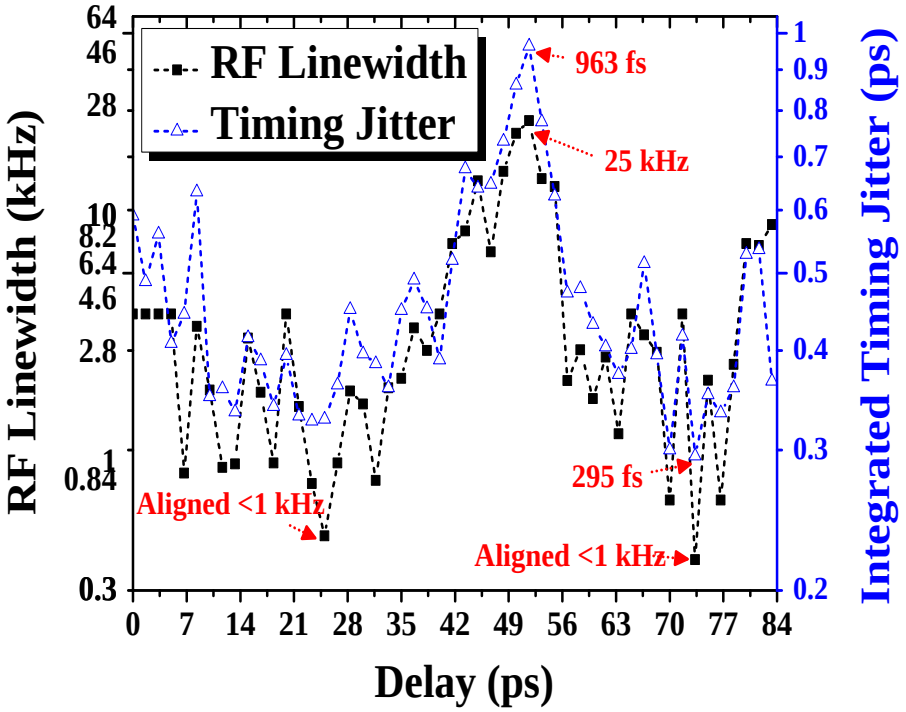

Figure 5.12: RF linewidth (black squares) and integrated timing jitters (blue triangles) of mode-locked pulse trains as a function of full optical delay tuning in asymmetric dual-loop feedback.

It was observed that at multiple optical delay ranges [Figs. 5.13 (a) and (b)] the

RF linewidth was instrument limited at less than 1 kHz, so the actual value may be lower. RF spectra is shown in Fig. 5.14. This shows that under these delay settings the RF linewidth was > 100x less than free-running. This behavior indicates that to maximise the RF linewidth, fine tuning of both optical delay lines is required. Furthermore, in this experiment, from delay settings 0-40 ps and 56 -78 ps, the RF linewidth was below the minimum RF linewidth measured for single-loop feedback; see Fig. 5.13(b).

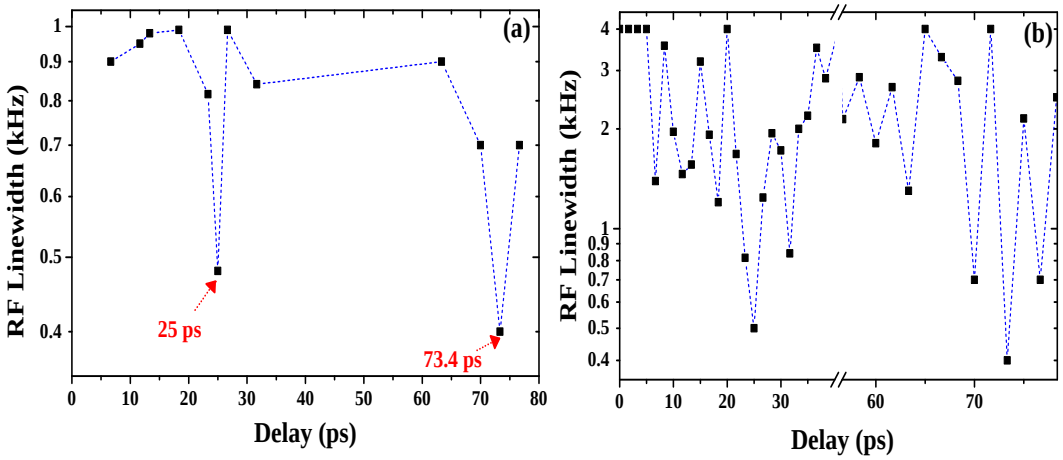

Figure 5.13: (a) 3 RF linewidth as a function of optical delay less than 1 kHz (instrumental limited) (b) RF linewidth as a function of optical delay [0-40 ps and 56 ps- 78 ps] less than 4 kHz (minimum RF linewidth measured in single-loop feedback).

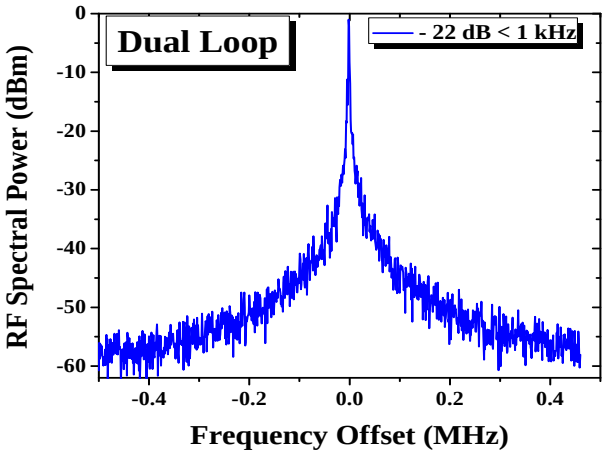

Figure 5.14: Measured RF spectrum for asymmetric dual-loop configurations using 1 MHz span (resolution bandwidth 1 kHz and video bandwidth 100 Hz).

Our results demonstrate that asymmetric dual-loop feedback is an effective and robust means of maintaining jitter stabilisation over wide delay phase tuning compared to single-loop feedback. The impact of asymmetric dual-loop optical feedback on the noise properties of our QDash lasers as a function of delay is

shown in Fig. 5.12 (blue triangles). Recently, the regime of resonance optical feedback configuration has been identified in the delay range 5 - 20 ps using single-loop feedback for a 40 GHz QDot mode-locked laser [78]. However, our proposed asymmetric dual-loop scheme maximises the resonant feedback regime from delay range 0 - 40 ps and 56 - 78 ps. Furthermore, we can see that the resonant condition in asymmetric dual-loop feedback is independent of optical delay, which makes it ideal for various practical applications because it offers a cost-effective control input.

Moreover, from the RF spectra, it is noticeable that the peak power of the RF spectrum in asymmetric dual-loop spectra rises by up to 63 dB. This increased RF peak power was 11 dB higher than single-loop feedback and 43 dB higher than free-running, and is a result of reduced RF linewidth and reduced threshold current which contributes to increase in optical power. The variation in RF peak power as a function of full delay phase tuning is shown in Fig. 5.15.

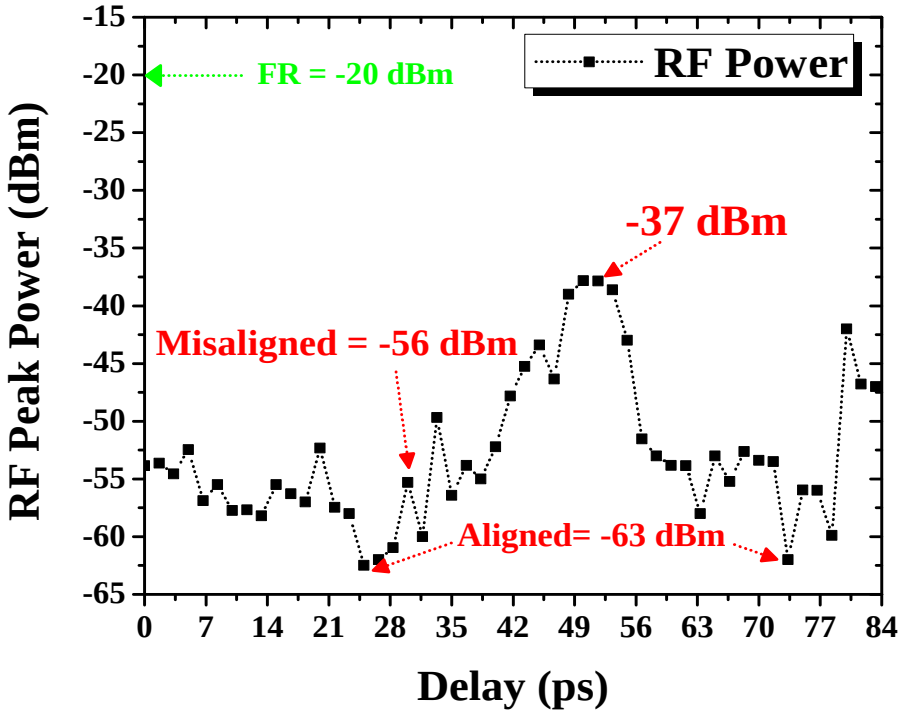

Figure 5.15: Peak power of RF spectra of mode-locked pulse trains as a function of full delay phase tuning (0 – 84 ps) for dual-loop optical feedback and its comparison with free-running situation.

5.5.1 Asymmetric dual-loop optical feedback subject to unbalanced feedback ratio

In the following, we observed the variation in RF linewidth versus delay with different percentage of power split ratio through two external feedback cavities based on asymmetric dual-loop optical feedback. Three combinations of feedback ratios studied in this study are presented in Table. 5.1. A schematic of asymmetric dual-loop feedback is shown in Fig. 5.16.

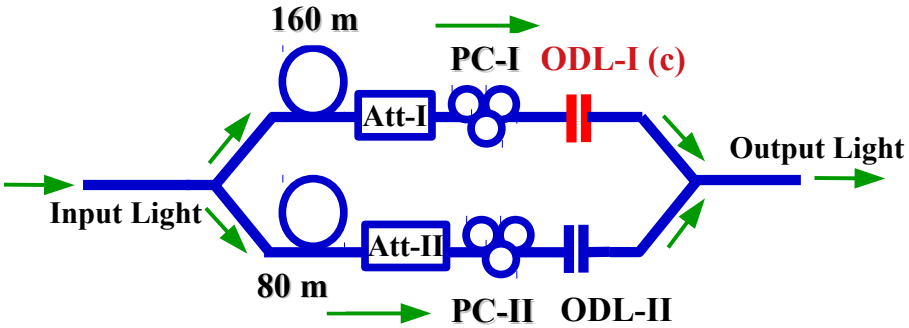

Figure 5.16: Schematic of asymmetric dual-loop feedback; Acronyms– ODL: Optical delay line; Att: Optical attenuator; PC: polarisation controller.

Table 5.1: Three chosen combinations of feedback ratio through either feedback loop and overall feedback strength into gain section.

Loop-I	Loop-II	Total Feedback at Gain
-22 dB (0.625%)	-22 dB (0.625%)	-22 dB (0.625%)
-23.29 dB (0.47%)(c)	-28.06 dB (0.16%)	-22 dB (0.625%)
-23.29 dB (0.47%)	-28.06 dB (0.16%)(c)	-22 dB (0.625%)

In above section, we experimentally investigated the RF linewidth and timing jitter over a wide range of delay tuning in SML QDash lasers subject to balanced asymmetric dual-loop optical feedback. However, in following, we further demonstrated and investigated stabilisation of SML QDash lasers subject to different power split ratio through the external feedback loops which is asymmetric dual-loop feedback. In this case, fine adjustment of polarisation controllers (PC-I and PC-II) and optical delay line (ODL-I) was done. In addition, phase delay attached with a weaker cavity (ODL-II) was set to integer resonance then we fine-tuned the stronger cavity (ODL-I (c)). Feedback ratio through loop-I and loop-II was fixed to -23.29 and -28.06 dB using variable optical attenuators (Att-I and Att-II), respectively. The RF linewidth versus delay is shown in Fig. 5.17(b) (red circles). These results demonstrates that

RF linewidth versus delay yields severe instabilities over a widest range of delay tuning when the weaker cavity (ODL-II) is set to an integer resonance the stronger cavity (ODL-I(c)) is fine tuned. When both feedback cavities were fully resonant, the RF linewidth narrowing to as low as 1.3 kHz was noted. Measured RF spectrum under integer resonance is shown in Fig. 5.18 (red line).

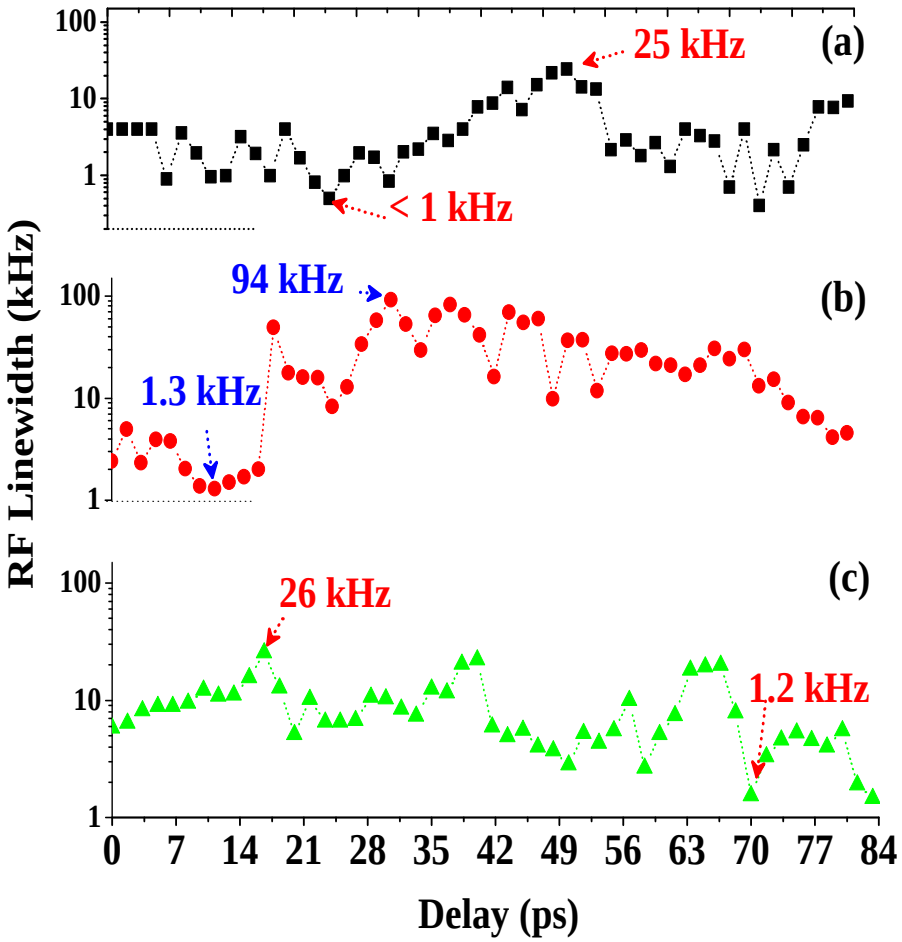

Figure 5.17: Measured RF linewidth versus delay using asymmetric dual-loop optical feedback with power split ratio (a) loop-I:-22 dB; loop-II:-22 dB (black squares) (b) loop-I(c):-23.29 dB; loop-II: -28.06 dB (red squares) (c) loop-I:-23.29 dB; loop-II(c):-28.06 dB (green triangle).

For the next combination of power split, the phase delay of the strong cavity (ODL-I=-23.29 dB) was set to integer resonance then fine-tunes the weaker cavity fine-tuned (ODL-II (c)) (-28.06 dB). RF linewidth versus delay is shown in Fig. 5.17(c) (green triangles) and under double resonance the RF linewidth was reduced to 1.2 kHz. However, for the widest delay range, a significant reduction in RF linewidth was observed. Measured RF spectra under integer resonance is shown in Fig. 5.18 (green line).

These results demonstrate that different power split ratios have significant in-

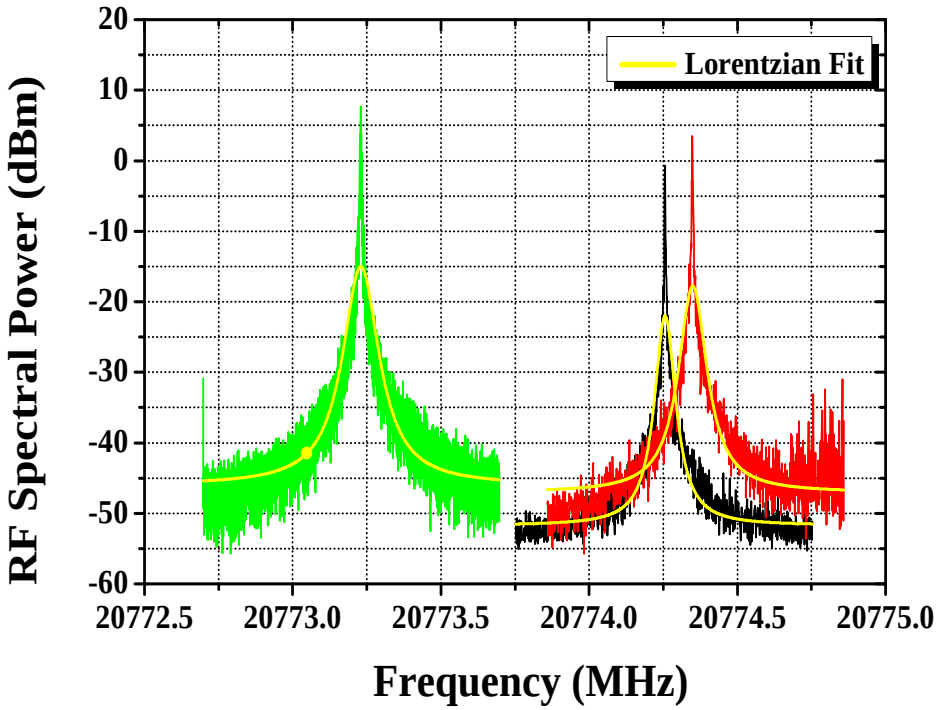

Figure 5.18: Measured RF spectra using frequency span 1 MHz (resolution bandwidth 1 kHz and video bandwidth 100 Hz) as a function of power split ratio (a) loop-I:-22 dB; loop-II:-22 dB (black line) (b) loop-I(c):-23.29 dB; loop-II: -28.06 dB (red line) (c) loop-I:-23.29 dB; loop-II(c) (green line).

Table 5.2: Three chosen combinations of feedback ratio through either feedback loop using asymmetric dual-loop optical feedback and measured minimum and maximum RF linewidth for each case.

Loop-I	Loop-II	Minimum RF	Maximum RF
-22 dB	-22 dB	1 kHz	25 kHz
-23.29 dB(c)	-28.06 dB	1.3 kHz	94 kHz
-23.29 dB	-28.06 dB(c)	1.4 kHz	26 kHz

fluences on the RF linewidth of our SML QDash laser subject to asymmetric dual-loop at integer resonance, as well as the widest range of delay tuning. In addition, these measurements further reveal that stabilisation of SML QDash lasers can be improved by controlling parameters such as the power split ratio and optical delay tuning using asymmetric dual-loop optical feedback.

5.6 Suppression of External Cavity Side-Modes using Asymmetric Dual-Loop Optical Feedback

As demonstrated in the above section, to achieve lower timing jitter, fine-tuning of both external feedback cavities is desirable. To investigate the side-mode suppression effects, a series of dual-loop feedback experiment was performed with the following lengths (shown in Table 5.3) in two external feedback cavities.

Table 5.3: Lengths of loop-I and loop-II in balanced asymmetric dual-loop optical feedback.

Feedback Scheme	Loop-I	Loop-II
Asymmetric dual-loop	160 m	80 m
Asymmetric dual-loop	205 m	40 m
Asymmetric dual-loop	2 km	200 m

5.6.1 Asymmetric Dual-Loop Optical Feedback with Loop Lengths 160 m and 80 m

For asymmetric dual-loop experiments, the optical feedback was split into two fibre cavities whose lengths were calibrated by measurement of RF spectra with each loop unblocked separately. For the first set, the cavity spacing was 1.28 MHz consistent with the 160 m nominal length of loop-I. For the second, the cavity frequency spacing was 2.6 MHz in agreement with the 80 m length of loop-II. RF spectral measurements with this arrangement are shown in Figs. 5.19(a) and (b).

To explore the influence of asymmetric dual-loop optical feedback on side-mode suppression ratio (SMSR), one delay (ODL-I) was set to 25 ps, the other (ODL-II) fixed to 15 ps then every second mode of loop-I coincided precisely with a mode of loop-II. As a result, a maximum of 30 dB suppression in the first order side-mode occurred (see Fig. 5.19(c)) the RF linewidth narrowed to 1 kHz. SSB phase-noise was as low as -80 dBc/Hz at frequency offset 10 kHz and the integrated timing jitter was reduced to 295 fs [10 kHz – 100 MHz]. Optimal suppression of external cavity side-modes occurred due to the interference of the two delayed feedback signals at the 3 dB coupler. Modal overlap in the RF spectrum was observed for spectral alignment of the modes of the two fibre loops having identical intensity and resemble as RF frequency comb (see Fig.

5.19(d)). Exact conditions for modal overlap, of course, depends on the precise optical lengths of the feedback loops; here we noted 2.60 MHz spacing between supermodes, in agreement with our 80 m outer loop.

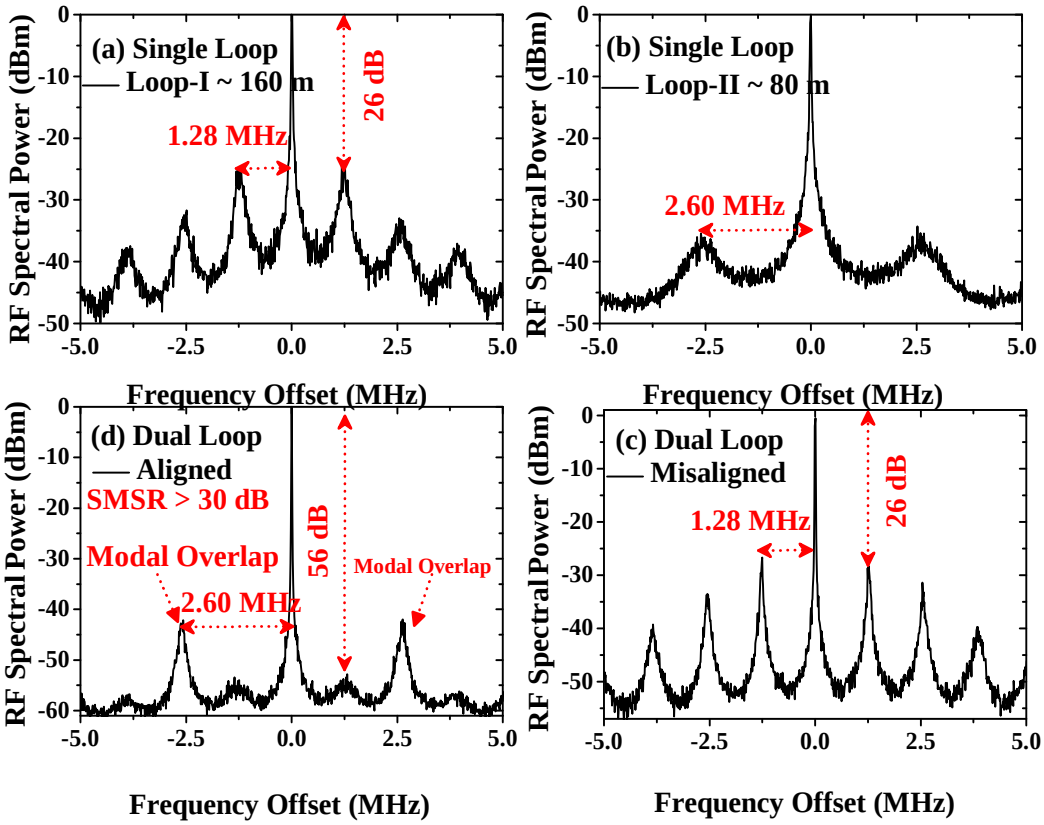

Figure 5.19: RF Spectra of single loop feedback with length (a) 160 m (b) 80 m (c) dual loop having spectrally aligned cavity lengths with > 30 dB sidemode suppression (d) RF spectrum of spectrally offset (misaligned) dual loop cavity with strong side-mode: All spectrums are measured using Span=10 MHz, resolution bandwidth=10 kHz and video bandwidth = 1 kHz.

However, with slight tuning offset between the modes of both fibre loops, strong side-modes appear with intensity -26 dBm (see Fig. 5.19(d)) and at the same time, the RF linewidth is reduced to 1.94 kHz and the integrated timing jitter approaches 450 fs [10 kHz – 100 MHz]. The SSB phase-noise traces for asymmetric dual-loops subjected to aligned (blue line) and misaligned (black line) cavity states are depicted in Fig. 5.20. From measured RF spectra of single-loop optical feedback and misaligned dual-loop feedback: the expected noise-resonances appear around the fundamental mode-locked frequency, contributing significantly to the phase-noise. The 155 fs reduction in timing jitter for the aligned cavity state as compared to the misaligned one, further confirms this argument.

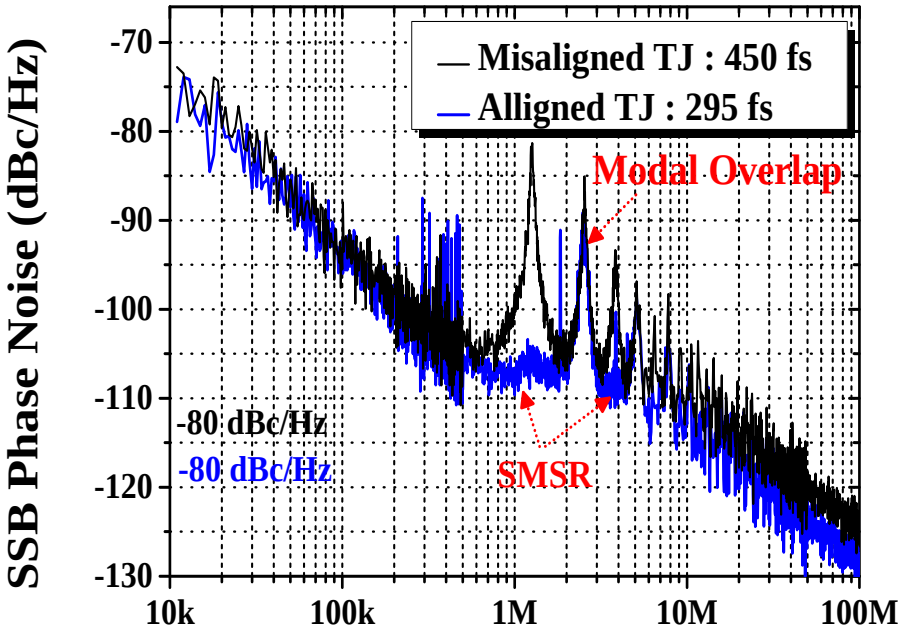

Figure 5.20: SSB phase-noise traces for misaligned asymmetric dual-loop (black line) and aligned asymmetric dual-loop (blue line) with integration limits 10 kHz - 100 MHz.

5.6.2 Asymmetric Dual-Loop Optical Feedback with Length of Loop-I=185 m and Loop-II $\sim$ 20 m

To further investigate side-mode suppression, we used another experimental arrangement, replacing 160 m and 80 m fibre loops with 185 m and 20 m fibre in the experimental arrangements shown in Fig. 5.2. The schematic of single and asymmetric dual-loop optical feedback configuration is depicted in Fig. 5.21.

The single-loop feedback was measured when loop-II was disconnected and the resulting spectrum was measured using a frequency span of 10 MHz (black line in Fig. 5.22) and 100 MHz (black line in Fig. 5.23). The spacing between the side-modes was 0.99 MHz which corresponded well with a feedback loop $\sim$ 206 m. When loop-I was disconnected, the configuration again acted as a single-loop, and the RF linewidth narrowed to 12 kHz. However, when the parallel arms of the two feedback loops were connected and the length of loop-I was varied so that every fourth mode of the inner fibre loop was in precise alignment with a mode of the outer, suppression of the first side-mode was demonstrated with SMSR > 23 dB. Measured RF spectra for asymmetric dual-loop feedback are shown in Fig. 5.22 (blue line) and Fig. 5.23 (blue line), respectively. This suppression occurred due to the interference of the two delayed optical signals

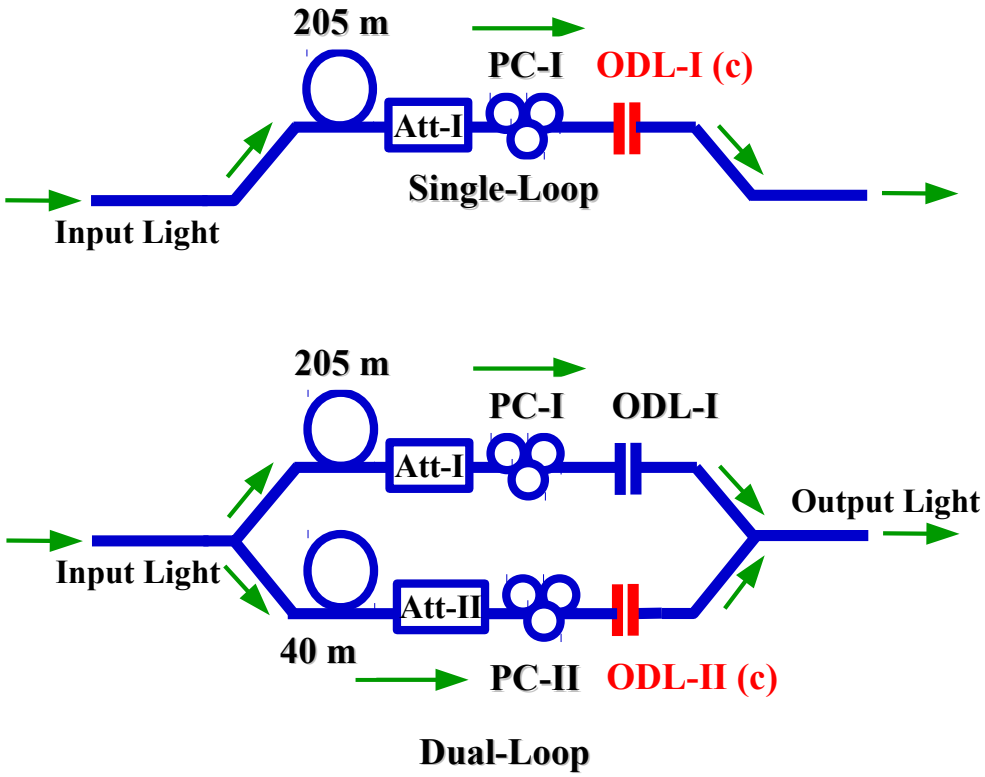

Figure 5.21: Schematic of single- and asymmetric dual-loop optical feedback; Acronyms– ODL: Optical delay line; Att: Optical attenuator; PC: polarisation controller.

at the 3-dB coupler. Consequently, a strong reduction in additional side-modes and phase-noise was observed. Modal overlap in the RF spectrum could be observed due to constructive interference of the modes of the inner and outer fibre loops. The modal overlap depends on the ratio of the two feedback loops. Under optimal feedback level and fully resonant condition, the RF linewidth was reduced from 100 kHz to < 1 kHz for dual-loops and 12 kHz for single-loop feedback. RF linewidth measured using asymmetric dual-loops was $>$ 100x lower than the free-running condition and $>$ 12x than single-loop feedback.

In addition, the timing jitter associated with optical pulses generated by our two-section QDash SML laser was also reduced from 3.9 ps free-running to 400 fs for asymmetric dual-loop feedback and 800 fs for a single-loop. RMS timing jitter was calculated by integrating the phase-noise trace from 10 kHz to 100 MHz.

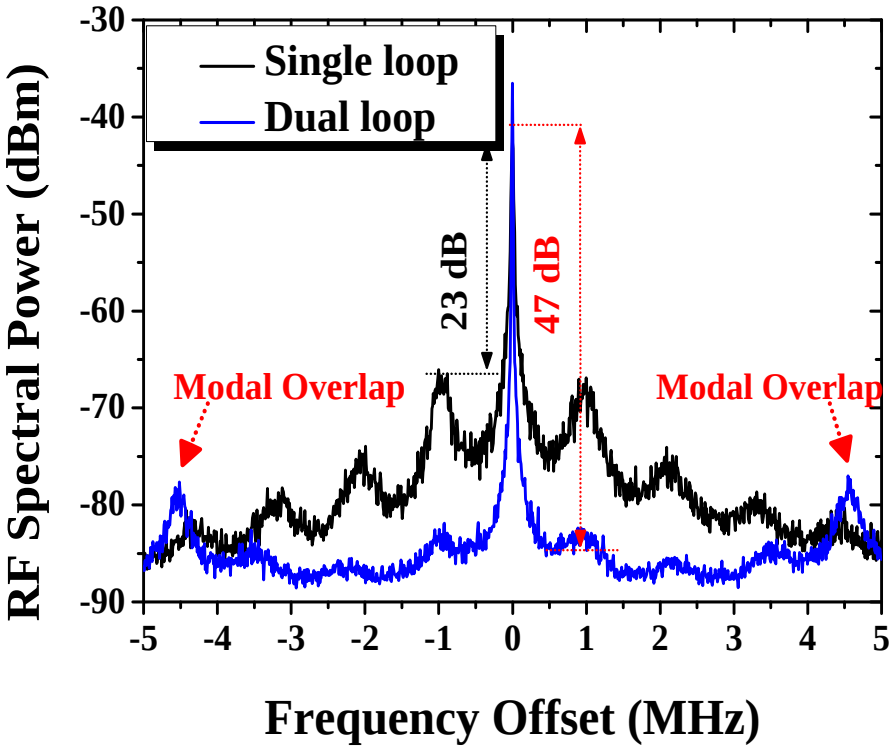

Figure 5.22: RF spectra measured using single (black line) and asymmetric dual-loop feedback (blue line) with frequency span 10 MHz (resolution bandwidth 10 kHz and video bandwidth 1 kHz).

5.6.3 Asymmetric Dual-Loop Optical Feedback with Length of Loop-I=2 km and Loop-II=200 m

Opto-electronic oscillators (OEOs) can generate signals or tens of gigahertz with fibre lengths of 1 km or more. That means the mode spacing in their RF spectra ranges from several hundred to tens of kilohertz. It is very difficult to design a filter with a bandwidth narrow enough to select a single mode at multiple GHz [103]. To overcome these issues, optoelectronic feedback [104] can also be utilized to stabilise timing jitter and to suppress cavity side-modes by conversion of the optical oscillation (using a fast photodetector) to an electrical signal used in a long feedback loop.

In this section, a simpler asymmetric dual-loop feedback technique without optical/electrical conversion has been demonstrated to improve timing jitter and to filter or suppress unwanted spurious side-bands. A schematic of the single and asymmetric dual-loop optical feedback setup is shown in Fig. 5.24. With fibre lengths of 2.25 km, signals of a few gigahertz are generated with mode spacing 90 kHz away from the fundamental mode-locked frequency, as shown

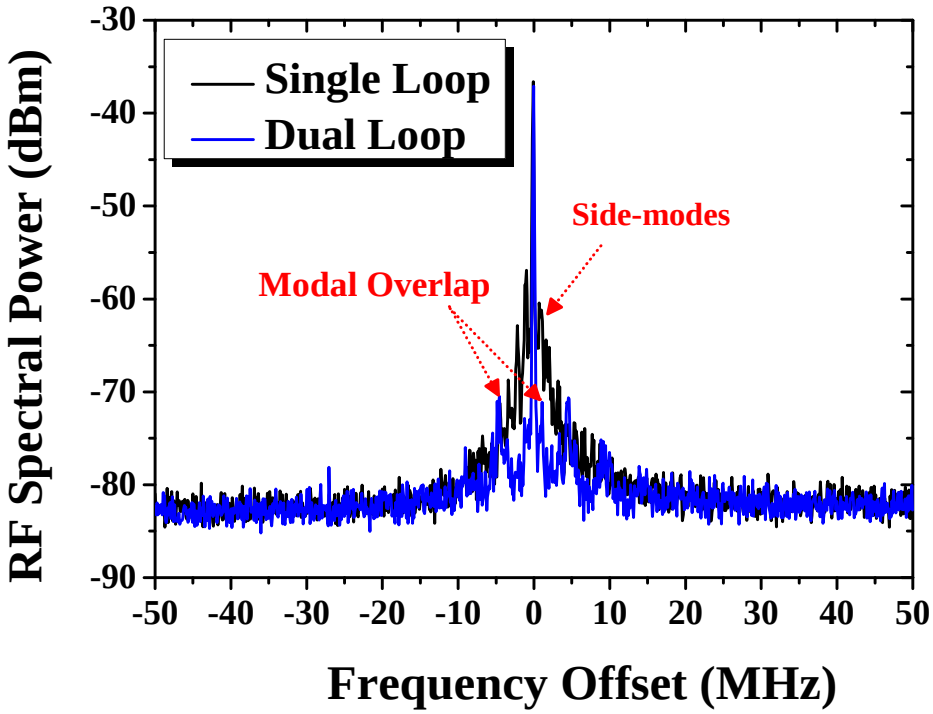

Figure 5.23: RF spectra measured using single (black line) and asymmetric dual-loop feedback (blue line) with frequency span 100 MHz (resolution bandwidth 100 kHz and video bandwidth 10 kHz).

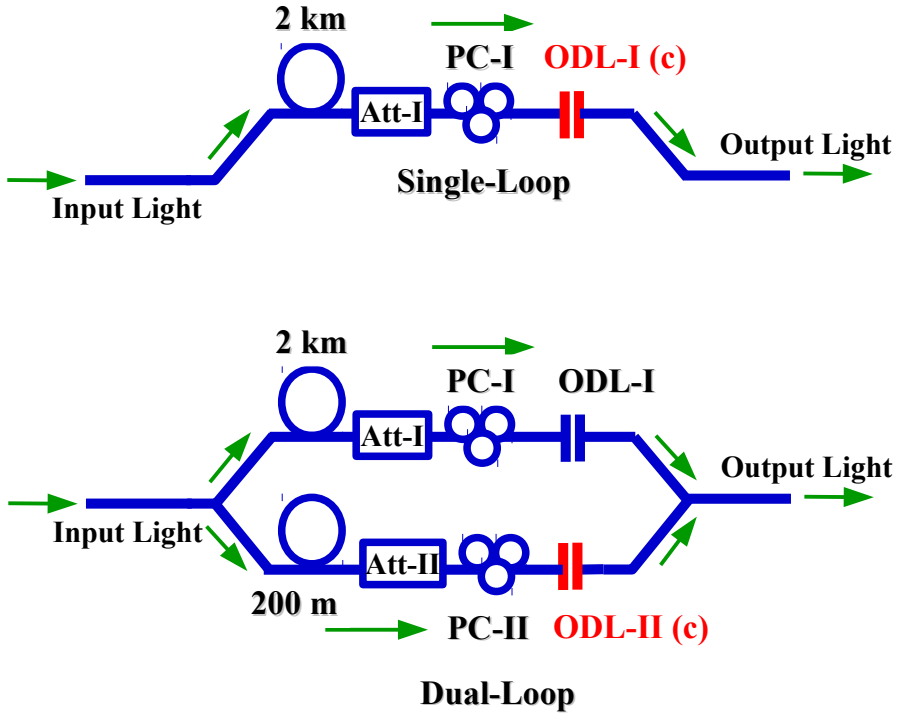

Figure 5.24: Basic schematic of single and asymmetric dual-loop optical feedback; Acronyms– ODL: Optical delay line; Att: Optical attenuator; PC: polarisation controller.

in Fig. 5.25 (black line). Upon fine-tuning of both external feedback loops, the asymmetric dual-loop configuration suggested here (Loop-I=2 km and Loop-II=200 m) is a promising approach which leads to significant suppression in external cavity side-modes closer to the main peak, and the fundamental frequency oscillates in the resonator cavity and becomes a carrier signal. Measured RF spectra are shown in Fig. 5.25 using single-loop feedback with fibre lengths 2 km (black line), 200 m (red line) and dual-loop (blue line) feedback. The asymmetric dual-loop feedback method demonstrated in this chapter is a robust and powerful technique which effectively suppresses unwanted noise-induced oscillations and yields side-band free RF spectra. Measured RF linewidth, integrated timing jitter and SMSR are summarised in Table 5.4 for single and asymmetric dual-loop feedback.

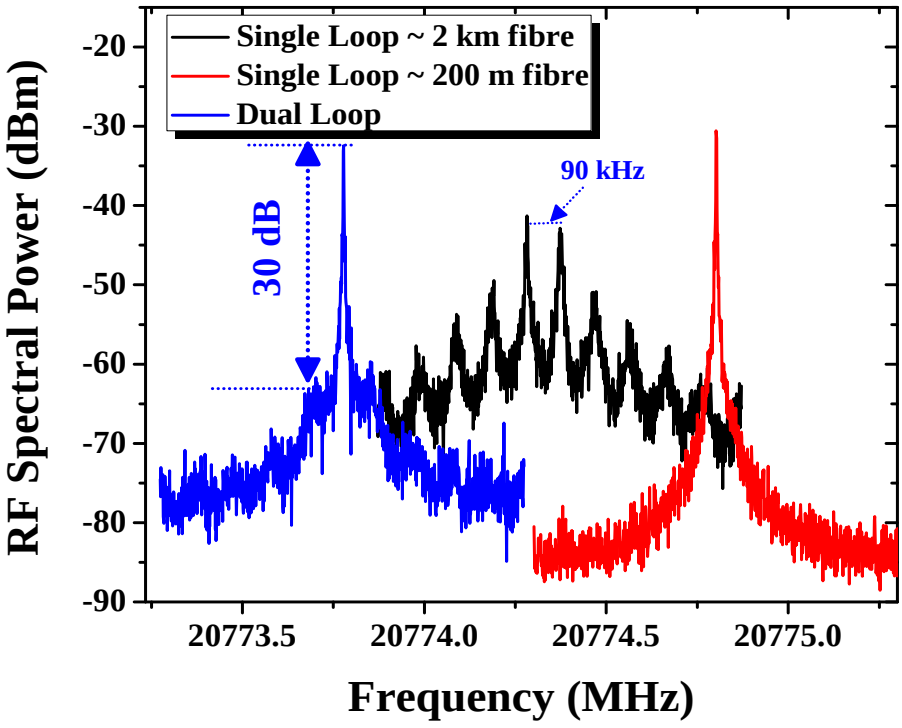

Figure 5.25: Measured RF spectra using single-loop feedback with length 2.25 km (black line), 200 m (red line) and asymmetric dual-loops having lengths 2.25 km for loop-I and 200 m for loop-II under frequency span 1 MHz (resolution bandwidth 1 kHz and video bandwidth 100 Hz).

5.7 Summary

This chapter has highlighted the effects of external optical feedback from asymmetric dual- and single-loop optical feedback on the RF linewidth and tim-

Table 5.4: Comparison of RF Linewidth, Timing Jitter and SMSR using single- and asymmetric dual-loop feedback configuration.

Feedback Scheme	**Loop-I**	**Loop-II**	**RF (kHz)**	**TJ (ps)**	**SMSR (dB)**
free-running	-	-	100	3.9	-
single-loop	160 m	-	4	0.7	-
single-loop	80 m	-	3 kHz	0.65	-
dual-loop	160 m	80 m	<1 kHz	0.295	30
single-loop	205 m	-	12 kHz	0.8	-
dual-loop	205 m	40 m	< 1 kHz	0.4	23
single-loop	-	200 m	< 1 kHz	-	-
dual-loop	2 km	200 m	< 1 kHz	-	30

ing jitter for a wide range of delay tuning. The feedback level which yielded narrowest RF linewidth and reduced timing jitter was identified to be $\sim$ -22 dB for single-loop and asymmetric dual-loop feedback. It was observed that single-loop feedback produced effective stabilisation near the resonant feedback regime (5 and 53 ps) and generated additional noise-resonances a few MHz away in the power spectrum. To extend the regime of resonant optical feedback and to suppress adverse noise fluctuations, a dual-loop feedback configuration with the second loop shorter than the main one was used. We showed that asymmetric dual-loop feedback has far greater tolerance to delay phase tuning than single-loop feedback. Moreover, optimised asymmetric dual-loop feedback extends the effective resonant feedback regime and maintains stable RF spectra, with narrow RF linewidth and reduced timing jitter across the entire accessible delay range, making this setup desirable for practical applications. Using external feedback loops which were doubly resonant achieved significant suppression in external cavity side-modes relative to single-loop feedback. These results suggest that optimised asymmetric dual-loop feedback is a robust and effective means to overcome the most difficult performance limitations of mode-locked diode lasers, namely large timing jitter and tendency to exhibit instabilities.

Chapter 6

Asymmetric Dual-Loop Feedback to Suppress Spurious-Tones in SML QDash Lasers

6.1 Introduction

In this chapter, we will show how additional noise-resonances induced in conventional single- and dual-loop feedback schemes can be suppressed by appropriately choosing the relative loop lengths. We will further explore the length ratio between the two cavities in asymmetric dual-loop configurations which are desired to achieve best SMSR and lowest timing jitter. It will be further observed that RF linewidth and integrated timing jitter were reduced by increasing the length of the second cavity. Measured experimental results will be compared with recently reported numerical simulations. Our findings suggest that noise stabilisation and side-mode suppression depend strongly on additional feedback delay times. The resulting setup was integrable in a transceiver package using hybrid integrated optics, passive optical networks (PONs) and/or compact fibre loops.

This chapter is structured as follows: In section 6.2, we will introduce the experimental setup. In section 6.3, we will show how additional noise-resonances induced in conventional single- and asymmetric dual-loop feedback schemes can be suppressed by appropriately choosing the length of the second feedback loop, and results will be compared with recently reported numerical simulations. Finally, the influence of side-mode suppression on the RF linewidth and

corresponding timing jitter of SML QDash laser will be presented in Section 6.4.

6.2 Suppression of Additional Noise-Resonances by Asymmetric Dual-Loop Feedback

Asymmetric dual-loop optical feedback, as proposed and demonstrated in the previous chapter, yielded sub-kHz linewidths and sub-picosecond timing jitter but produced additional noise peaks (modal overlaps) at frequencies resonant with the inverse of the delay time in the second cavity. These modal overlaps depend on the ratio of the two feedback loops and are undesirable in many applications where low noise and flat spectra are required, as in frequency comb generation. To eliminate these adverse dynamical effects, we have proposed and demonstrated an asymmetric dual-loop feedback with long and short optical cavities. The combinations of optical delay times used are given in Table 6.1.

Table 6.1: Comparison of RF Linewidth, Timing Jitter and SMSR using single- and dual-loop feedback configuration.

Feedback Scheme	**Loop-I**	**Loop-II**
Single-loop	160 m	-
Asymmetric dual-loop	160 m	80 m
Asymmetric dual-loop	160 m	53 m
Asymmetric dual-loop	160 m	20 m

A schematic for the asymmetric dual-loop experiment is depicted in Fig. 6.1. For single and dual-loop feedback configurations, a calibrated fraction of light was fed back through port 1 of an optical circulator, then injected into the laser cavity via port 2. Optical coupling loss from port 2 to port 3 was -0.64 dB. The output of the circulator was sent to a semiconductor optical amplifier (SOA) with a gain of 9.8 dB, then split into two arms by a 50/50 coupler. 50% went to an RF spectrum analyser (Keysight, E4407B) via a 21 GHz photodiode and to optical spectrum analysers (Ando AQ6317B and Advantest Q8384). The other 50% of power was split into two equal parts by a 3-dB splitter. For single-loop feedback, all power passed through loop-I. For asymmetric dual-loop configurations (feedback loops-I and-II) the power was split into two loops at the 3-dB splitter. Feedback strengths in both loops were controlled by variable optical

attenuators and monitored using power meters. In this experimental arrangement, the length of loop-I was fixed to 160 m while the length of the second feedback loop was set to one of the following lengths: 20, 53 and 80 m. polarisation controllers in each loop plus one polarisation controller before port 1 of the circulator ensured the light fed back through both loops matched the emitted light polarisations to maximise feedback effectiveness. In this experiment, the feedback ratio into the gain section was limited to -22 dB.

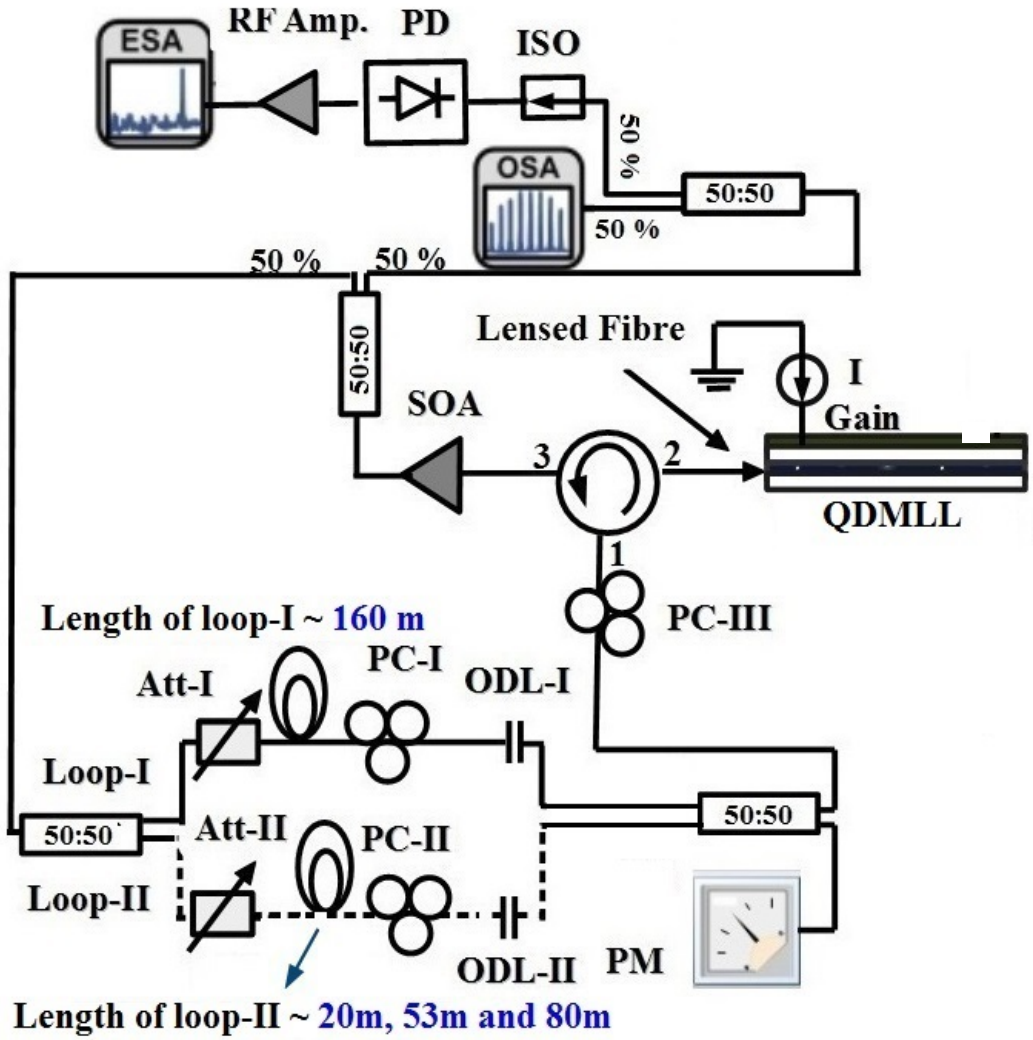

Figure 6.1: Schematic of the experimental arrangement for single (excluding dashed portion) and asymmetric dual-loop configurations (with dashed portion). *Acronyms*– SOA: Semiconductor Optical Amplifier; ISO: Optical isolator; PD: Photodiode; RF Amp.: RF Amplifier; ODL: Optical delay line; Att: Optical attenuator; PC: polarisation controller; ESA: Electrical spectrum analyser; OSA: Optical spectrum analyser; PM: Power Meter; QDMLL: Quantum-dash mode-locked laser.

6.3 Results and Discussions

In this section, we experimentally show that a second feedback loop can suppress additional noise-resonances, and how this influences the RF linewidth and timing jitter of MLLs.

6.3.1 RF Spectra of Single-Loop Feedback using 160 m Loop

To observe RF spectra with single-loop feedback, the loop was initially set at 160 m; optimally stable resonance occurred when the feedback length was fine-tuned using an optical delay line (ODL-I) which spanned 0 to 84 ps in steps of 1.67 ps. Such optimisation provides a resonant condition (at delay setting=13 ps) under which the RF linewidth was reduced from 100 kHz free-running to as low as 4 kHz, with integrated timing jitter to 0.7 ps from 3.9 ps [10 kHz - 100 MHz]. RF spectra and measured phase-noise traces as functions of frequency offset from fundamental mode-locked frequency are given in Figs. 6.2(a) and (b), for the free-running laser (gray line) and single-loop feedback (blue line), respectively. Under similar delay settings, external cavity side-modes appear in the RF spectrum with frequency spacing 1.28 MHz, the inverse of the loop round-trip delay. RF spectra are shown in Figs. 6.3(a) and (b), respectively. Frequency resonances can be seen in both frequency spans which contribute significantly to timing jitter, particularly for the longer feedback cavities as they are closer to the main peak and are less suppressed [100]. To eliminate these fluctuations and to improve the SMSR, asymmetric dual-loop feedback was implemented as described in the next section.

6.3.2 RF Spectra of Dual-Loop Feedback with Loop-I=160 m and Loop-II=80 m

To assess suppression of these frequency resonances, a shorter feedback cavity corresponding to half the period of the noise-induced oscillations of Loop-I was introduced. Feedback strengths of both cavities were equalised using the variable optical attenuators (Att-I and Att-II) plus polarisation controllers (PC-I and PC-II). One optical delay (ODL-II) was adjusted to full integer resonance and the length of the other delay line (ODL-I) was tuned over the maximum range available 0-84 ps. When ODL-I and ODL-II were fine-tuned (ODL-I=15 ps and

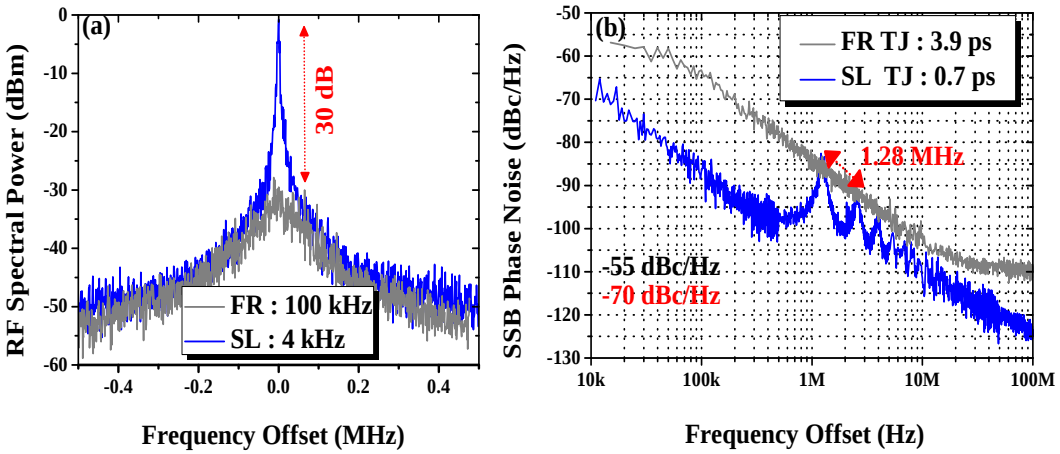

Figure 6.2: (a) Comparison of RF spectra for single-loop feedback (blue line) with free-running (gray line) using frequency span 1 MHz (resolution bandwidth 1 kHz and video bandwidth 100 Hz) (b) Comparison of phase-noise traces of free-running laser (gray line) with single-loop feedback (blue line) as a function of frequency offset from fundamental mode-locked frequency with integration limits 10 kHz - 100 MHz.

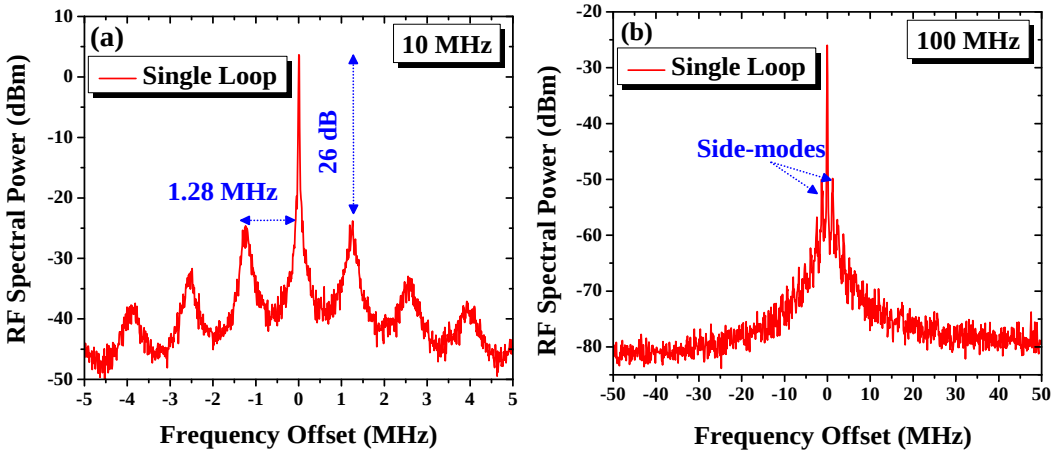

Figure 6.3: (a) RF Spectra of single-loop feedback of length 160 m (red line) using frequency span 10 MHz (resolution bandwidth 10 kHz and video bandwidth 1 kHz) (b) RF Spectra of single-loop feedback of length 160 m (red line) using frequency span 100 MHz (resolution bandwidth 100 kHz and video bandwidth 10 kHz).

ODL-II=25 ps) so that every second mode of loop-I coincided precisely with a mode of Loop-II, maximum >30 dB suppression in the first order side-mode was achieved. However, additional fluctuations (modal overlaps) appeared at frequencies resonant with the inverse of the length of the second delay time which became the carrier signal. These noise fluctuations depend on the ratio of the loop lengths. Here these fluctuations at frequency spacing 2.60 MHz are consistent with the length of the second feedback loop 80 m. RF spectra of the

asymmetric dual-loop configuration are shown in Figs. 6.4(a) and (b), respectively. In this fully resonant configuration, the RF linewidth narrowed to < 1 kHz (instrument limited), with timing jitter reduced to 295 fs. Comparison of RF spectra and phase-noise traces with free-running conditions are shown in the Figs. 6.5(a) and (b), respectively. Most recently, relative modulation suppression was determined from Floquet exponents and numerically calculated power spectra for a mode-locked laser were compared with Floquet spectra [112]]. It was observed that the n_2=495 [see Fig. 5(c) of Ref [112] fundamental mode was suppressed but additional fluctuations appeared at frequencies resonant with the inverse of the second delay time which agrees well with our experimentally measured power spectra [see Fig. 6.4(a)]. The RF spectra illustrated in Figs. 6.6 and 6.7 show that this feedback configuration is not suitable to achieve effective suppression in frequency resonances, as the second delay time will be resonant with the second mode of the first feedback loop. This restricts practical applications where flat and side-band free RF spectra are required. To improve this situation, a different dual-loop feedback configuration with non-resonant shorter second loop (53 m) was investigated, as described in the next section.

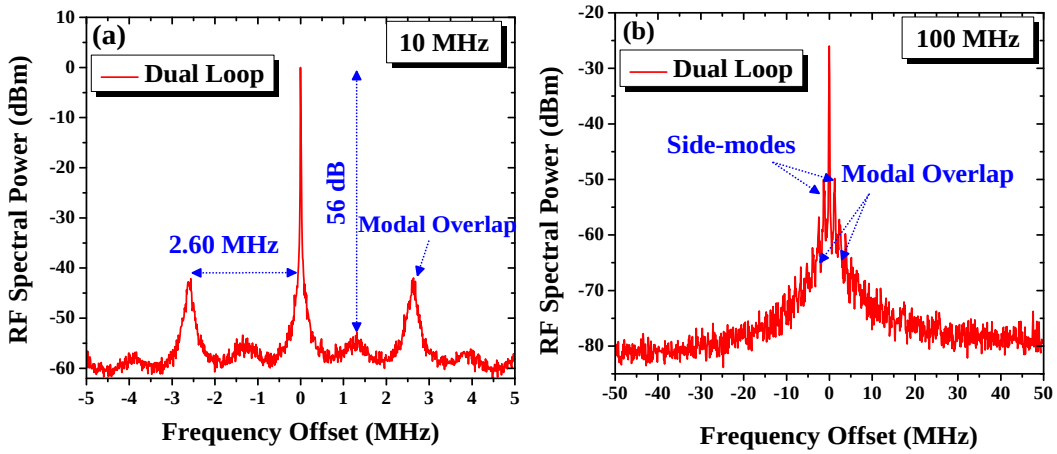

Figure 6.4: RF Spectra of asymmetric dual-loops having lengths 160 m for loop-I and 80 m for loop-II using frequency span (a) 10 MHz (resolution bandwidth 10 kHz and video bandwidth 1 kHz) (b) and frequency span 100 MHz (resolution bandwidth 100 kHz and video bandwidth 10 Hz).

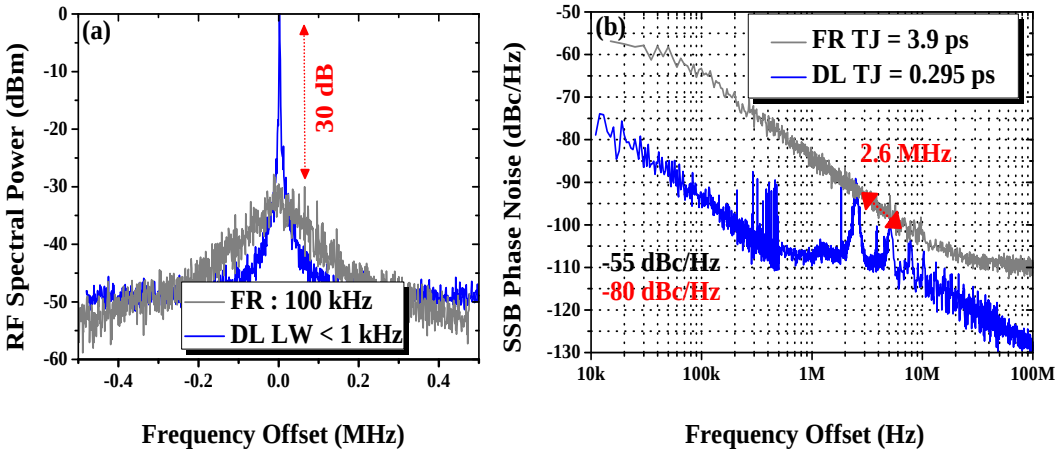

Figure 6.5: (a) Comparison of RF spectra for asymmetric dual-loop (blue line) and free-running (gray line) with frequency span 1 MHz (resolution bandwidth 1 kHz and video bandwidth 100 Hz) (b) Comparison of phase-noise traces of free-running laser (gray line) with asymmetric dual-loop feedback (blue line) using integration limits 10 kHz - 100 MHz.

6.3.3 RF Spectra of Dual-Loop Feedback with Loop-I=160 m and Loop-II=53 m

In the asymmetric dual-loop configuration presented in this section, the length of loop-I was initially set to 160 m while that of loop-II was 53 m. Upon fine-tuning of both optical delay lines (ODL-I=13 ps and ODL-II=15 ps), when the second delay time was resonant with the third harmonic of the first loop, suppression of the first two frequency resonances occurred, while the third harmonic (modal overlap) was unsuppressed. This harmonic was observed at a frequency offset 3.9 MHz, corresponding to the 53 m length of the outer feedback loop. RF spectra for the asymmetric dual-loop configuration are shown in Figs. 6.6(a) and (b), respectively. In this configuration, when both external cavities are fully resonant, the RF linewidth narrowed to 2 kHz with integrated timing jitter 0.45 ps. Comparison of RF spectra and phase-noise traces for asymmetric dual-loop (blue line) with free-running (gray line) are shown in Figs. 6.7(a) and (b), respectively. These measured results show that external cavity side-modes cannot be optimally suppressed by simply choosing the second feedback delay time to be a fraction of the first. Numerically it was observed that the n_2=325 [refer to Fig. 5(b) of Ref [112]], the first harmonic was suppressed but modal overlap occurred at a frequency resonant with the inverse of the third delay time which agrees well with our measured power spectra [Figs. 6.6(a) and (b)]. To achieve stable and flat RF spectra, we designed an asymmet-

ric dual-loop feedback configuration for effective suppression of external cavity side-modes. This produced flat RF spectra close to the main peak compared to conventional single- and asymmetric dual-loop feedback.

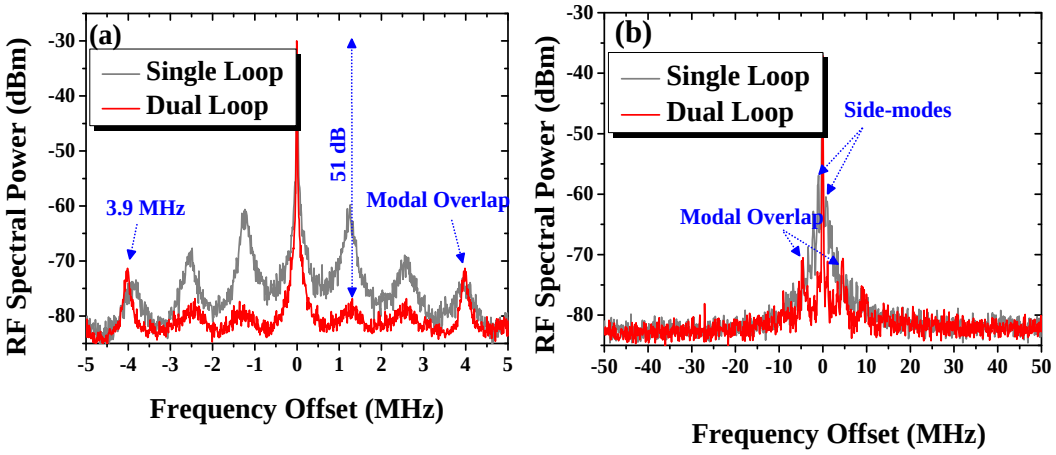

Figure 6.6: RF Spectra of single-loop feedback with length 160 m (gray line) and dual-loops having lengths 160 m for loop-I and 53 m for loop-II (red line) using frequency span (a) 10 MHz (resolution bandwidth 10 kHz and video bandwidth 1 kHz) (b) 100 MHz (resolution bandwidth 100 kHz and video bandwidth 10 kHz).

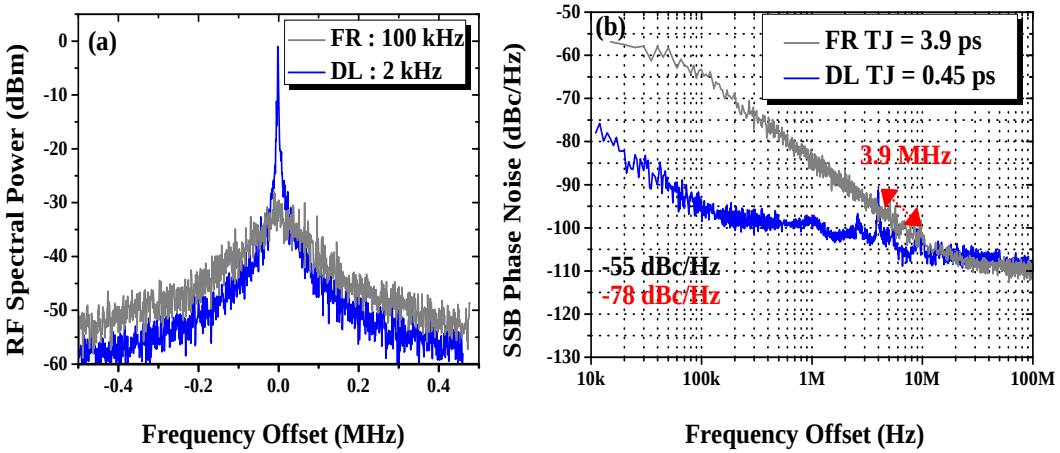

Figure 6.7: (a) Comparison of RF spectra measured for asymmetric dual-loop (blue line) and free-running (gray line) with frequency span 1 MHz (resolution bandwidth 1 kHz and video bandwidth 100 Hz) (b) Comparison of phase-noise traces of free-running laser (gray line) with asymmetric dual-loop feedback (blue line) with integration limits 10 kHz - 100 MHz.

6.3.4 RF Spectra of Dual-Loop Feedback with Loop-I=160 m and Loop-II $\sim$ 20 m

In this asymmetric dual-loop feedback, the length of Loop-I was fixed (160 m) and Loop-II was set $\sim$ 8x shorter than loop-I. Fine-tuning of both cavities (ODL-I=15 ps and ODL-II=21 ps) produced precise coincidence of every eighth mode of Loop-I with a mode of Loop-II so that strong side-mode suppression occurred and all feedback-induced side-modes and spectral resonances were eliminated. RF spectra for this asymmetric dual-loop feedback configuration (red line) are shown in Figs. 6.8(a) and 6.(b) using span 10 and 100 MHz, respectively. Furthermore, when both external cavities were fully resonant, the RF linewidth narrowed to 8 kHz with integrated timing jitter 0.6 ps. Comparison of RF spectra and phase-noise traces under double resonance with free-running conditions is shown in Figs. 6.9(a) and (b), respectively. In this configuration, the RF linewidth was higher than for single-loop feedback, but the measured timing jitter was lower; this is due to suppression of external cavity side-modes. In Ref [112], it was predicted that for n_2=90, the fundamental frequencies of the first feedback cavity would be significantly suppressed. However, modes corresponding to the 9th, 10th, and 11th harmonics are weakly suppressed. Our measured RF spectra [Figs. 6.8(a) and (b)], showed weak modal overlap (with intensity $\sim$ -6 dBm) at 10.2 MHz frequency spacing, consistent with our 20 m outer loop; this is shown in Fig. 6.8(b) (red line).

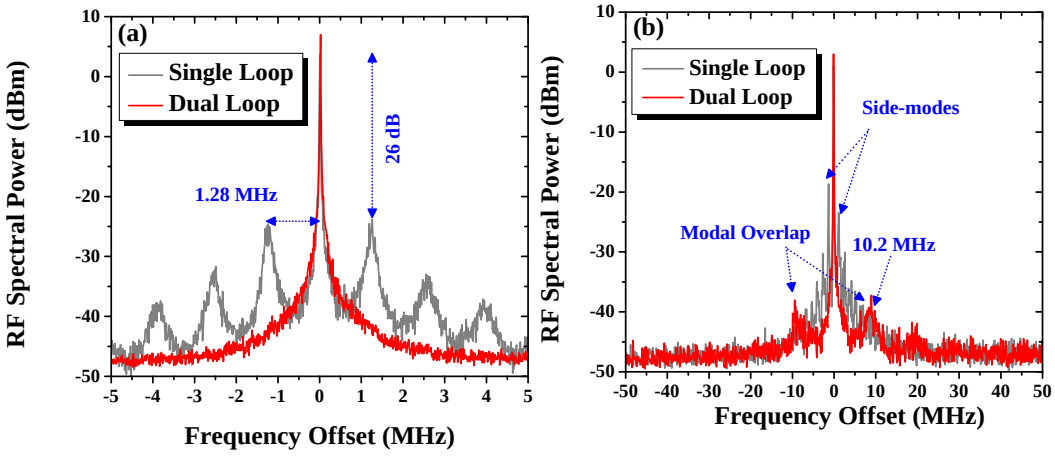

Figure 6.8: RF Spectra of single-loop feedback with length 160 m (gray line) and asymmetric dual-loops having lengths 160 m for loop-I and 20 m for loop-II (red line) using frequency span (a) 10 MHz (resolution bandwidth 10 kHz and video bandwidth 1 kHz) (b) 100 MHz (resolution bandwidth 100 kHz and video bandwidth 10 kHz).

Comprehensive analysis based on the above three different experimental configurations shows that the second feedback delay has a significant influence on the side-mode suppression, due to the long feedback cavity. This behaviour shows that effective suppression of external cavity side-modes and reduced timing jitter can be achieved by appropriately fine-tuning the length of the second feedback loop.

It should be noted that the length of loop-II ($\sim$ 20 m) is only optimal in our specific experimental setup. Further reduction in the length of the second feedback loop is not possible, as the combined variable optical attenuator, optical delay line, polarisation controller and 3-dB coupler have a minimum length of $\sim$ 20 m. Better suppression of cavity side-modes could be achieved in an arrangement not subject to this limitation, such as a photonic integrated circuit.

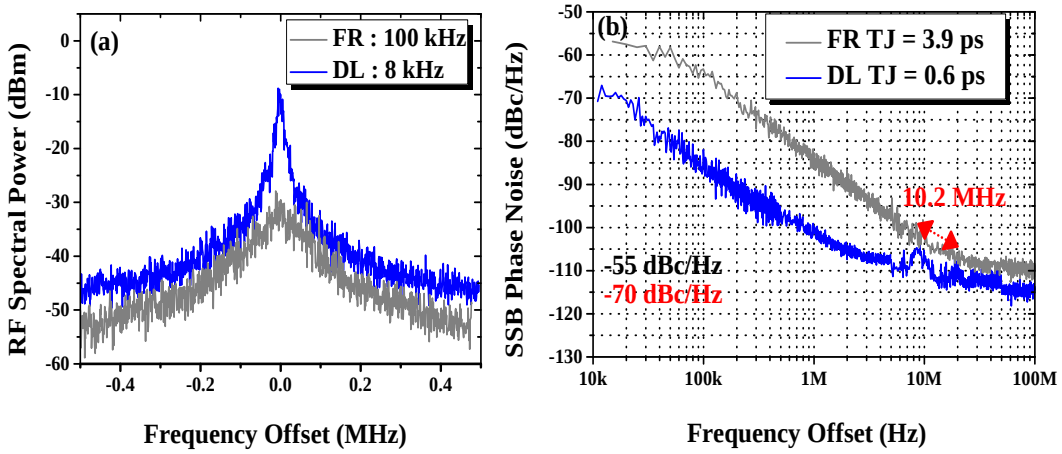

Figure 6.9: (a) RF Spectra measured for asymmetric dual-loop (blue line) and free-running (gray line) with frequency span 1 MHz (resolution bandwidth 1 kHz and video bandwidth 100 Hz) (b) Phase-noise trace of free-running conditions (gray line) with asymmetric dual-loops having lengths 160 m for loop-I and 20m for loop-II (blue line) with integration limits 10 kHz - 100 MHz.

Measured phase-noise traces for free-running condition (green line), single-loop (gray line) and asymmetric dual-loop feedback with loop-II at 20 m (red line), 53 m (black line) and 80 m (blue line) as functions of frequency offset from the fundamental mode-locked frequency, are given in Fig. 6.10. From measured phase-noise traces of single-loop optical feedback and asymmetric dual-loop feedback, the expected noise-resonances can be seen as functions of frequency offset from the fundamental mode-locked frequency, contributing significantly to the timing jitter.

Measured RF spectra under integer resonance are shown in Fig. 6.11 for free-running condition (green line), single-loop (gray line) and dual-loop feedback

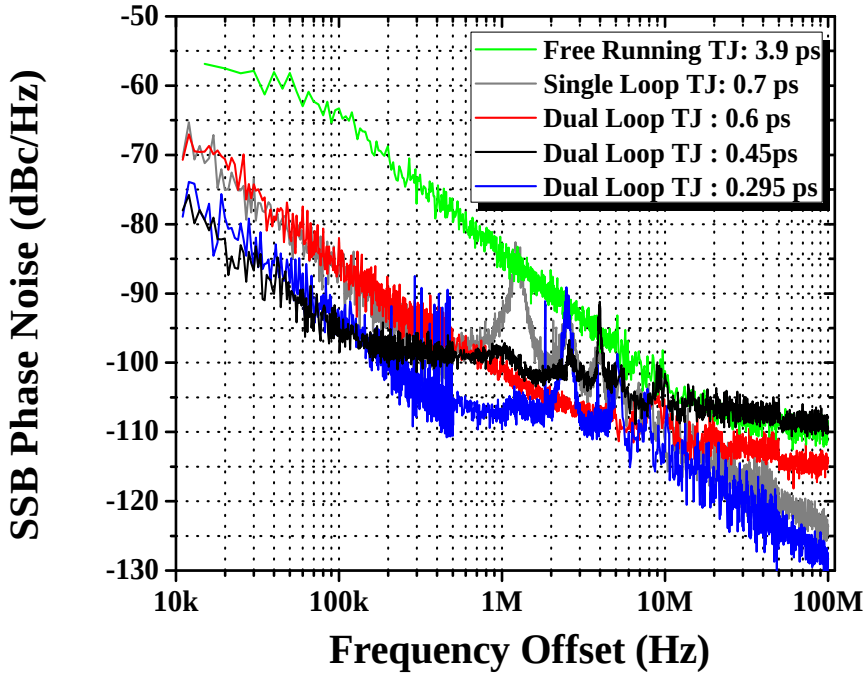

Figure 6.10: SSB phase-noise trace of free-running, single- and asymmetric dual-loop feedback configurations with loop-I = 160 m and loop-II ∼ 20 m (red line), 53 m (black line) and 80 m (blue line) under fully resonant condition with integration limits 10 kHz - 100 MHz.

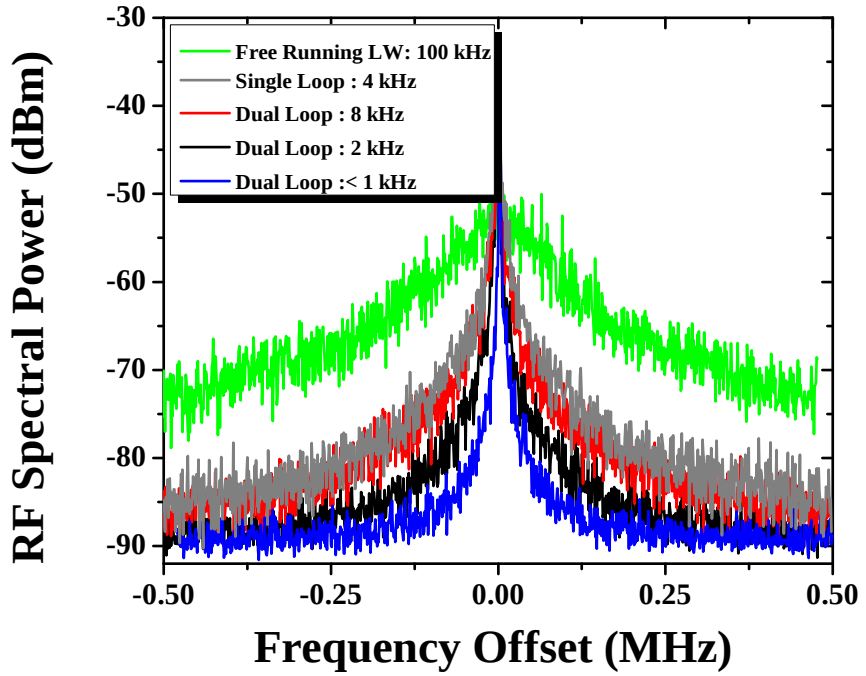

Figure 6.11: RF spectra for free-running, single- and dual-loop feedback with loop-I = 160 m and loop-II ∼ 20 m (red line), 53 m (black line) and 80 m (blue line) using frequency span 1 MHz (resolution bandwidth 1 kHz and video bandwidth 100 Hz).

with Loop-II at 20 m (red line), 53 m (black line) and 80 m (blue line). Variation in RF linewidth and timing jitter in single- and asymmetric dual-loop feedback followed a similar trend when feedback approached the optimal value, which agrees well with reported analytical results (square root dependence of the RF linewidth on integrated timing jitter) [116].

6.4 Influence of Side-Mode Suppression on Integrated Timing Jitter

We now describe investigation of the influence of side-mode suppression on the timing jitter of our QDash mode-locked laser. As observed in section 6.3, the external cavity side-modes for conventional single- and dual-loop feedback play a significant role in timing jitter. A comparison of RF linewidth and integrated timing jitter under stable resonant conditions, for three chosen lengths of the second feedback cavity, is shown in Fig. 6.12. Measured integrated timing jitter in all dual-loop configurations was lower than for single-loop feedback. However, the best suppression in external cavity side-modes was achieved with the second delay time $\sim$ 8x shorter than the first. Furthermore, the integrated timing jitter in this case was 16% lower than for single-loop feedback. Reduction in timing jitter occurs due to suppression of external cavity side-modes relative to single-loop feedback.

In the literature [109, 110], it was reported that side-mode suppression was achieved when both feedback delays had a common multiple. This shows that effective suppression in external cavity side-modes is highly dependent on the length of the second loop. Recently, the influence of the second loop delay on the suppression of external cavity side-modes [112] and timing jitter [112] was studied numerically. In this work, experimentally measured suppression of cavity side-modes and integrated timing jitter as a function of the second cavity delay corresponds well with published numerical simulations [112, 114].

6.5 Summary

In this chapter, we have reported a novel asymmetric dual-loop feedback scheme, suppressing parasitic noise-resonances when single-loop and dual-loop optical

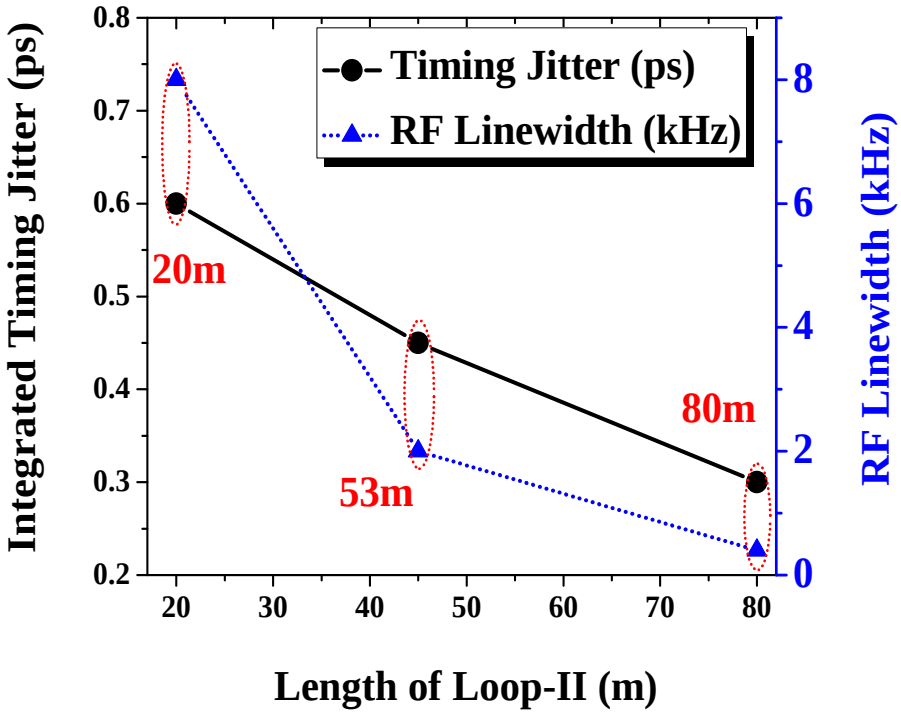

Figure 6.12: RF Linewidth (blue triangles) and Integrated timing jitter (black circles) for asymmetric dual-loop feedback with loop-I = 160 m and loop-II = 20, 53 and 80 m.

Table 6.2: Comparison of RF Linewidth, Timing Jitter and SMSR using single- and dual-loop feedback configuration.

Feedback Scheme	Loop-I	Loop-II	RF (kHz)	TJ (ps)	SMSR (dB)
Free-running	-	-	100	3.9	-
Single-loop	160 m	-	4	0.7	-
Dual-loop	160 m	80 m	<1 kHz	0.295	30
Dual-loop	160 m	53 m	2 kHz	0.45	25
Dual-loop	160 m	20 m	8 kHz	0.6	-

feedback was used to stabilise our InP based SML QDash laser. Conditions for optimum suppression were determined and compared with published theory.

To assess the SMSR, RF spectra were measured with fixed loop length 160 m, in which frequency resonances given by the inverse of the loop round-trip delay appeared spaced by 1.28 MHz from the fundamental mode-locked frequency. To eliminate these fluctuations and to improve the SMSR, asymmetric dual-loop feedback with successively three discrete lengths [80, 53, and 20 m] of the second loop was implemented. It was observed that with Loop-I=160 m and Loop-II=80 m, maximum >30 dB suppression in the first-order side-mode was achieved. However, additional noise fluctuations (modal overlap) appeared at frequencies resonant with the inverse of the second cavity which affects timing

jitter. To study the suppression of these parasitic frequency resonances, loop-I was fixed at 160 m and loop-II set to 53 m, then suppression of the first two frequency resonances occurred, while the third harmonic (modal overlap) remained unsuppressed. These modal overlaps depend on the ratio of the lengths of the two feedback loops. Experimental results using this two configurations showed that external cavity side-modes cannot be optimally suppressed by simply choosing the second feedback delay time to be a simple fraction of the first. To achieve stable flat RF spectra, we designed an asymmetric dual-loop feedback configuration with loop-I=160 m and loop-II $\sim$ 20 m which effectively suppresses cavity side-modes and produces flat RF spectra close to the main peak, superior to conventional single- and dual-loop feedback schemes. This behavior showed that effective suppression of external cavity side-modes and reduced timing jitter can be achieved by roughly setting the first loop and fine-tuning the length of the second feedback loop. Furthermore, by increasing the length of the second loop, a significant reduction in RF linewidth and RMS timing jitter was produced. Our experimental results have validated predictions of recently published numerical simulations. Measured integrated timing jitter in all asymmetric dual-loop configurations was lower than for single-loop feedback. However, best suppression in the external cavity side-modes was achieved with the second delay time $\sim$ 8x shorter than the first. Furthermore, integrated timing jitter, in this case, was 16% lower than single-loop feedback. Reduction in timing jitter occurs due to suppression of external cavity side-modes relative to single-loop feedback. Using this method, stable side-band-free integrated photonic oscillators based on MLLs may be developed which are feasible and attractive for many applications in optical telecommunications, time-domain multiplexing, frequency comb generation and as synchronised pulse sources or multi-wavelength lasers for wavelength-diversity or multiplexing.

Chapter 7

stabilisation of SML QDash Lasers by Simultaneous Optical Injection and Optical Feedback

7.1 Introduction

In this chapter, we report investigation of the simultaneous effects of external optical feedback and CW optical injection-locking on the stability of two-section SML QDash lasers over a wide range of delay tuning. The RF linewidth and a shift in the fundamental mode-locked frequency were reported as functions of CW optical injection. Various wavelength ranges were investigated and optimum wavelengths were determined which yield the narrowest RF linewidth and lowest timing jitter. We have also observed that incorporation of single-loop feedback and CW optical-injection leads to significant reduction in RF linewidth across a wide range of delay tuning compared to single-loop feedback.

This chapter is organised as follows: In Section 7.2, we introduce the CW injection properties and the experimental setup. In Section 7.3, variation in RF linewidth and pulse repetition frequency as functions of injected wavelength are investigated, and wavelength ranges for best stability were identified. A comprehensive analysis of RF linewidth versus delay range will be presented in Section 7.4 using single-loop optical feedback plus CW optical-injection.

7.2 CW Injection

In previous chapters, we enhanced the stability of our SML QDash laser using external optical feedback. However, in this section, we use optical injection for this technique. The behaviour of the slave laser when the external light is injected depends on three external parameters: frequency detuning (frequency or wavelength difference between the master and the slave), and slave laser power. Under certain conditions, the slave laser becomes locked with the wavelength phase of the master which is known as injection locking.

The device under investigation was a two-section InAs/InP QDash mode-locked laser with an active region consisting of nine InAs quantum dash monolayers grown by gas source molecular beam epitaxy (GSMBE) embedded within two barrier layers (dash-in-barrier device), and separate confinement heterostructure layers of InGaAsP, emitting at $\sim$ 1.55 μm. A detailed description of the laser can be found in Chapter 2.

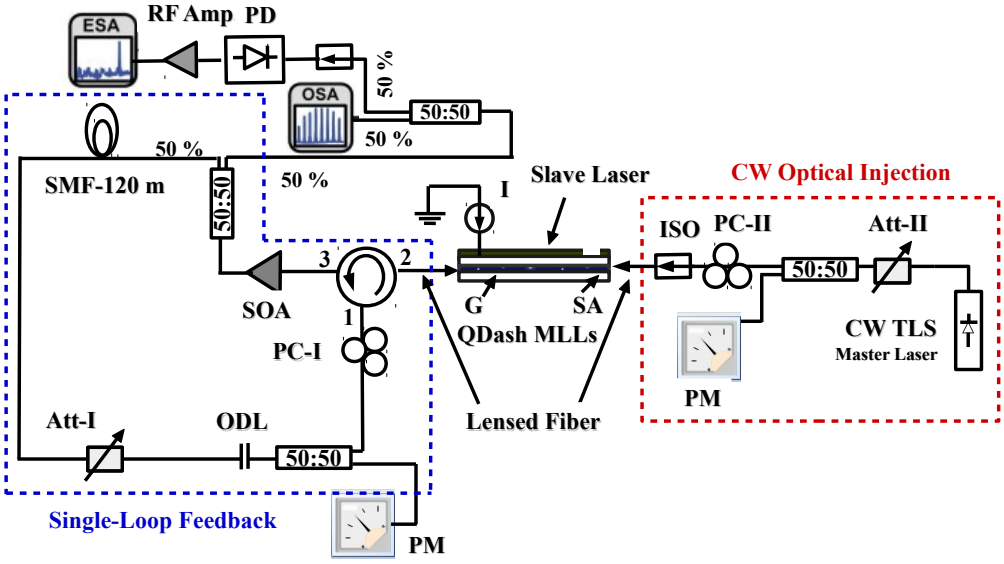

Figure 7.1: Schematic of the experimental arrangement for single-loop feedback plus CW optical- injection *Acronyms*– SOA: Semiconductor Optical Amplifier; ISO: Optical isolator; PD: Photodiode; RF Amp.: RF Amplifier; ODL: Optical delay line; Att: Optical attenuator; PC: polarisation controller; ESA: Electrical spectral analyser; OSA: Optical spectrum analyser; SMF: Single mode fibre; PM: Power Meter; QDash MLLs: Quantum dash mode-locked lasers; CW TLS: continuous-wave tunable laser source.

A schematic of the experimental arrangement is shown in Fig. 7.1. For single-loop feedback, a calibrated fraction of light was fed back through port 1 of an

optical circulator, then injected into the laser cavity via port 2. The optical coupling loss from port 2 to port 3 was -0.64 dB. The output of the circulator was sent to a semiconductor optical amplifier (SOA) with a gain of 9.8 dB and then split into two arms by a 50/50 coupler. Half of the amplified signal went to an RF spectrum analyser (Keysight, E4407B) via a 21 GHz photodiode and optical spectrum analysers (Ando AQ6317B and Advantest Q8384). The other half of power was directed to the feedback circuit containing an optical delay line combined with a variable optical attenuator and a polarisation controller. For the optical-injection part, we used a commercial external cavity tunable laser (New Focus 6328, 1520-1570 nm) with an optical linewidth $<$1 MHz and fine-tuning resolution of $\sim$ 0.5 pm was used as the master laser. The feedback intensity incident on the slave laser absorber section was controlled with a variable optical attenuator (Att-II) and was set to -13.6 dB. A polarisation controller was used to align the polarisation of the master laser with that of the slave. Master laser wavelengths were precisely controlled by a LabView® program.

7.3 Variation in RF Linewidth and Pulse Repetition Frequency as a Function of Injected Wavelength

In order to investigate the influence of CW optical-injection on the RF spectra of the free-running slave laser, first fine adjustment of a polarisation controller (PC-II) was made and part of the feedback intensity was fed back to the absorber section of the slave laser. The power injected from the master laser was controlled by a variable optical attenuator (Att-II). The measured RF linewidth (blue triangles) and the shifting in RF peak frequency (black squares) as functions of injected wavelength are shown in Fig. 7.2. Four different spectral regimes were identified, under which the injected laser makes the RF linewidth narrower or broader relative to free-running. It can be seen that the RF linewidth becomes narrower and RF peak frequency gets closer to that of free-running when the injected wavelengths were 1571.725 - 1572.10 nm. However, the injected wavelengths 1572.25 to 1578 nm, the RF linewidth becomes much wider and RF peak frequency gets farther away from the free-running RF peak frequency. The comparison of free-running optical spectra with that of optical-injection is shown in Figs. 3(a) - 3(d). When the CW laser

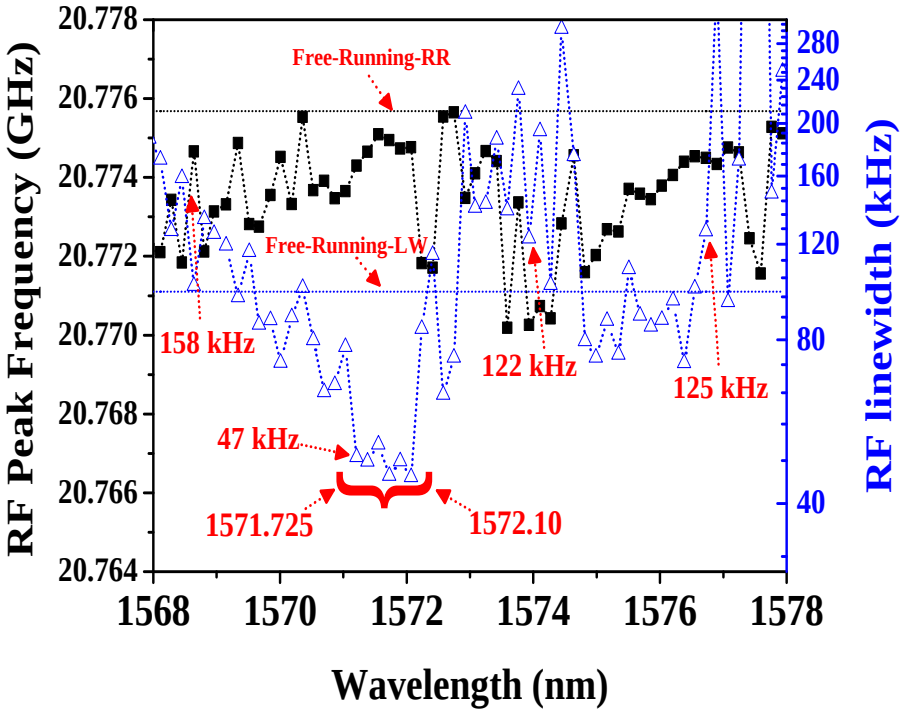

Figure 7.2: Dependences of the RF linewidth and RF peak frequency as a function of different injected wavelengths of the master laser.

was injected at 1568.45 nm, the RF linewidth was 158 kHz which is $\sim$ 1.5x higher than free-running. At this wavelength, comparison of the free-running optical spectra with that using optical-injection (1568.45 nm) is shown in Fig. 7.3(a) which is narrower than the free-running optical spectrum. With further detuning of the injected wavelength (1571.725 to 1572.10 nm), significant reductions in RF linewidth and timing jitter were observed. From this analysis, we have identified the wavelength range of master laser (1571.725 to 1572.10 nm) which yields narrowest RF linewidth and reduced RMS timing jitter of slave laser. In this range, the RF linewidth was reduced from 100 kHz free-running-laser to 44 kHz, with RMS timing jitter as low as 1.39 ps from 3.9 ps free-running (integrated from 10 kHz to 100 MHz). Comparisons of measured RF spectra and phase-noise traces of the free-running laser (gray line) with the injection-locked laser (blue line) are shown in Figs. 7.4(a) and (b), respectively. The optical spectrum of the injected light (1571.725 nm) was shown in Fig. 7.3(b) (red line) and we see that most of the side-modes were suppressed by at least 3 dB.

Furthermore, in Fig. 7.3(c), injection at 1573.935 nm makes the optical spectrum narrower than that of the free-running laser. However, some short wavelength optical modes were suppressed and some long wavelength side-modes

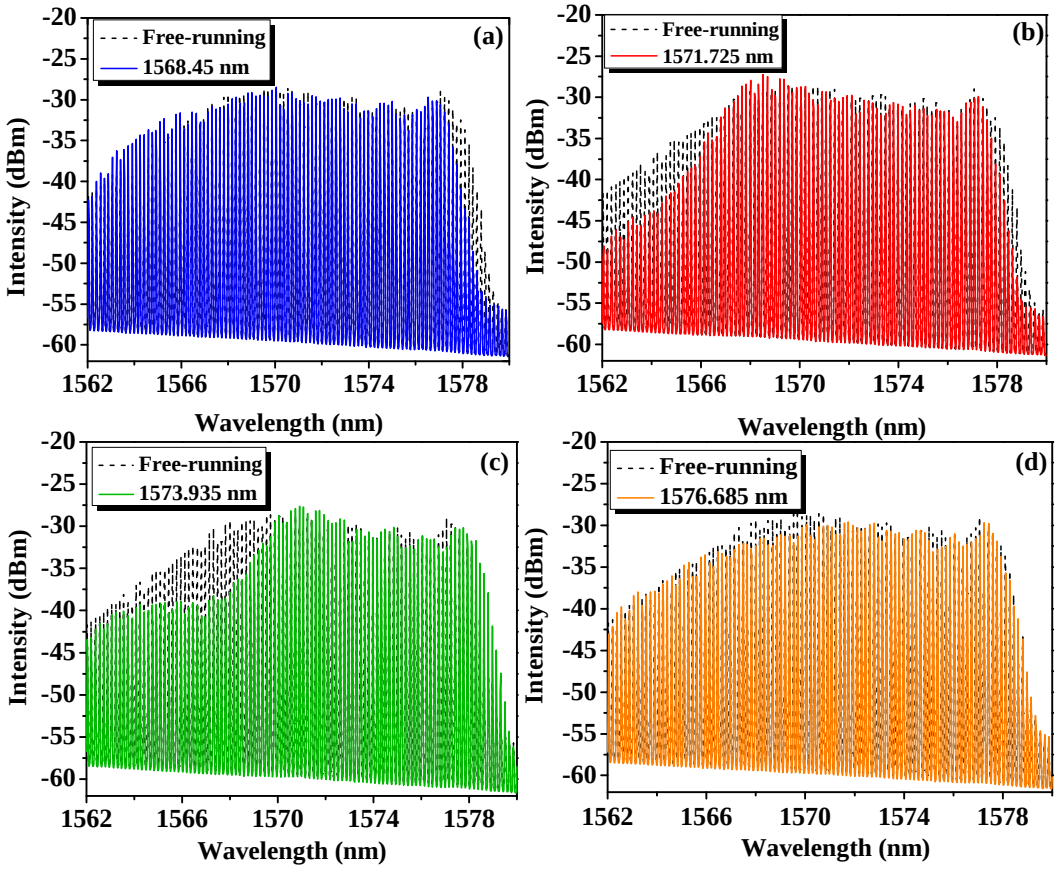

Figure 7.3: Optical spectra for free-running mode-locked laser compared with the optical spectra of the injected master laser at wavelength (a) 1568.45 nm (b) 1571.725 nm (c) 1573.935 nm and (d) 1576.685 nm.

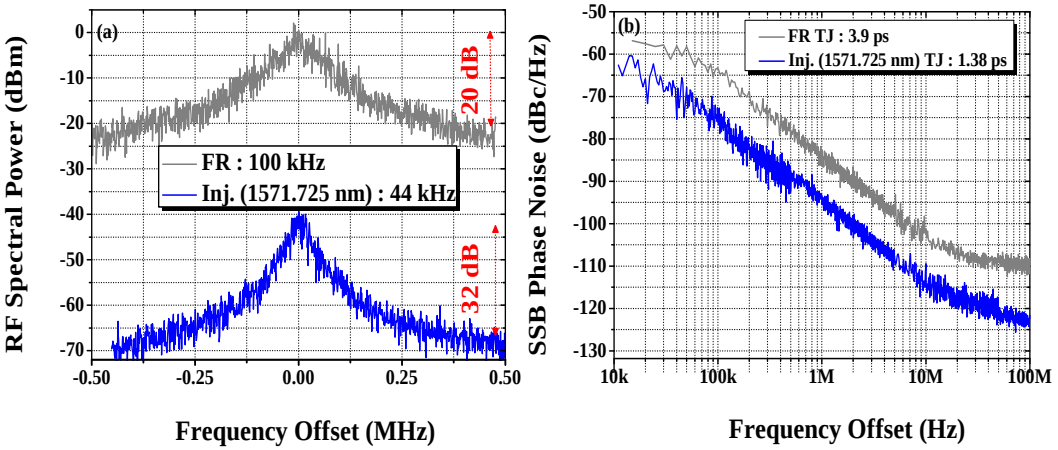

Figure 7.4: (a) Comparison of measured RF spectra of free-running mode-locked laser (gray line) and injected wavelength 1571.25 nm (blue line) using frequency span 1 MHz (resolution bandwidth 1 kHz and video bandwidth 100 Hz) (b) Comparison of measured phase-noise traces of free-running mode-locked laser (gray line) and injected mode-locked laser at wavelength 1571.725 nm (blue line) with integration limits 10 kHz - 100 MHz.

arose, resulting in wider RF linewidth (122 kHz) than that of the free-running laser (100 kHz). Moreover, when the CW laser was injected at 1576.685 nm, there is no obvious effect on the laser stability: the optical spectrum and RF linewidth of injected mode-locked laser were both similar to free-running. From this detailed analysis, the injected wavelength range 1571.725 to 1572.10 nm was identified to be most efficient to stabilise the optical pulses of our SML QDash mode-locked laser.

7.4 Comparison of RF Linewidth Versus Delay

From above detailed investigations, we determined the range of injected wavelength (1568 nm - 1578 nm) which yields significant reduction in RF linewidth and integrated timing jitter. Next we compared the effect of external optical feedback with simultaneous optical feedback and optical-injection at (1571.725 nm).

7.4.1 Using Single-Loop Feedback

To study the effects of single-loop feedback on the RF linewidth of the laser for the widest delay range [0-70 ps], maximum feedback to the gain section was limited to -22 dB. For single-loop feedback, a single 120 m fibre span was used, stable resonant condition being achieved by optimising optical delay line ODL-I which was adjustable in steps of 1.67 ps. Resulting RF linewidths (black squares) are shown in Fig. 7.5 versus delay from 0-70 ps. This behaviour shows that timing stability depends strongly on feedback delay. This effect occurs because for feedback delay times which are detuned from the main resonance condition, the system needs to adapt its periodicity for synchronisation to occur between the pulses in the laser and feedback cavities [112]. The periodicity in the RF linewidth as a function of delay tuning can be seen to be 48.4 ps, which agrees well with the fundamental mode-locked frequency (20.7 GHz) of our QDash mode-locked laser. Furthermore, this optimisation of the single feedback loop delay reduced the RF linewidth and corresponding timing jitter considerably, as for other reported experiments [77, 79] and theoretical predictions [85]. Effective and stable mode-locking could be achieved when the external cavity length was close to an integer multiple of that of the solitary

laser. When fully resonant, the RF linewidth decreased from 100 kHz free-running to 2 kHz, and integrated timing jitter from 3.9 ps to 0.7 ps (10 kHz - 100 MHz). Under this feedback delay time, the arrival time of the pulses from the laser cavity and the feedback cavity coincide precisely, at the laser facet. At full resonance, the comparisons of measured RF spectra and phase-noise traces with single-loop feedback (blue line) and free-running (gray line) are shown in Figs. 7.7(a) and (b), respectively. Upon tuning of the optical delay to 6 and 54 ps, synchronization of the optical pulses emitted from the laser cavity did not occur with the optical pulses inside the feedback cavity. At these delay values, the RF spectra became highly deformed and non-resonant feedback regime (6 to 54 ps) was observed. Our experimental results using single-loop feedback show that for practical use of QDash mode-locked laser, the most suitable and stable delay ranges are located at delays 5 and 53 ps. However, this is still quite sensitive to packaging and production. In the next section, we describe how to reduce the sensitivity of resonant single-loop feedback using simultaneous CW optical-injection and external optical feedback.

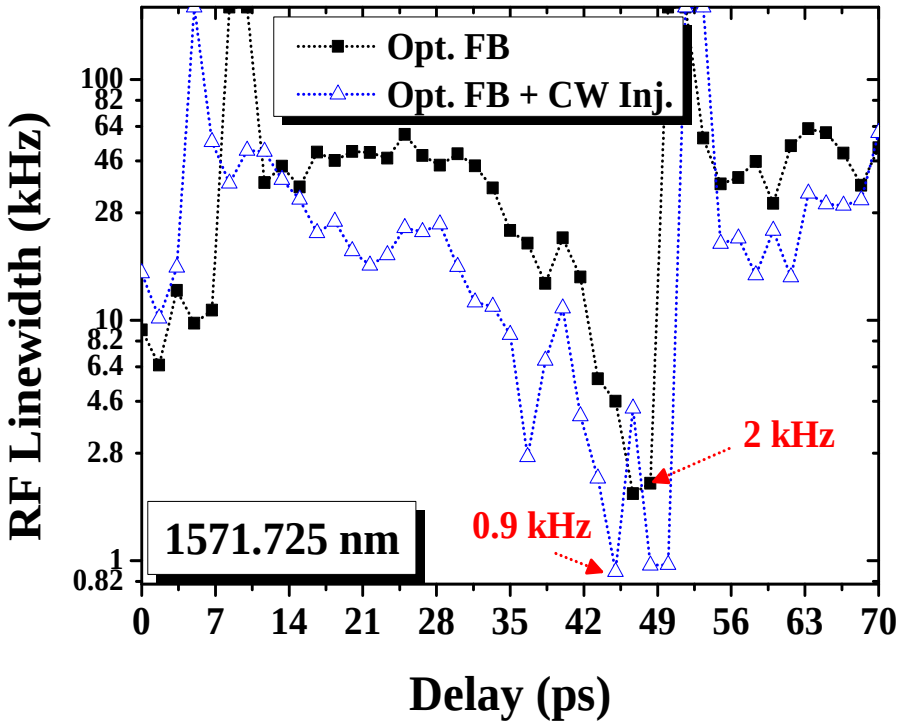

Figure 7.5: Variation of RF linewidth versus delay with optical feedback (black squares) and optical feedback plus simultaneous CW optical-injection (blue triangles) of wavelength 1571.725 nm.

7.4.2 Simultaneous Single-Loop Optical Feedback Plus CW Optical-Injection

After investigating the effects of single-loop feedback on the RF linewidth and timing jitter, the simultaneous effects of both CW optical-injection and external optical feedback were demonstrated. For this purpose, experimental arrangements for single-loop feedback were kept fixed and light from the tunable laser source was fed back into the laser absorber section. The optical delay line (ODL-I) and polarisation controller (PC-I) were fine-adjusted and the master laser with fixed wavelength (1571.725 nm) was shone into the slave laser's absorber section, the injected power controlled by a variable optical attenuator (Att-II). Measured RF linewidth data for single-loop feedback (black squares) alone and optical feedback plus optical-injection (blue triangles) are shown in Fig. 7.5. With both optical feedback and CW optical-injection, a minimum RF linewidth of $<$ 1 kHz (instrumental limited) was achieved which was 2x lower than external optical feedback and $>$ 100x lower than the free-running condition. Moreover, integrated timing jitter was reduced from 3.9 ps for the free-running laser to 0.45 ps for optical feedback alone and 0.4 ps for simultaneous optical feedback and CW optical-injection.

Measured RF spectra for free-running, single-loop feedback (blue line) and optical feedback plus optical-injection (red line) of integer cavity resonances are shown in Fig. 7.6. The cavity frequency spacing was 1.45 MHz in accordance with the 140 m nominal length of the external feedback loop. Comparison of RF spectra and phase-noise traces of the free-running laser (gray line) with external optical feedback (blue line) and simultaneous feedback plus optical-injection scheme (red line) are shown in Figs. 7.7(a) and (b), respectively. With both CW injection and optical feedback, we achieved sub-kHz RF linewidth, sub-ps timing jitter under full resonance, which was better than using optical feedback only. However, over the full delay range, CW optical-injection plus optical feedback yielded much more stable dynamics: narrow RF spectra and reduced timing jitter were found over a widest delay range, unlike external optical feedback alone. Recently,timing jitter reduction have been investigated using optical injection technique [100, 120]. The optical-injection-locked laser, double-locked with optical feedback, showed 2x TBP reduction and RF linewidth reduction by two orders of magnitude.

Measured RF linewidths versus delay for optical feedback plus injection at

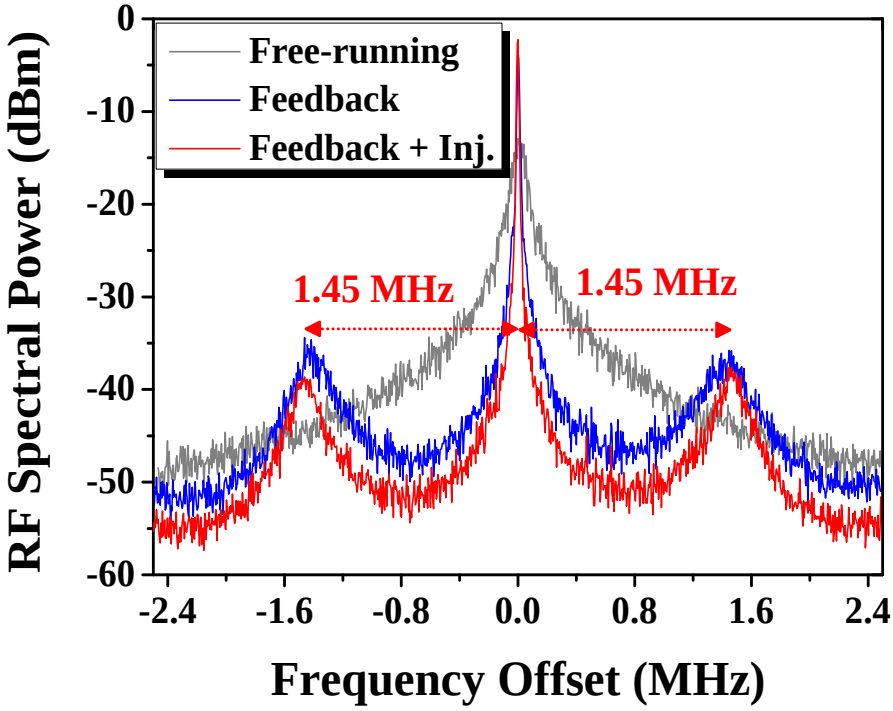

Figure 7.6: Comparison of RF spectra of free-running (gray line) with optical feedback (blue line) and optical feedback plus simultaneous optical-injection (red line) of wavelength 1571.725 nm with frequency span 10 MHz (resolution bandwidth 10 kHz and video bandwidth 1 kHz).

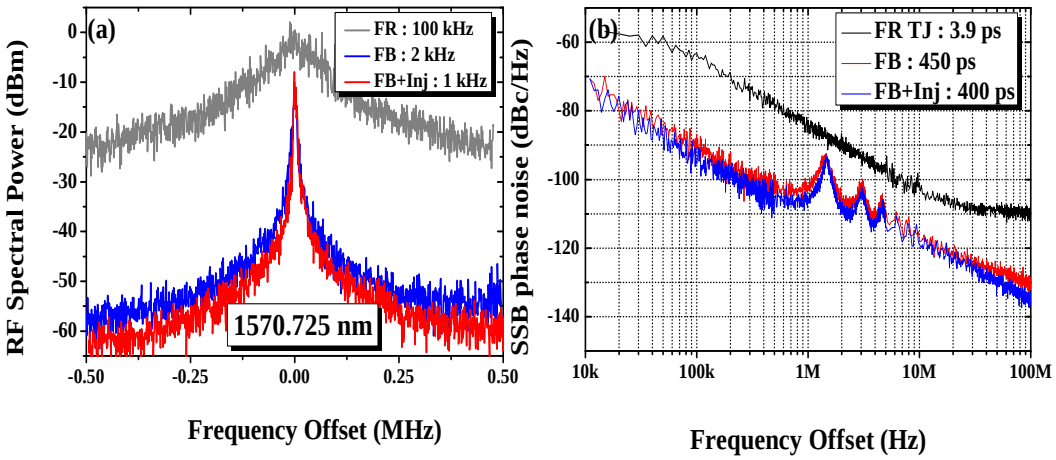

Figure 7.7: (a) Comparison of measured RF spectra of single-loop feedback (blue line), simultaneous optical-injection plus optical feedback (red line) and free-running (gray line) with frequency span 1 MHz (resolution bandwidth 1 kHz and video bandwidth 100 Hz) (b) Comparison of measured SSB phase noise traces of single-loop feedback (blue line), simultaneous optical-injection plus optical feedback (red line) and free-running (gray line) with integration limits 10 kHz - 100 MHz.

three chosen injected wavelengths (1571.685, 1571.710 and 1571.720 nm), are shown in Fig. 7.8. The RF linewidth reduced to its minimum when the

round-trip time of the feedback loop became an integer multiple of the laser's round-trip time which was modified by optical-injection. At stable resonance, simultaneous optical feedback plus optical-injection narrows the linewidth to 1.35, 5 and 1.3 kHz for optical-injection wavelengths 1571.685, 1571.710 and 1571.720 nm, respectively. These results show that optical feedback plus optical-injection technique reduced the RF linewidth at an integer resonance. However, over a wider delay range, several instabilities were observed. Therefore, these wavelengths are not suitable to achieve stabilisation of our SML QDash laser. Measured RF spectra under full resonance are shown in Fig. 7.9 for feedback plus simultaneous injected wavelengths 1571.685 (black line), 1571.710 nm (red line), 1571.720 nm (green line) and 1571.725 nm (blue line), respectively.

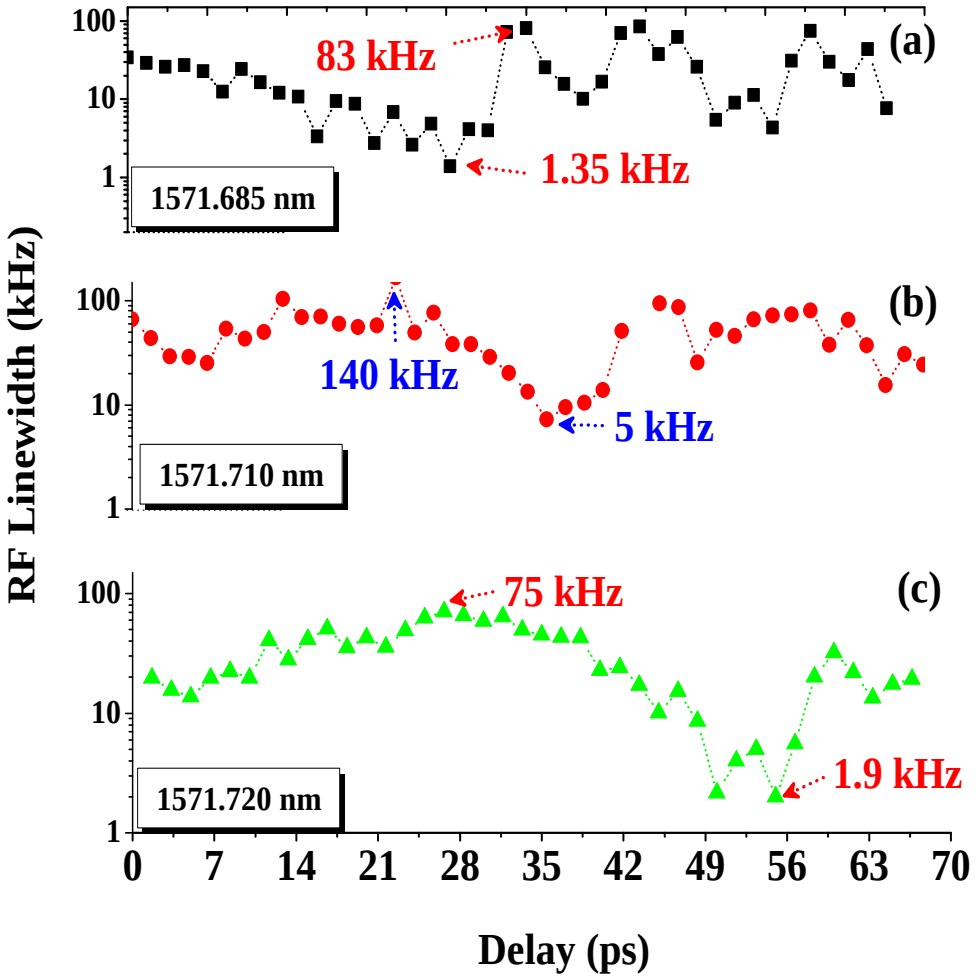

Figure 7.8: Measured RF linewidth versus delay using feedback loop plus injected wavelength 1571.685 (black squares), 1571.710 nm (red circles), and 1571.725 nm (green triangles).

In summary, we have demonstrated the potential of the combination of optical-injection and optical feedback. Measured experimental results suggest that this

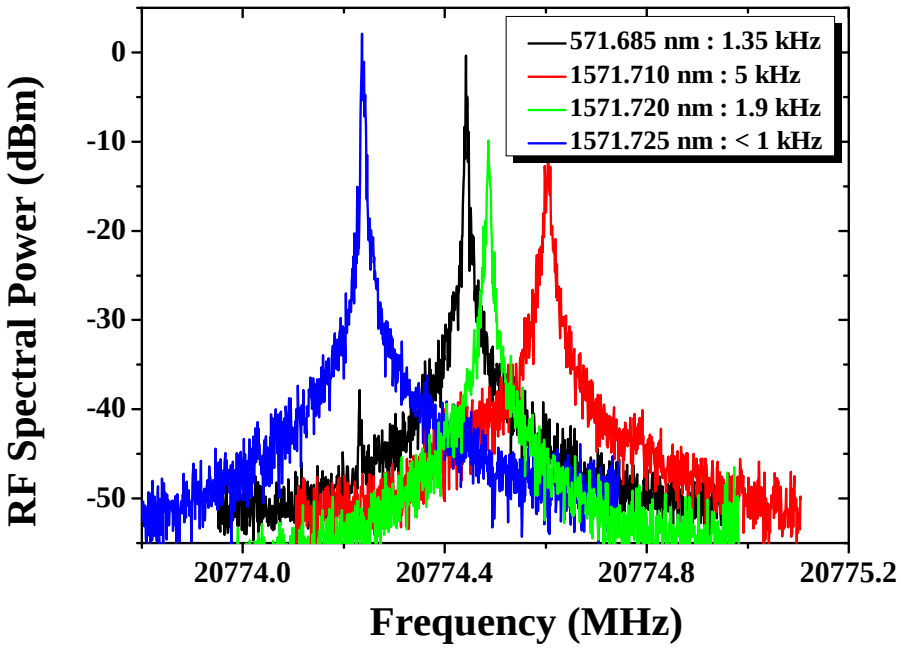

Figure 7.9: Measured RF spectra for feedback plus simultaneous injected wavelength 1571.685 (black line), 1571.710 nm (red line), 1571.720 nm (green line) and 1571.725 nm (blue line) under frequency span 1 MHz (resolution bandwidth 1 kHz and video bandwidth 100 Hz).

approach is an efficient technique to improve the stabilisation of QDash mode-locked lasers compared to optical feedback alone, though at the price of additional cost, bulk and complexity.

7.5 Summary

This chapter has highlighted the effects of single-loop feedback plus CW optical-injection on the RF linewidth and timing jitter, over the widest delay range, compared to results with single-loop optical feedback. The regime of injected wavelengths from the master laser leading to optimal RF linewidth narrowing and shifting of the fundamental frequency was identified to be 1571.725 - 1572.10 nm. First, variation in RF linewidth versus delay was observed using single-loop optical feedback and it was observed that single-loop feedback yields effective stabilisation near the resonant condition, while over the full delay range several instabilities were observed. In order to improve jitter stabilisation on widest delay ranges, the simultaneous effects of single-loop feedback plus CW optical-injection were studied. It was observed that optical feedback plus CW optical-injection maximised the resonant regime across the entire ac-

cessible delay range relative to results measured with single-loop feedback and the free-running. In addition, under double resonance, with both optical feedback and CW injection, a minimum RF linewidth of < 1 kHz (instrumental limited) was achieved which was 2x lower than external optical feedback and > 100x lower than free-running.

Chapter 8

Summary and Future Work

In this chapter, we present a summary of research work carried out in this thesis. In addition, we highlight the problems corresponding to each technical contribution, to be investigated for future extensions of this research work.

8.1 Summary of the Work Presented

The primary goal of this thesis was to achieve stabilisation of SML QDash lasers under external optical feedback and optical-injection. A brief summary of the experimental investigations described in this thesis is given below.

Chapter 1 provided a brief introduction to pulsed semiconductor lasers, and their potential applications in high-speed optical telecommunications and clocking. Mode-locking mechanism to generate ultra-short optical pulses including three major mode-locking techniques (active, passive and hybrid mode-locking), were reviewed. In addition, a brief overview of stabilisation techniques (external optical feedback and external optical-injection) performed in the thesis to investigate the stability of our QDash mode-locked laser was given. The motivation for this work and outline of this thesis was also presented in this Chapter.

Chapter 2 presented a basic characterisation of the SML QDash lasers. After introducing the device, the main measurement techniques to investigate optical/electrical spectra, optical power, and integrated timing jitter were briefly introduced.

Chapter 3 focused on the effectiveness of symmetric dual-loop optical feedback with predictable delay difference between the two external feedback cavities as means of robust stabilisation of SML QDash lasers operating at 21 GHz pulse repetition rate and emitting at 1550 nm wavelength. Various feedback schemes were investigated and the optimum feedback level determined to be -22 dB, narrowest RF linewidth and low timing jitter, for single- and symmetric dual-loop feedback. In addition, the fibre delay length (80 m) yielded the lowest RF linewidth and a reduced timing jitter was also identified. Two symmetric dual-loops configurations, with balanced and unbalanced feedback ratios were studied. For symmetric dual-loop with balanced feedback ratios equal power was coupled to both external cavities. However, for unbalanced symmetric dual-loop feedback more power (-20 dB) was coupled to loop-I than Loop-II (-26 dB). We demonstrated that unbalanced symmetric dual-loop feedback, with the inner cavity resonant and fine delay tuning of the outer loop, gives the narrowest RF linewidth and reduced timing jitter over a wide range of delay, unlike single and balanced symmetric dual-loop configurations. This configuration with feedback lengths 80 and 140 m narrowed the RF linewidth by $\sim$ 4-67x ($\sim$ 2-9x timing jitter reduction) and $\sim$ 10-100x ($\sim$ 2.5-10x timing jitter reduction), respectively, across the widest delay range, compared to free-running. For symmetric dual-loop feedback, the influence of different power split ratios through the feedback loops was further determined. A dual-loop scheme with 4:1 power ratio between loops was most successful, reducing RF linewidth by up to two orders of magnitude (70x) compared to free-running, 2-5x over single-loop and 5-8x relative to balanced symmetric dual-loop feedback. Longer 140 m fibre loops proved to be more effective than shorter 80 m loops. Our results showed that symmetric dual-loop feedback is markedly more effective than single-loop feedback in reducing RF linewidth and timing jitter, and is much less sensitive to delay phase, making this technique ideal for applications where robustness and alignment tolerance are essential.

Chapter 4 explored the variation in RF linewidth versus a wide range of delay tuning [0-84 ps] followed by different percentages of the power split ratio through either external feedback cavity using the symmetric dual-loop feedback configuration. RF linewidth narrowing and broadening over a broad range of delay phase was demonstrated when each cavity was set to an integer resonance and the second cavity was fine-tuned, which produced RF linewidth reduction over a broad range of phase delay.

Chapter 5 briefly discussed the effects of optical feedback from asymmetric

dual and single feedback loops on the RF linewidth and timing jitter for a wide range of delay tuning in SML QDash lasers. The feedback ratio which yielded the narrowest RF linewidth and low timing jitter was identified for single and asymmetric dual-loop feedback. Our measurements reveal that asymmetric dual-loop feedback with one loop shorter than the main one maximises tolerance to delay phase mismatch relative to single-loop feedback. Moreover, optimised dual-loop feedback extends the effective resonant feedback regime and maintains stable RF spectra, with narrow RF linewidth and reduced timing jitter across the entire accessible delay range, making this setup desirable for practical applications. It was further observed that at multiple optical delay ranges, the RF linewidth was instrument limited at less than 1 kHz, so the actual value may be lower. This behaviour indicates that to maximise the RF linewidth, delicate tuning of both optical delay lines is required. Furthermore, in this experimental arrangement, from delay settings 0-40 ps and 56.7-78.4 ps, the RF linewidth was below the minimum RF linewidth measured for single-loop feedback. In addition, this asymmetric dual-loop scheme reduced RF linewidth $\sim$ 2.5-4x compared to single-loop and 4-100x relative to free-running conditions. Our results demonstrate that asymmetric dual-loop feedback is more effective than single-loop feedback at reducing linewidth and jitter, across a much wider range of delay phase. The resonant condition in asymmetric dual-loop feedback is nearly independent of optical delay, making it ideal for practical applications. We also assessed the influence of asymmetric dual-loop optical feedback on SMSR and observed that suppression of external cavity side-modes leads to a significant reduction in timing jitter. It was demonstrated that when the length of loop-I was fixed to 160 m and loop-II was set to 80 m then 30 dB fundamental side-mode suppression was achieved. However, when the length of loop-I was adjusted to 185 m and loop-II was fixed to 20 m, 23 dB suppression occurs for first harmonic. Furthermore, the influence of the long fibre loop-I (up to order of $>$ 2 km) relative to Loop-II on the suppression of external cavity side-modes was investigated.

Chapter 6 described an asymmetric dual-loop feedback method to suppress external cavity side-modes induced in SML QDash lasers with conventional single-loop and dual-loop feedback. An asymmetric dual-loop feedback configuration discussed in Chapter 5 suppressed noise-resonances but additional noise fluctuations (modal overlap) appeared at frequencies resonant with the inverse of the round trip delay in the second cavity. However, for some particle applications of MLLs, narrow and flat RF spectra are required. For this purpose, an

asymmetric dual-loop feedback has been demonstrated to suppress additional noise-resonances found in conventional single and dual-loop feedback setups. In this experimental arrangement, the length of loop-I was fixed to 160 m while the length of the second feedback loop was varied in three chosen lengths: 20, 53 and 80 m. It was observed that with loop-I=160 m and loop-II=80 m, maximum > 30 dB suppression in the first order side-mode was achieved. However, additional noise fluctuations (modal overlap) appeared at frequencies resonant with the inverse of the length of the second delay time which becomes the carrier signal. To assess suppression of these frequency resonances, when the length of loop-I was fixed to 160 m and loop-II was kept 53 m then suppression of the first two frequency resonances occurred, while the third harmonic (modal overlap) remained unsuppressed. These modal overlaps depends on the ratio of the length of two feedback loops. Experimental results using these two feedback configurations show that external cavity side-modes cannot be optimally suppressed by simply choosing the second feedback delay time to be a fraction of the first. To achieve stable and flat RF spectra, we designed an asymmetric dual-loop feedback configuration with length of loop-I=160 m and loop-II $\sim$ 20 m which effectively suppress cavity side-modes and produced flat RF spectra close to the main peak compared to conventional single and dual-loop feedback schemes. This behaviour shows that effective suppression of external cavity side-modes and reduced timing jitter can be achieved by appropriately fine-tuning the length of the second feedback loop. Furthermore, by increasing the length of the second loop, a significant reduction in RF linewidth and integrated timing jitter was produced. Our experimental results have validated predictions of recently published numerical simulations.

Chapter 7 discussed the influence of simultaneous external optical feedback and CW optical-injection on the timing stability of the SML QDash laser. We identified the wavelength ranges which yielded narrow RF linewidth and reduced timing jitter under full resonance. It was further found that simultaneous injection-locking and optical feedback leads to narrow RF linewidth across the full delay range compared to optical feedback alone. Furthermore, the relationship between RF linewidth and repetition rate tuning as a function of the injected wavelength was also investigated.

Measured RF linewidth and integrated timing jitter in each experimental performed is summarized in Table 8.1. In addition, SMSR for the balanced asymmetric dual-loop feedback was presented in Table 8.2.

8.2 Future Work

Some suggestions for future extension of this research work are listed below:

- Mode-locking in our QDash mode-locked laser was obtained without reverse bias applied to the absorber section. This was a two-section device but was packaged similarly to a single-section SML laser since the absorber was unbiased: its minimal absorption does not affect the self-mode-locking mechanism. Non-linear effects such as self-phase modulation (SPM), cross-phase modulation (XPM) and four-wave-mixing (FWM) in the cavity has been proposed as the reason for this coherent self-pulsing behavior. Probably an important problem which is still open is the development of a theoretical model for explanation of the self-mode-locking present in QDash MLLs.
- In Chapter 6, we demonstrated that the best side-mode suppression and lower timing jitter relative to single-loop feedback were achieved with the length ratio between the two cavities $\sim$ 8x. It should be noted that the length of loop-II ($\sim$ 20 m) is only optimal in our specific experimental setup. Further reduction in the length of second feedback loop are not possible, as the combined variable optical attenuator, ODL, PC, and 3 dB coupler have a minimum length of $\sim$ 20 m. Better suppression in external cavity side-modes could be achieved in an arrangement not subject to this limitation, such as experimental arrangements in free space.
- This thesis is based on self mode-locking. However, similar experimental studies could be performed for passive mode-locking which has a significant influence on repetition rates and pulse duration of semiconductor QDash MLLs.
- As discussed in various experimental studies, the minimum RF linewidth can be achieved when the phase of the emitted light matches the phase of the injected light. In addition, the coupling efficiency plays a crucial role in narrowing and broadening of the RF linewidth. Mechanical vibrations of the systems can lead to severe instabilities and cause degradation in the RF linewidth. To improve stabilisation of MLLs, robust integration of laser systems is highly desirable.
- In Chapters 3-6, we demonstrated that jitter stabilisation on the full range of delay phase tuning can be achieved using dual-loop feedback. In Chap-

ter 7, we improved the timing stability of SML QDash laser subject to single-loop feedback plus CW optical-injection. We believe that further improvement in the timing stability of QDash mode-locked laser is possible using simultaneous CW injection into the absorber section and asymmetric dual-loop feedback into the gain section of the laser. The proposed experimental arrangement for this experimental setup is shown in Fig. 8.1.

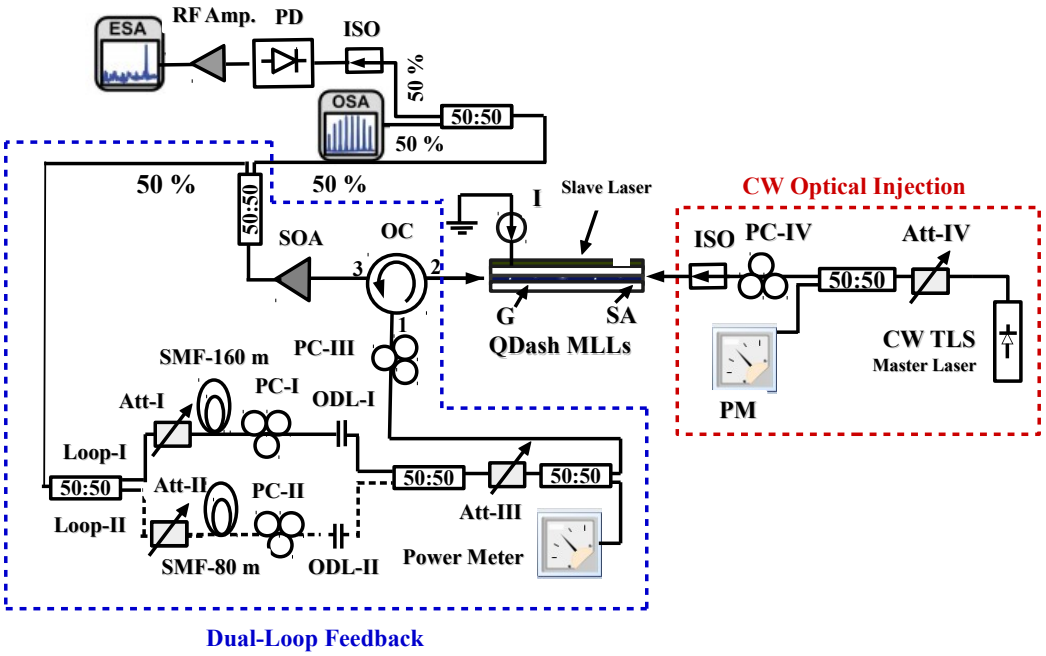

Figure 8.1: Schematic of the experimental arrangement for dual-loop feedback plus cw optical- injection *Acronyms*– SOA: Semiconductor Optical Amplifier; ISO: Optical isolator; PD: Photodiode; RF Amp.: RF Amplifier; ODL: Optical delay line; Att: Optical attenuator; PC: polarisation controller; ESA: Electrical spectral analyser; OSA: Optical spectrum analyser; SMF: Single mode fibre; PM: Power Meter; QDash MLLs: Quantum dash mode-locked lasers; CW TLS: continuous-wave tunable laser source

Table 8.1: Comparison of RF Linewidth (RF), and Timing Jitter (TJ) using single- and dual-loop feedback performed in this thesis; *Acronyms*– FS: Feedback Scheme; FBR: feedback ratio through either feedback loop; FR: Free-running; SL: Single-loop; BSDL: Balanced symmetric dual-loop; USDL: Unbalanced symmetric dual-loop; ADL: Asymmetric dual-loop; Opt. Inj: Optical-Injection.

FS	**Loop-I**	**Loop-II**	**FBR**	**RF**	**TJ**
	m	**m**	**dB**	**kHz**	**ps**
FR	-	-	-	100	3.9
SL	20	-	-22	4	1.2
SL	48	-	-22	4	0.8
SL	80	-	-22	4	0.6
SL	80	-	-20	68	-
SL	80	-	-26	8	-
SL	80	-	-46.6	72.7	3
SL	80	-	-39.6	64	2.9
SL	80	-	-36.6	50	2.3
SL	80	-	-31.8	40.1	2.1
SL	80	-	-29.59	28.7	1.75
SL	80	-	-26.58	12.9	1.1
SL	80	-	-24.82	7	0.89
SL	80	-	-23.57	5	0.98
SL	80	-	-22.6	3	0.6
SL	120	-	-22	2	0.7
SL	145	-	-22	4	0.65
SL	160	-	-22	4	0.7
SL	160	-	-46.6	80	3
SL	160	-	-39.6	61.3	2.7
SL	160	-	-36.6	60.3	2.6
SL	160	-	-31.8	34.7	2
SL	160	-	-29.59	10	1.3
SL	160	-	-26.58	9.12	1
SL	160	-	-24.82	6.2	0.9
SL	160	-	-23.57	4.03	0.72
SL	160	-	-22.6	4	0.7
SL	200	-	-22	< 1	-
SL	205	-	-22	12	0.8
BSDL	80	-	-22:-22	12	0.89
BSDL	80	-	-46.6: -46.6	75	3.1
BSDL	80	-	-39.6: -39.6	70	3
BSDL	80	-	-36.6: -36.6	48	2.5
BSDL	80	-	-31.8: -31.8	33	2
BSDL	80	-	-29.59: -29.59	28.7	1.8
BSDL	80	-	-26.58: -26.58	17	1.35
BSDL	80	-	-24.82: -24.82	16.5	1.3
BSDL	80	-	-23.57: -23.57	16	0.98

FS	Loop-I	Loop-II	FBR	RF	TJ
	m	m	dB	kHz	ps
BSDL	80	-	-22.6: 22.6	15	0.9
BSDL	140	-	-22:-22	8	-
BSDL	220	-	-22:-22	4	0.75
USDL	80	-	-26:-20(c)	4.1	-
USDL	80	-	-24.3:-20.6(c)	3.4	-
USDL	80	-	-23:-21.3(c)	2.1	-
USDL	80	-	-21.3:-23(c)	30	-
USDL	80	-	-20.6:-24.3(c)	1.6	-
USDL	80	-	-20:-26(c)	1.5	0.45
USDL	80	-	-46.6: -46.6	69	2.9
USDL	80	-	-39.6: -39.6	57	2.5
USDL	80	-	-36.6: -36.6	52.8	2.3
USDL	80	-	-31.8: -31.8	32.1	1.9
USDL	80	-	-29.59: -29.59	21.5	1.6
USDL	80	-	-26.58: -26.58	7.23	1
USDL	80	-	-24.82: -24.82	3.36	0.8
USDL	80	-	-23.57: -23.57	2.78	0.69
USDL	80	-	-22.6: 22.6	2	0.45
USDL	140	-	-19.5:-29.03(c)	1	0.4
USDL	220	-	-19.5(c):-29.03	11	-
USDL	220	-	-20.6(c):-24.3	3	-
USDL	220	-	-21(c):-22.7	3	-
USDL	220	-	-21.3(c):-23	10	-
USDL	220	-	-19.5:-29.03(c)	1	-
USDL	220	-	-20.6:-24.3(c)	3	-
USDL	220	-	-21:-22.7(c)	14	-
USDL	220	-	-21.3:-23(c)	7	-
BADL	160	80	-22:-22	<1	0.295
BADL	160	53	-22:-22	2	0.45
BADL	160	20	-22:-22	8	0.6
BADL	205	40	-22:-22	< 1	0.4
BADL	2000	200	-22:-22	< 1	-
UADL	160	80	-22:-22	1.3	-
UADL	160	80	-23.29(c):-28.06	1.3	-
UADL	160	80	-23.29:-28.06(c)	1.4	-
UADL	160	80	-46.6	70	3
UADL	160	80	-39.6	57	2.5
UADL	160	80	-36.6	52.8	2.4
UADL	160	80	-31.8	32.1	1.9
UADL	160	80	-29.59	10	1.3
UADL	160	80	-26.58	7.23	98
UADL	160	80	-24.82	3.36	0.8
UADL	160	80	-23.57	2.78	0.5
UADL	160	80	-22.6	0.4	0.29

FS	Loop-I	Loop-II	FBR	RF	TJ
	m	m	dB	kHz	ps
FB plus 1571.725 nm	120	-	-22	< 1	0.4
FB plus 1571.685 nm	120	-	-22	1.35	-
FB plus 1571.710 nm	120	-	-22	5	-
FB plus 1571.720 nm	120	-	-22	1.9	1.9

Table 8.2: Side mode suppression ratio (SMSR) dual-loop feedback performed in this thesis; *Acronyms*– FS: Feedback Scheme; FBR: feedback ratio through either feedback loop; BADL: Balanced asymmetric dual-loop

FS	Loop-I	Loop-II	FBR	SMSR
	m	m	dB	dB
BADL	160	53	-22:-22	25
BADL	160	80	-22:-22	30
BADL	205	40	-22:-22	23
BADL	2000	200	-22:-22	30

References

[1] T. Miyazaki, H. Sotobayashi, and W. Chujo, "Optical sampling and demultiplexing of 80 Gb/s OTDM signals with optically recovered clock by injection mode-locked laser diode," in *European Conference on Optical Communication (ECOC)*, (2002).
[Available: http://ieeexplore.ieee.org/document/1600923/]

[2] K. Merghem, V. Panapakkam, Q. Gaimard, F. Lelarge, and A. Ramdane, "Narrow linewidth frequency comb source based on self-injected quantum-dash passively mode-locked laser," in *Conference on Lasers and Electro-Optics (CLEO)*, paper SW1C.5 (2017).
[Available: http://ieeexplore.ieee.org/document/8084420/]

[3] V. Moskalenko, K. Williams, J. Koelemeij, and E. Bente, "42 nm wide coherent frequency comb generated by a QW based integrated passively mode-locked laser," in *Semiconductor Laser Conference (ISLC)*, (2016).
[Available: http://ieeexplore.ieee.org/document/7765756/]

[4] E. Sooudi, S. Sygletos, Andrew D. Ellis, G. Huyet, John G. McInerney, F. Lelarge, K. Merghem, R. Rosales, A. Martinez, A. Ramdane, Stephen P. Hegarty, "Optical frequency comb generation using dual-mode injection-locking of quantum-dash mode-locked lasers: Properties and Applications," IEEE J. Quantum Electron. **48**(10), 1327–1338 (2012).

[5] H. Sotobayashi, "Ultra-wideband 40 GHz optical-combs generation and distribution through WDM optical fibre netwroks," in *Frequency Control Symposium* , 984–985 (2007).
[Available: http://ieeexplore.ieee.org/abstract/document/4319227/]

[6] F. Gao, S. Luo, H.-M. Ji, S.-T. Liu, D. Lu, C. Ji, and T. Yang, "Single-section mode-locked 1.55-μm InAs/InP quantum-dot lasers grown by MOVPE," Opt. Communication **370**, 18–21 (2016).

[7] J. Luo, J. Parra-Cetina, P. Landais, H. J. S. Dorren, and N. Calabretta, “40 G burst mode optical clock recovery after 52 km transmission enabled by a dynamically switched quantum dash mode-locked laser,” in *European Conference and Exhibition on Optical Communication (ECOC)*, paper Th.2.A.2 (2013).
[Available: http://ieeexplore.ieee.org/abstract/document/6647721/]

[8] H. Schmeckebier, G. Fiol, C. Meuer, D. Arsenijević, and D. Bimberg, “Complete pulse characterization of quantum-dot mode-locked lasers suitable for optical communication up to 160 Gbit/s," Opt. Express **18**(4), 3415–3425 (2010).

[9] E. U. Rafailov, M. A. Cataluna, and W. Sibbett, “Mode-locked quantum-dot lasers," Nature Photon **1**, 395–401 (2007).

[10] M. Kuntz, G. Fiol, M. Laemmlin, C. Meuer, and D. Bimberg, “High-speed mode-locked quantum-dot lasers and optical amplifiers," Proc. IEEE **95**(9), 1767–1778 (2007).
[Available: http://ieeexplore.ieee.org/abstract/document/4362703/]

[11] D. Bimberg, G. Fiol, M. Kuntz, C. Meuer, M. Lämmlin, N. N. Ledentsov, and A. R. Kovsh, “High speed nanophotonic devices based on quantum-dots," Phys. Stat. Sol. (a) **203**(14), 3523–3532 (2006).

[12] D. J. Bradley and M. H. Holbrook, “Mode-Locked semiconductor lasers and their spectroscopic applications,” Phil. Trans. R. Soc. Lond. A. **307**(1500), 521–530 (1982).

[13] A. Ellis and F. C. G. Gunning, “Spectral density enhancement using coherent WDM,” IEEE Photonics Technol. Lett. **17**(2), 504–506 (2005).

[14] V. Vujicic, C. Calò, R. Watts, F. Lelarge, C. Browning, K. Merghem, A. Martinez, A. Ramdane, and L. P. Barry, “Quantum-dash mode-locked lasers for data centre applications,” IEEE J. Sel. Top. Quantum Electron. **21**(6), 53–60 (2015).

[15] A. Sano, Y. Takatori, and Y. Miyamoto, “No-guard-interval coherent optical OFDM for 100-Gb/s/ch long-haul transmission systems,” in *Optical Fibre Communication Conference and National Fibre Optic Engineers Conference*, paper OTuO3, (2009).
[Available: https://www.osapublishing.org/abstract.cfm?uri=OFC-2009-OTuO3]

[16] P. Kumar, F. Grillot, "Control of dynamical instability in semiconductor quantum nanostructures diode lasers: role of phase-amplitude coupling," Eur. Phys. J. Special Topics **222**, 813–820 (2013).

[17] A. Einstein, "The quantum theory of radiation," Phys. Z. **18**(121) (1917).

[18] D. N. Nasledov, A. A. Rogachev, S. M. Ryvkin, and B. V. Tsarenkov, 1962, "Recombination radiation of galiun arsenic," Sov. Phys. Solid State. **4**, 782–785 (1962).

[19] R. N. Hall, G. E. Fenner, J. D. Kingsley, T. J. Soltys, and R. O. Carlson, "Coherent light emission from GaAs junctions," Phys. Rev. Lett. **9**(9), 366–369 (1962).

[20] M. I. Nathan, W. P. Dumke, G. Burns, F. H. Dill and G. Lasher, "Stimulated emission of radiation from GaAs p-n junctions," Appl. Phys. Lett. **1**(3), 62 (1962).

[21] N. Holonyak and S. F. Bevacqua, "Coherent (visible) light emission from Ga($As_{1-x}P_x$ junctions," Appl. Phys. Lett. **1**(4), 82 (1962).

[22] T. M. Quist, R. H. Rediker, R. J. Keyes, W. E. Krag, B. Lax, A. L. McWhorter, and H. J. Zeigler, " Semiconductor maser of GaAs," Appl. Phys. Lett. **1**(4), 91 (1962).

[23] Zh. I. Alferov, V. M. Andreev, D. Z. Garbuzov, Yu. V. Zhilyaev, E. P. Morozov, E. L. Portnoi, and V. G. Trofim, "Investigation of the influence of the AlAs–GaAs heterostructure parameters on the laser threshold current and realization of continuous emission at room temperature," Sov. Phys.-Semicond. **4**(9) 1573–1575 (1971).

[24] I. Hayashi, M. B. Panish, P. W. Foy, and S. Sumski, "Junction lasers which operate continuously at room temperature," Appl. Phys. Lett. **17**(3), 109 (1970).

[25] G. Tandoi, "Monolithic high power mode-locked GaAs/AlGaAs quantum-well lasers," Ph.D. Thesis (School of Engineering, University of Glasgow) (2011).
[Available: http://theses.gla.ac.uk/2721/]

[26] I. Esquivias, S. Weisser, J. D. Ralston, and D. F. G. Gallagher, "High-speed GaAs/AlGaAs multiple-quantum-well lasers: design and characterization," IEEE Trans. Electron Dev. **39**(11), 2660–2661 (1992).

[27] E. U. Rafailov, M. A. Cataluna, and E. A. Avrutin, "Ultrafast lasers based on quantum-dot structures: Physics and Devices," Wiley-VCH Verlag Co. KGaA, (2011).

[28] R. Paschotta, "Field guide to laser pulse generation", in *SPIE Press*, Bellingham, WA (2007)

[29] S. Arahira, S. Oshiba, Y. Matsui, T. Kunii, and Y. Ogawa, "500 GHz optical short pulse generation from a monolithic passively mode-Locked distributed bragg reflector laser diode," Appl. Phys. Lett **64**(15), 1917 (1994).

[30] R. Ludwig, S. Diez, A. Ehrhardt, L. Kuller, W. Pieper, and H. G. Weber, "A tunable femtosecond mode-locked semiconductor laser for applications in OTDM-systems," IEICE Trans. Electron **E81-C**(2), 140–145 (1998).

[31] F. Lelarge, B. Dagens, J. Renaudier, R. Brenot, A. Accard, F. V. Dijk, D. Make, O. Le Gouezigou, J. Provost, F. Poingt, J. Landreau, O. Drisse, E. Derouin, B. Rousseau, F. Pommereau, and G. -H. Duan, "Recent advances on InAs/InP quantum dash based semiconductor lasers and optical amplifiers operating at 1.55μm," IEEE J. Sel. Top. Quantum Electron. **13**(1), 111–124 (2007).

[32] O. Svelto, "Principles of Lasers," 4th ed., USA: Springer, (1998).

[33] A. Yariv, "Quantum Electronics," 39th ed., USA: John Wiley Sons, (1975).

[34] P. Paulus, R. Langenhorst, and D. Jager, "Generation and optimum control of picosecond optical pulses from gain-switched semiconductor lasers," IEEE J. Quantum Electron. **24**(8), 1519–1523 (1988).

[35] C. Rulliere, "Femtosecond laser pulses, principles of experiments," 2nd ed., USA: Springer, (2003).

[36] K. Merghem, A. Akrout, A. Martinez, G. Aubin, A. Ramdane, F. Lelarge, and G.-H. Duan, "Pulse generation at 346 GHz using a passively mode locked quantum-dash-based laser at 1.55 μm," Appl. Phys. Lett. **94**(2), 021107 (2009).

[37] S. Latkowski, R. Maldonado-Basilio, and P. Landais, "Sub-picosecond pulse generation by 40-GHz passively mode-locked quantum-dash 1-mm-long Fabry-Prot laser diode," Opt. Express **17**(21), 19166–19172 (2009).

[38] Y. M. Chang, J. Lee, Y. M. Jhon, and J. H. Lee, "Active Q-switching in an

erbium-doped fibre laser using an ultrafast silicon-based variable optical attenuator," Opt. Express **19**(27), 26911–26916 (2011).

[39] G. J. Spühler, R. Paschotta, R. Fluck, B. Braun, M. Moser, G. Zhang, E. Gini, and U. Keller, "Experimentally confirmed design guidelines for passively Q-switched microchip lasers using semiconductor saturable absorbers," J. Opt. Soc. Am. B. **16**(3), 376–388 (1999).

[40] J. J. Degnan, "optimisation of passively Q-switched lasers," IEEE J. Quantum Electron. **31**(11), 1890–1901 (1995).

[41] R. A. Griffin, D. A. Jackson, and D. D. Sampson, "Coherence and noise properties of gain switched Fabry-Perot semiconductor lasers," IEEE J. Sel. Top. Quantum Electron. **1**(2), 569–576 (1995).

[42] H. Ito, H. Yokoyama, S. Murata, and H. Inaba, "Picosecond optical pulse generation from an r.f. modulated AlGaAs d.h. diode laser," IEEE J. Quantum Electron. **15**(23), 738–740 (1979).

[43] L. P. Barry, P. Anandarajah, and A. Kaszubowska, "High frequency, wavelength-tunable pulse generation using a gain-swicthed commercial Fabry-perot laser with strong external-injection," in *Lasers and Electro-Optics Society (LEOS)*, 587-588, paper WV5 (2000).
[Available: http://ieeexplore.ieee.org/abstract/document/893978/]

[44] P. W. Smith, "Mode-locking of lasers," in *Proc. IEEE* , **58**(9), 1342–1357 (1970).
[Available: http://ieeexplore.ieee.org/abstract/document/1449856/]

[45] H. A. Haus, "Mode-locking of lasers," IEEE J. Sel. Top. Quantum Electron. **6**(6), 1173–1185 (2000).

[46] L. E. Hargrove, R. L. Fork, and M. A. Pollack, "Locking of He–Ne laser modes induced by synchronous intracavity modulation," Appl. Phys. Lett. **5**(1), 4 (1964).

[47] R. Paschotta and U. Keller, "Passive mode locking with slow saturable absorbers," Appl. Phys. B **73**(7), 653–662 (2001).

[48] B. K. Garside and T. K. Lim, "Laser mode locking using saturable absorbers," J. Appl. Phys. **44**(5), 2335 (1973).

[49] E. P. Ippen, C. V. Shank, and A. Dienes, "Passive mode locking of the cw dye laser," Appl. Phys. Lett. **21**(8), 348 (1972).

[50] G. M. Roger, P. Koumans and R. V. Roijen, "Theory for passive mode-locking in semiconductor laser structures including the effects of self-phase modulation, dispersion, and pulse collisions," IEEE J. Quantum Electron. **32**(3), 478–492 (1996).

[51] R. Arkhipov, A. Pimenov, M. Radziunas, D. Rachinskii, A. G. Vladimirov, D. Arsenijević, H. Schmeckebier, and D. Bimberg, "Hybrid mode locking in semiconductor lasers: Simulations, Analysis, and Experiments," IEEE J. Sel. Top. Quantum Electron., **19**(4), 1100208–1100208 (2012).

[52] A. Yariv, "Quantum Electronics," 3rd ed., USA: John Wiley Sons, Inc., (1988).

[53] J. Renaudier, G.-H. Duan, J.-G. Provost, H. Debregeas-Sillard, and P. Gallion, "Phase correlation between longitudinal modes in semiconductor self-pulsating DBR lasers," IEEE Photonics Technol. Lett. **17**(4), 741–743 (2005).

[54] C. Gosset, K. Merghem, A. Martinez, G. Moreau, G. Patriarche, G. Aubin, A. Ramdane, J. Landreau, and F. Lelarge, "Subpicosecond pulse generation at 134 GHz using a quantum-dash-based Fabry-Perot laser emitting at 1.56 μm," Appl. Phys. Lett. **88**(24), 241105 (2006).

[55] C. Gosset, K. Merghem, A. Martinez, G. Moreau, G. Patriarche, G. Aubin, J. Landreau, F. Lelarge, and A. Ramdane, "Subpicosecond pulse generation at 134 GHz and low radiofrequency spectral linewidth in quantum dash-based FabryPerot lasers emitting at 1.5 μm," Electronics Letters. **42**(2), 91–92 (2006).

[56] Z. G. Lu, J. R. Liu, S. Raymond, P. J. Poole, P. J. Barrios, and D. Poitras, "312-s pulse generation from a passive c-band InAs/InP quantum dot mode-locked laser," Opt. Express. **16**(14), 10835–10840 (2008).

[57] G. P. Agrawal , and N. A. Olsson, "Self-phase modulation and spectral broadening of optical pulses in semiconductor laser amplifiers," IEEE J. Quantum Electron. **25**(11), 2297–2306 (1989).

[58] N. A. Olsson, and G. P. Agrawal, "Spectral shift and distortion due to self-phase modulation of picosecond pulses in 1.5 μm optical amplifiers," Appl. Phys. Lett. **55**(1), 13–15 (1989).

[59] M. Y. Hong, Y. H. Chang, A. Dienes, J. P. Heritage, P. J. Delfyett, Sol Dijaili, and F. G. Patterson, "Femtosecond self- and cross-phase modulation in

semiconductor laser amplifiers," IEEE J. Sel. Top. Quantum Electron. **2**(3), 523–539 (1996).

[60] G. P. Agrawal , "Population pulsations and nondegenerate four-wave mixing in semiconductor lasers and amplifiers," J. Opt. Soc. Am. B. **5**(1), 147–159 (1988).

[61] G. P. Agrawal , " Four-wave mixing and phase conjugation in semiconductor laser media," Opt. Lett. **12**(4), 260–262 (1987).

[62] L. Tiemeijer, P. Kuindersma, P. Thijs, and G. Rikken, "Passive FM locking in InGaAsP semiconductor lasers," IEEE J. Quantum Electron. **25**(6), 1385–1392 (1989).

[63] H. Bachert, P. Eliseev, M. Manko, V. Strahov, S. Raab, and C. Thay, "Multimode operation and mode-locking effect in injection lasers," IEEE J. Quantum Electron. **11**(7), 507–510 (1975).

[64] S. Chinn and E. Swanson, "Passive FM locking and pulse generation from 980-nm strained-quantum-well Fabry-Perot lasers," IEEE Photonics Technol. Lett. **5**(9), 969–971 (1993).

[65] K. Sato, "Optical pulse generation using Fabry-Perot lasers under continuous-wave operation," IEEE J. Sel. Top. Quantum Electron. **9**(5), 1288–1293 (2003).

[66] Y. Nomura, S. Ochi, N. Tomita, K. Akiyama, T. Isu, T. Takiguchi, and H. Higuchi, "Mode locking in Fabry-Pérot semiconductor lasers," Phys. Rev. A. **65**(4), 043807 (2002).

[67] R. Lang and K. Kobayashi, "External optical feedback effects on semiconductor injection laser properties," IEEE J. Quantum Electron. **16**(3), 347–355 (1980).

[68] S. Wieczorek, B. Krauskopf, D. Lenstra, "Mechanisms for multistability in a semiconductor laser with optical injection," Opt. Comm.. **183**(2000), 215–226 (2000).

[69] G.-Q. Xia, S.-C. Chan, and J.-M. Liu, "Mechanisms for multistability in a semiconductor laser with optical injection," Opt. Comm.. **15**(2), 572–576 (2007).

[70] J. Mork, J. Mark, and B. Tromborg, "Route to Chaos and Competition

between Relaxation Oscillations for a Semiconductor Laser with Optical Feedback," Phys. Rev. Lett. **65**(16), 1999–2002 (1990).

[71] M. Y. Hong, Y. H. Chang, A. Dienes, J. P. Heritage, P. J. Delfyett, Sol Dijaili, and F. G. Patterson, "Chaos in semiconductor lasers with optical feedback: theory and experiment," IEEE J. Quantum Electron. **28**(1), 93–108 (1992).

[72] G. H. M. van Tartwijk, D. Lenstra, " Low-frequency fluctuations in semiconductor lasers with optical feedback," Asian Journal of Physics. **7**, 562–575 (1998).

[73] L. Goldberg, H. F. Taylor, A. Dandridge, J. F. Weller, R. O. Miles, "Spectral characteristics of semiconductor lasers with optical feedback," IEEE Transactions on Microwave Theory and Techniques. **30**(4), 401–410 (1982).

[74] M. Tamburrini, P. Spano, and S. Piazzolla, "Influence of an external cavity on semiconductor laser phase-noise," Appl. Phys. Lett. **43**(5), 410 (1983).

[75] E. Patzak, H. Olesen, A. Sugimura, S. Saito, and T. Mukai, "Spectral linewidth reduction in semiconductor lasers by an external cavity with weak optical feedback," Electronics Letters. **19**(22), 938–940 (1983).

[76] G. Agrawal, "Line narrowing in a single-mode injection laser due to external optical feedback," IEEE J. Quantum Electron. **20**(5), 468–471 (1984).

[77] O. Solgaard and K. Y. Lau, "Optical feedback stabilisation of the intensity oscillations in ultrahigh-frequency passively modelocked monolithic quantum-well lasers," IEEE Photonics Technol. Lett. **5**(11), 1264–1267 (1993).

[78] D. Arsenijević, M. Kleinert, and D. Bimberg, "Phase-noise and jitter reduction by optical feedback on passively mode-locked quantum dot lasers," Appl. Phys. Lett. **103**(23), 231101 (2013).

[79] C.-Y. Lin, F. Grillot, N. A. Naderi, Y. Li, and L. F. Lester, "rf linewidth reduction in a quantum dot passively mode-locked laser subject to external optical feedback," Appl. Phys. Lett. **96**(5), 051118 (2010).

[80] K. Merghem, R. Rosales, S. Azouigui, A. Akrout, A. Martinez, F. Lelarge, G.-H. Duan, G. Aubin, and A. Ramdane, "Low noise performance of passively mode locked quantum-dash-based lasers under external optical feedback," Appl. Phys. Lett. **95**(13), 131111 (2009).

[81] L. Drzewietzki, S. Breuer, and W. Elsäßer, “Timing jitter reduction of passively mode-locked semiconductor lasers by self- and external-injection: Numerical description and experiments," Opt. Express **21**(13), 16142–16161 (2013).

[82] C. Otto, K. Lüdge, A. G. Vladimirov, M. Wolfrum, and E. Schöll, "Delay induced dynamics and jitter reduction of passively mode-locked semiconductor laser subject to optical feedback," New J. Phys. **14**, 113033 (2012).

[83] L. C. Jaurigue, A. S. Pimenov, D. Rachinskii, E. Schöll, K. Lüdge, and A. G. Vladimirov, "Timing jitter of passively mode-locked semiconductor lasers subject to optical feedback: a semi-analytic approach," Phys. Rev. A. **92**(5), 053807 (2015).

[84] C. Otto, L. C. Jaurigue, E. Schöll, and K. Lüdge, "optimisation of timing jitter reduction by optical feedback for a passively mode-locked laser," IEEE Photon. J. **6**(5), 1501814 (2014).

[85] E. A. Avrutin, and B. M. Russell, “Dynamics and spectra of monolithic mode-locked laser diodes under external optical feedback,” IEEE J. Sel. Top. Quantum Electron. **45**(11), 1456–1464 (2009).

[86] Y. Cho and M. Umeda, "Observation of chaos in a semiconductor laser with delayed feedback," Opt. Commun. **59**(2), 131–136 (1986).

[87] D. Lenstra, B. Verbeek, A. D. Boef, "Coherence collapse in single-mode semiconductor lasers due to optical feedback," IEEE J. Quantum Electron. **21**(6), 674–679 (1985).

[88] F. Grillot, C.-Y. Lin, N. A. Naderi, M. Pochet, and L. F. Lester, “Optical feedback instabilities in a monolithic InAs/GaAs quantum dot passively mode-locked laser,” Appl. Phys. Lett. **94**(15), 153503 (2009).

[89] S. Azouigui, B. Kelleher, S. P. Hegarty, G. Huyet, B. Dagens, F. Lelarge, A. Accard, D. Make, O. Le Gouezigou, K. Merghem, A. Martinez, Q. Zou, and A. Ramdane , “Coherence collapse and low-frequency fluctuations in quantum-dash based lasers emitting at 1.57 μm,” Opt. Express. **15**(21), 14155–14162 (2007).

[90] R. Adler, "A Study of Locking Phenomena in Oscillators," Proceedings of the IRE. **34**(6), 351 – 357 (1946).
[Available: http://ieeexplore.ieee.org/abstract/document/1451222/]

[91] H. L. Stover and W. H. Steier, “Locking of laser oscillators by light injection,” Appl. Phys. Lett. **8**(4), 91 (1966).

[92] S. Kobayashi, and T. Kimura, “Injection locking in AlGaAs semiconductor laser,” IEEE J. Quantum Electron. **17**(5), 681–689 (1981).

[93] R. Lang, "Injection-locking properties of a semiconductor laser," IEEE J. Quantum Electron. **18**(6), 976–983 (1982).

[94] F. Mogensen, H. Olesen, and G. Jacobsen, “Locking conditions and stability properties for a semiconductor laser with external light injection,” IEEE J. Quantum Electron. **21**(7), 784–793 (1985).

[95] G. H. M. van. Tartwijk and D. Lenstra, “Semiconductor lasers with optical injection and feedback,” Quantum Semiclass. Opt. **7**(2), 87–143 (1995).

[96] A. Sano, E. Yamada, H. Masuda, E. Yamazaki, T. Kobayashi, E. Yoshida, Y. Miyamoto, R. Kudo, K. Ishihara, and Y. Takatori, “No-guard-interval coherent optical OFDM for 100-Gb/s long-haul WDM transmission,” J. Lightwave. Technol. **27**(16), 3705–3713 (2009).

[97] T. Yilmaz, C. DePriest, T. Turpin, J. Abeles, and P. Delfyett, “Toward a photonic arbitrary waveform generator using a mode-locked external cavity semiconductor laser,” IEEE Photon. Technol. Lett. **14**(11), 1608–1610 (2002).

[98] C. J. Misas, P. Petropoulos, and D. Richardson, “All-optical signal processing of periodic signals using a brillouin gain comb,” J. Lightw. Technol. **26**(17), 3110–3117 (2008).

[99] S. Fukushima, C. F. C. Silva, Y. Muramoto, and A. J. Seeds, “Optoelectronic millimeter-wave synthesis using an optical frequency comb generator, optically injection locked lasers, and a unitraveling-carrier photodiode,” J. Lightwave Technol. **21**(12), 3043–3051 (2003).

[100] E. Sooudi, C. D. Dios, J. G. McInerney, G. Huyet, F. Lelarge, K. Merghem, R. Rosales, A. Martinez, A. Ramdane, and S. P. Hegarty, “A novel scheme for two-level stabilisation of semiconductor mode-locked lasers using simultaneous optical injection and optical feedback,” IEEE J. Sel. Top. Quantum Electron. **19**(4), 1101208 (2013).

[101] J.-H. Cho, H. Kim, and H.-K. Sung, “Reduction of spurious tones and

phase-noise in dual-loop OEO by loop-gain control," IEEE Photonics Technol. Lett. **27**(13), 1391–1393 (2015).

[102] F. V. Dijk, A. Enard, X. Buet, F. Lelarge, and G.- H. Duan, "Phase-noise reduction of a quantum-dash mode-locked laser in a millimeter-wave coupled opto-electronic oscillator," J. Lightwave Technol. **26**(15), 2789–2794 (2008).

[103] J. Yang, Y. J.-Long, W. Y.-Tian, Z. L.-Tai, and Y. En-Ze, "An optical domain combined dual-loop optoelectronic oscillator," IEEE Photonics Technol. Lett. **19**(11), 807–809 (2007).

[104] X. S. Yao and L. Maleki, "Optoelectronic microwave oscillator", J. Opt. Soc. Am. B. **13**(8), 1725–1735 (1996).

[105] V. F. Olle, A. Wonfor, L. A. M. Sulmoni, P. P. Vasilèv, J.-M. Lamy, J.-F. Carlin, N. Grandjean, R. V. Penty, and I. H. White, "Hybrid and passive mode-locking of a monolithic two-section MQW InGaN/GaN laser diode," IEEE Photonics Technol. Lett. **25**(15), 1514–1516 (2013).

[106] Y. Cheng, X. Luo, J. Song, T.-Y. Liow, G.-Q. Lo, Y. Cao, X. Hu, X. Li, P. H. Lim, and Q. J. Wang, "Passively mode-locked III-V/silicon laser with continuous-wave optical injection," Opt. Express. **23**(5), 6392–6399 (2015).

[107] E. Sooudi, G. Huyet, J. G. McInerney, F. Lelarge, K. Merghem, R. Rosales, A. Martinez, A. Ramdane, and S. P. Hegarty, "Injection-Locking properties of InAs/InP based mode-locked quantum-dash lasers at 21 GHz," IEEE Photonics Technol. Lett. **23**(20), 1544–1546 (2011).

[108] F. Quinlan, S. Gee, S. Ozharar, and P. J. Delfyett, "Greater than 20-dB supermode noise suppression and timing jitter reduction via cw injection of a harmonically mode-locked laser," IEEE Photonics Technol. Lett. **19**(16), 1221–1223 (2007).

[109] O. Nikiforov, L. Jaurigue, L. Drzewietzki, K. Lüdge, and S. Breuer, "Experimental demonstration of change of dynamical properties of a passively mode-locked semiconductor laser subject to dual optical feedback by dual full delay-range tuning," Opt. Express. **24**(13), 14301–14310 (2016).

[110] M. Haji, L. Hou, A. E. Kelly, J. Akbar, J. H. Marsh, J. M. Arnold, and C. N. Ironside, "High frequency optoelectronic oscillators based on the opti-

cal feedback of semiconductor mode-locked laser diodes," Opt. Express. **20**(3), 3268–3274 (2012).

[111] S. Breuer, W. Elsäßer, J. G. McInerney, K. Yvind, J. Pozo, E. A. J. M. Bente, M. Yousefi, A. Villafranca, N. Vogiatzis and J. Rorison, "Investigations of repetition rate stability of a mode-locked quantum dot semiconductor laser in an auxiliary optical fiber cavity," IEEE J. Quantum Electron. **46**(2), 150–157 (2010).

[112] L. Jaurigue, E. Schöll, and K. Lüdge, "Suppression of noise-induced modulations in multidelay systems," Phys. Rev. Lett. **117**, 154101 (2016).

[113] L. Jaurigue, "Dynamics and stochastic properties of passively mode-locked semiconductor lasers subject to optical feedback," P.hD. Thesis (Technischen Universität Berlin) (2016).
[Available: http://dx.doi.org/10.14279/depositonce-5543]

[114] R. Rosales, K. Merghem, A. Martinez, A. Akrout, J.-P. Tourrenc, A. Accard, F. Lelarge, and A. Ramdane, "InAs/InP quantum-dot passively mode-locked lasers for 1.55- μm applications," IEEE J. Sel. Top. Quantum Electron. **17**(5) 1292 –1301 (2011).

[115] S. Bouchoule, S. Azouigui, G. Patriarche, S. Guilet, L. Le Gratiet, A. Martinez, F. Lelarge, and A. Ramdane, "Processing of InP-based shallow ridge laser waveguides using a HBr ICP plasma," in *Indium Phosphide Related Material Conference*, 218 –221 (2007).
[Available: http://ieeexplore.ieee.org/abstract/document/4265919/]

[116] F. Kèfèlian, O$'$. Donoghue, M. T. Todaro, J. G. McInerney, and G. Huyet, "RF linewidth in monolithic passively mode-locked semiconductor laser," IEEE Photonics Technol. Lett. **20**(16), 1405–1407 (2008).

[117] S. Römisch, J. Kitching, E. Ferré-Pikal, L. Hollberg, and F. L. Walls, "Performance evaluation of an optoelectronic oscillator," IEEE Trans. Ultrason. Ferroelectr. Freq. Control. **47**(5), 1159–1165 (2000).

[118] W. Wei, H. Asghar, P. Kumar, D. Marah, and J. G. McInerney, "Sub-kHz RF linewidth of quantum-dash mode-locked laser by self-injection from symmetric dual-loop feedback and fibre delay," in *Conference on Lasers and Electro-Optics (CLEO)*, paper STh4L. (2016).
[Available: 10.1364/CLEO-SI.2016.STh4L.4]

[119] J.-H. Cho, H. Kim, and H.-K. Sung, "Performance optimisation of an op-

tically combined dual-loop optoelectronic oscillator based on optical interference analysis," Optical Engineering. **56**(6), 066111 (2017).

[120] T. Habruseva, D. Arsenijević , K. Kleinert, D. Bimberg, G. Huyet and S. P. Hegarty, "Optimum phase noise reduction and repetition rate tuning in quantum-dot mode-locked lasers," Appl. Phys. Lett. **104**, 021112 (2017).